Adsorption Characteristics of Organic Anions onto Large α-Alumina Beads with Positively Charged Surface

September 2014

Tien Duc PHAM

Adsorption Characteristics of Organic Anions onto Large α-Alumina Beads with Positively Charged Surface

A Dissertation Submitted to

the Graduate School of Life and Environmental Sciences,

the University of Tsukuba

in Partial Fulfillment of the Requirements

for the Degree of Doctoral of Philosophy in Agricultural Science

(Doctoral Program in Appropriate Technology and Sciences for Sustainable Development)

Tien Duc PHAM

Contents

Chapter 1. General introduction

1.1. Important environmental science properties

Earth science generally considers that the Earth consists of four spheres: the lithosphere, the hydrosphere, the atmosphere, and the biosphere, corresponding to rocks (including soil), water (including ice), air and life. Environmental science is close to earth science that seems to be a central of the relations to numerous branches of science such as biology, chemistry, physics, etc. The natural environment encompasses all living and non-living things occurring naturally on Earth with the interactions of all living species [1]. For example, physical, chemical and biological changes proceed ceaselessly in soil and water. These changes make the existence of life in soil. Plants and animals of the field cannot live without the changes.

Soil or sediments can be regards as the mixtures of inorganic minerals, organic materials and biochemicals. Minerals consist of clays (montmorillonite, kaolinite, illite,…) and non-clays (quartz and carbonate) [2]. Organic materials include plant and animal detritus and bacteria [3]. Also, both inorganic and organic contaminants are in water and soil. In order to evaluate the quality of soil and water environment, analytical science becomes necessarily. Inorganic contaminants in soils and sediments including metal cations and anions can be simultaneously determined by inductively couple plasma mass spectrometry (ICP-MS) [4] and ion chromatography (IC) [5], respectively. However, organic pollutants are very complicated because of a great number of organic compounds can exist in soils and sediments with complex interactions. It should be noted that all substances become the hazardous pollutants if they can cause a potential hazard to human health or the environment when improperly treated, stored, transported, or disposed of, or otherwise managed. Furthermore, the quantity of a contaminant in a given medium and the existing state affect the environmental impact. It is therefore important to consider what drives a contaminant from one medium to another and the manner and extent that a contaminant related to the different media or phases within a local environmental system. Contaminant adsorption by natural organic substance or solid surface can be treated in some detail to elucidate the relevant physicochemical parameters. Another feature is that the structure of organic compounds on the surface can be estimated on the basis of surface modification and adsorption properties. In this thesis, we focus on some kinds of organic ions, surfactants, polymers and dyes, to

emphasize their adsorption characteristics that can guide us toward a sufficiently accurate understanding of the activity and fate of contaminants in the environment.

1.2. Surfactants

Surfactant is one of the most versatile products used for detergents, chemical industry, pharmaceuticals, drilling muds, flotation agents and so on. A surfactant, known as ***surf***ace ***act***ive ***a***ge***nt***, is a substance that has property of adsorbing onto surfaces or interfaces to a marked degree and reduces the interfacial free energies of those surfaces or interfaces. The interfacial free energy is the minimum amount of work required to create that interface [6]. The most important point on the groups of surfactants is that surfactants are amphiphilic molecules consisting of a hydrophobic part such as a hydrocarbon (the tail) and a hydrophilic part (the head) [7]. Therefore, a surfactant molecule contains both a water insoluble component and a water soluble component. Depending on the nature of hydrophilic groups, surfactants are normally classified to 4 groups: nonionic, anionic, cationic, and zwitterionic surfactants (Figure 1.1). The differences in the hydrophobic groups are usually less pronounced than those in the hydrophilic groups. Surfactants are classified by different structures such as: straight chain or branched chain with long alkyl groups, long chain with alkylbenzene residues, alkylnaphtalene residues, high molecular weight propylene oxide polymers, etc [6]. In this study, an anionic surfactant with linear long chain hydrocarbon is considered.

Surfactants are effective chemicals that are used to perform a particular function in some process. For instance, surfactants are widely used chemicals for cleaning because surfactants in aqueous solution can lead to the solubilization of substances that would not dissolve in an aqueous solution [7]. Furthermore, in the bulk aqueous phase, surfactants form aggregates, such as micelles, where the hydrophobic tails form the core of the aggregate and the hydrophilic heads are in contact with the surrounding liquid. The concentration of surfactant at which micelles begin to form is called critical micelle concentration (CMC). The CMC is a function of the structure of the surfactant, temperature of the surfactant solution, the concentration of added electrolyte and the concentration of solubilizates and other amphiphilies [8]. The CMC seems to be very important factor to study interfacial properties of surfactant.

A fundamental property of surfactants is their tendency to adsorb at interface in an oriental fashion [6]. Adsorption of surfactants at the liquid-solid interface plays an important role in

many technological, environmental and industrial applications [9]. For the understanding of adsorption, adsorption isotherms have been the most important pieces of the experimental information. Thus, many experimental studies have been focused on the adsorption isotherms of surfactant at solid-aqueous interfaces [9-15]. Recently, the removal of organic contaminants by adsorption from aqueous solutions using ionic surfactant modified solid surface to enhance the removal efficiency has attracted intense studies [16-26]. However, adsorption behavior of surfactant molecules at such an interface is complex due to the presence of different micelles [10]. These micelles are called hemimicelles [27-31] (head groups of surfactant molecules toward solid surface) and admicelles [32-34] (a local bilayer structure with head groups of surfactant toward solution). The information about the adsorbed layer of surfactants on solid surfaces is unclear when the surface charge of an adsorbent is regulated upon surfactant adsorption. In order to evaluate adsorption mechanisms of surfactant, theory and model are needed. Nevertheless, simple models of adsorption of surfactant with the effect of charge adjustment have not been fully developed. The improvement in modeling is important when the model is applied for other complex systems and the understanding of adsorption under natural conditions is considered.

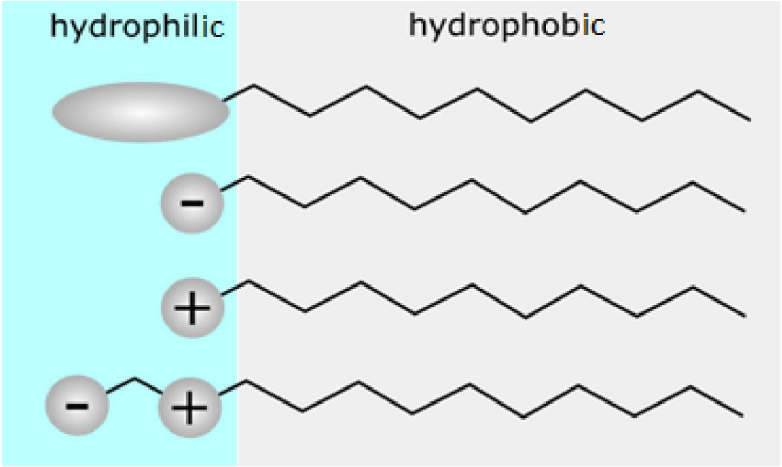

Fig. 1.1. Schematic representation of four groups of surfactant. Surfactant molecules consist of hydrophilic head and hydrophobic tail parts.

1.3. Polyelectrolytes

Polymers are very long molecules with a repetitive structure. The polymer chains may consist of identical units called monomers or segments. Polymers are broadly characterized

by their ionic nature: cationic, anionic and non-ionic [35]. Polyelectrolytes are polymers in which the monomers carry an electrical charge in solution. Strong and weak polyelectrolytes can be distinguished due to the dissociation of chargeable groups on the segments with the pH of solution [36]. While charges of strong polyelectrolytes are independent on pH, those of weak polyelectrolytes are highly dependent on pH.

The main applications of organic polyelectrolyes in portable water production are coagulation and flocculation, and in the dewatering of treatment plant sludges [35]. In the principle of physical chemistry, there are three mechanism of flocculation of particles by polyelectrolytes: polymer bridging, depletion flocculation and charge neutralization (including electrostatic patch effect) [35, 37]. Except for depletion flocculation, other mechanisms are dependent on adsorption of polymers on particle surfaces so that adsorption of polyelectrolyte is important to evaluate flocculation behavior of particles. Adsorption of polymers from solution takes place when the adsorption energy is high enough to compensate for the loss of entropy [38]. At very low concentration, polymer can be adsorbed on the surface of particles with a flat conformation (Fig. 1.2a). In a realistic situation, many chains of polymer adsorb and compete for the available surface sites. The adsorbed layer thickness increases as loops and tails develop (Fig. 1.2b) [36]. A train is a sequence of polymer segments in contact with surface while a loop is a part of chain which toward solution but ends on both sides in a train. A tail is non-adsorbed, dangling end of the chain.

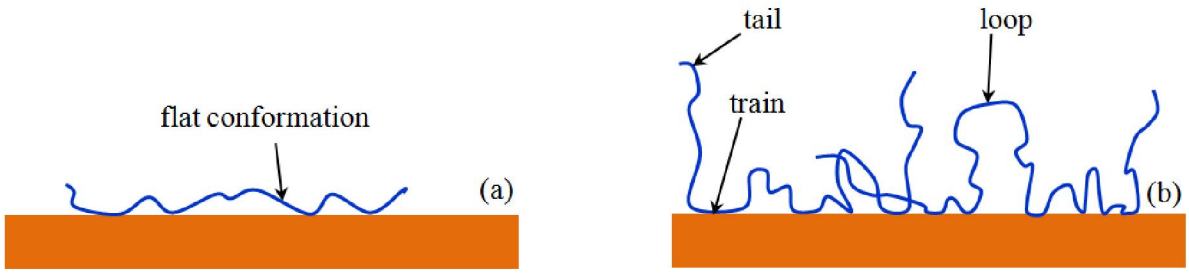

Fig. 1.2. The conformation of adsorbed polymer on the surface. Adsorbed layer of polymer at a low surface coverage (a) and at high coverage (b).

In the adsorption of polyelectrolytes, charge effect is very important but it is rather complex. The adsorption system is more complicated when the solid surface also contains electrical charge. Driving force for the adsorption of strong polyelectrolyte on oppositely charged surface can only be electrostatic or a combination of electrostatic and non-electrostatic contributions [36, 39]. When a non-electrostatic interaction is induced, a slight

overcompensation of surface charge is found. Polyelectrolyte chains adopt a flat conformation due to the repulsion between the chains in the low concentration of salt solution. Due to specific adsorption characterization of polyelectrolyte on the solid surface, numerous polymers were used to modify solid particles to enhance removal efficiency of organic contaminants [40-42]. In almost cases of adsorption of polyelectrolytes for removal of pollutants in aqueous solutions, charge effects have to be considered. Furthermore, the charge regulation of mineral surface upon adsorption of strong polyelectrolyte was obtained theoretically and experimentally [43]. The self consistent field (SCF) calculation showed the large effect of pH and the small effect of the salt concentration to the adsorbed amount while the proton co-adsorption was dependent on both pH and salt concentration. Nevertheless, the measured adsorption isotherms of polyanion on positively charged mineral surface did not show a high affinity character as expected from theoretical calculations because of fast flocculation and non-equilibrium polymer conformation [43, 44]. It is therefore preferable to make an equilibrium study of polyelectrolyte adsorption using absorbents which are free flocculation such as large particles.

1.4. Organic dyes

Dyes are a class of pollutants and can be identified by human eye [45]. Many industries such as textile, paint, cosmetic, paper and plastic use dyes to color their products and also substantial volume of water. As the results, they generate a large amount of colored wastewater that influence to the quality of water by the color [46]. A number of dyes are toxic and serious hazardous to human body and living organisms. Synthetic dyes exhibit considerable structure diversity and are classified in several ways [45, 47]. They can be classified on the basis of their solubility: soluble dyes including acid, mordant, metal complex, direct, basic and reactive dyes; and insoluble dyes which include azoic, sulfur, vat and disperse dyes. In addition, both a major azo linkage and anthraquinone unit also characterize dyes chemically. It should be noted that organic azo dyes are one of the most widely used and account for 65 -70 % of total dyes produced [45]. In this thesis, a soluble azo dye with sulfonic groups will be investigated.

A wide range of methods have been developed for the removal of organic dyes from waters and wastewaters in order to decrease their impact on the environment [45, 47] such as adsorption [48-51], photocatalytic degradation [52-54], electrochemical oxidation [55, 56], coagulation flocculation [57], biological process [58], etc. Among them, adsorption becomes

one of the most common technology that can be applicable for developing countries by using low-cost or natural adsorbents [45, 46, 59]. Recently, many studies focused on the removal of organic dyes by adsorption from aqueous solutions using solid surface modified with ionic surfactant or polyelectrolyte [16-19, 21-26, 35, 52, 60-62]. So far, ionic surfactants [16, 20, 23] and polyelectrolyte [40-42] were used to modify large particles to enhance the removal efficiency of ionic dyes. Higher performance for the removal organic dyes was obtained when ionic surfactants are combined with polyelectrolytes [61, 63, 64]. Another feature is that using large particles is not only limited in laboratorial investigations but also applicable in the chemical engineering process by packed bed adsorbents in columns. However, the mechanisms of dye adsorption on surfactant and polyelectrolyte modified solid surfaces are still inadequate. It is necessary to make a comparative adsorption studies between polyelectrolyte, ionic surfactant, or ionic dyes with the similar charge (same cationic or same anionic) on large beads with oppositely charged solid surfaces.

1.5. Metal (hydr)oxides

Metal (hydr)oxides and/or mineral (hydr)oxides are one of major inorganic components of soils. Furthermore, metal (hydr)oxides are also used as the important absorbents in a wide range of applications. The interfacial properties of metal (hydr)oxides are important to study adsorption of solutes and colloids in soil and water environments. While a lot of studies carried out adsorption and transport using large particles such as silica sand with negative charge), not so many studies have been conducted on porous material with positive charge. Therefore, this thesis interests the interfacial properties of alumina and the adsorption characteristics of some organic anions onto alumina (normally positive charge at lower neutral pH).

Hydroxides and oxides of aluminum are often found in soil system with different amount as independent particles or as mixture with other minerals [65]. Many interests to interfacial characterizations of aluminum hydroxides have been improving the understanding of these properties of aluminum oxides. The crystal structure of aluminum hydroxide was analyzed by applying the Pauling rules [66]. The trivalent Al^{3+} ions distribute their charge over six surrounding oxygen ions of the octahedron to form hexa-coordination with oxygens [67]. The aluminum ion attributes haft a unit charge to the surface oxygen groups per Al-O bond. As the surface oxygens are formed singly or doubly to Al^{3+} ions, the surface groups are two types of $AlOH^{1/2-}$ and Al_2OH^0, respectively. The charge of $AlOH^{1/2-}$ group can become

reserved by the adsorption of a proton. The proton affinities of various types of groups are different. The adsorption of proton can also be influenced by adsorbed organic ions. When proton co-adsorption upon the adsorption of organic ions is significant, surface charge of aluminum (hydr)oxides is dependent on both of the adsorption of proton and organic ions. Conversely, if proton co-adsorption is negligible, charging property of aluminum (hydr)oxides will only be affected by the adsorption of organic ions.

1.6. Modeling the adsorption of organic ions

Modeling the adsorption of organic ions onto (hydr)oxide surfaces is a major challenge. At the (hydr)oxide solid-solution interface, some types of surface groups can exist and each reacting group follows its own affinity constant (*K*) for proton. A general MUltiSIte Complexation (MUSIC) model, which was presented by Hiemstra et al. [68, 69] was successfully applied to several (hydr)oxides to predict proton affinity constants. The protonation of reactive oxygen is strongly dependent on pH and ionic strength. The pH at which the net charge of surface equals zero in the absence of chemically bond ions other than $H^+$and OH^-, is called the point of zero charge (PZC). At pH below or above the PZC, the surface sites become positively or negatively charged due to the reaction with either H^+or OH^-, respectively [70].

In the calculation of particle charge, electrostatic theory is often applied to the adsorbing protons and other ions. Ions form complexes at the (hydr)oxides surface so that repulsive or attractive force by electrostatic field need to be taken into account [67]. The Charge Distribution (CD) has been developed to improve the MUSIC model. The CD-MUSIC model is based on the 1-pK approach in which the only one protonation of different oxygen surface groups is described by single reaction. The CD-MUSIC model was successfully tested for many ions binding to different mineral surfaces in aqueous environment. However, the CD-MUSIC cannot be applied for some kinds of organic ions (such as surfactants or polyelectrolytes) systems where the interactions between organic ions and (hydr)oxides surface probably induce the surface charge regulation.

In the cases of regulating charge surface, the self-consistent field lattice (SCFA) theory was used to describe adsorption behaviors of polymer [71, 72] and surfactant [7, 73]. The theory was extended by taking account of electrostatic interactions and association structures of some organic ions [7, 74]. For surfactant adsorption, the SCFA theory describes well the adsorption amount, effects of charged surface, chain length and branching [7]. The SCFA

theory indicates that the two-step adsorption and four-region isotherm models coexist and are valid under different conditions depending on the charging properties of solid surface [75]. While two-step adsorption model [10, 76] suggests the hemimicelles on a linear – linear scale plot, the four-region isotherm is indicative for the case of both hemimicelles and admicelles (as mentioned in section 1.2) on a log – log scale. The extended SCFA model also predicts successfully at a quantitative level the surface charge density in the presence of polyelectrolyte and the charge overcompensation upon polyelectrolyte adsorption [77]. However, the adsorption amounts of polyelectrolyte on metal oxides are poorly described when compared with experimental results [43, 77]. The SCFA model is rather complicated because this model requires so many choices of parameters. It is practically preferable to choose a simple model that can be applicable for different adsorption situations.

Two-step adsorption model was firstly presented by Zhu et al. [76, 78] by assuming that the adsorption on solid-liquid interface occurs in two steps. This simple model was originally described for the adsorption of surfactant with hemimicelle formation. On the basis of two-step model, a general adsorption isotherm was derived. This equation was also applied to various types of surfactant adsorption isotherms for numerous systems. In addition, works of Koopal and co-workers [79, 80] indicated that, at low salt concentration, almost every adsorbing surfactant molecule adsorbs a proton. It suggests that the uptake of proton due to surfactant adsorption is probably described by two step model if this model is successful in predicting the surfactant adsorption. Recently, adsorption isotherms of some kinds of polymers on ZrO_2 nanoparticle [81] and onto cotton fiber [82] were fitted and interpreted by the general equation. The multilayer model which was introduced by Brunauer-Emmett-Teller (BET) was used to describe adsorption isotherms of some ionic dyes [83-86]. However, the complex multilayer adsorption of ionic dyes fitted by the general equation has not been reported. In this thesis, two-step model will be examined for describing the adsorption isotherms of some organic anions including surfactant, polyelectrolyte, dye and predict proton co-adsorption.

1.7. Objectives and outline of this thesis

The treatment of wastewater containing organic pollutants is of a great importance in environmental remediation. Adsorption is one of the most popular methods for removing organic wastes such as dyes in aqueous solutions is widely seen in many developing countries. The modified adsorbent surface by surfactant and/or polyelectrolyte can enhance

the removal efficiency. The understanding of adsorption characteristics of organic ions onto large particles is a challenging problem in the relation to issues mentioned above sections. While the uptake of organic contaminants on natural porous media with negatively charged surface such as silica sand has attracted numerous researches, not so many studies have been conducted on positively charged large beads. In order to better understand the adsorption in natural environmental porous media, the investigation and comparison should be carried out on both negatively and positively charged large particles. Therefore, we will focus on the large alumina beads with positively charged surface in all topics in this thesis. The objectives of this thesis are to investigate the adsorption of anionic surfactant, sodium dodecyl sulfate (SDS), anionic azo dye, new coccine (NC), and polyanion, polystyrene sulfonate (PSS), onto large α-Al_2O_3 beads as functions of pH and NaCl concentration after characterizing the interfacial properties of these beads. The two-step model is performed to describe the adsorption of these organic anions onto positively charge surface of α-Al_2O_3 beads. The interfacial properties and surface modifications of α-Al_2O_3 beads before and after adsorption are also studied. The structures of adsorbed SDS, NC and PSS onto α-Al_2O_3 are discussed on the basis of surface charge effect, surface modification and adsorption isotherms.

This thesis consists of the four research topics that will be introduced from the chapter 2 to chapter 5.

Chapter 2 is devoted to the interfacial characterization of Al_2O_3 materials by streaming potential and chromatographic methods. The large particles are difficult to be characterized with standard methods but streaming potential and chromatography are applicable for the interface of Al_2O_3 beads in our research. Streaming potential will be used to monitor the zeta potential at several pH values to discuss electrokinetic property and to identify isoelectric point (IEP) of α-Al_2O_3 materials. The surface charge density of α-Al_2O_3 materials is evaluated by chromatographic method from measuring pH breakthrough curves. It will be shown that the combination of streaming potential and chromatography compared with the 1-pK model are promising to obtain the electrokinetic potential and surface charge density of large bead particles.

In chapter 3 the adsorption of SDS onto Al_2O_3 beads with variably charged surface will be investigated. The adsorption isotherms of SDS by batch experiments at different pH and NaCl concentrations are discussed by two-step and four-region models. Proton uptake upon surfactant adsorption will also be fitted by two-step model. At different salt concentrations, the structure of adsorbed layer based on hemimicelle and admicelle concepts are proposed.

Chapter 4 deals with the comparison of SDS to NC in adsorption. For this purpose, streaming potential will be used again to evaluate the effect of SDS and NC at the plateau adsorption on surface charge of α-Al_2O_3. The surface modifications of α-Al_2O_3 after adsorption of SDS and NC are confirmed by Fourier transform infrared attenuated total reflection spectroscopy (FTIR-ATR). Two-step adsorption model is applied to predict NC isotherms. The influence of salt induced charge effect in SDS and NC systems are shown for the comparison of their adsorption behaviors. The structure of adsorbed NC and SDS will be discussed based on adsorption isotherms with surface charge effect and surface modifications.

In chapter 5 we study the adsorption of strong polyelectrolyte, PSS with different molecular weights onto α-Al_2O_3 beads and effect of added SDS on the isotherms. The pH independent nature of PSS is also confirmed by ultraviolet spectrophotometry. From low to high molecular weights, the adsorption isotherms show the typical high affinity and can be represented well by two-step model. Proton co-adsorption upon the adsorption of PSS of different molecular weight is also investigated. The salt effect to isotherms will be shown to demonstrate the influence of electrostatic, and non-electrostatic interactions. The prevention of SDS uptake onto α-Al_2O_3 beads to the adsorption of PSS is evaluated with pre-adsorbed SDS. The structure of adsorbed PSS of different molecular weight at low and high salt concentrations will be proposed.

Lastly, in chapter 6 the obtained results from chapter 2 to chapter 5 are summarized and the perspectives for further studies will be proposed.

References

[1] D.L. Johnson, S.H. Ambrose, T.J. Bassett, M.L. Bowen, D.E. Crummey, J.S. Isaacson, D.N. Johnson, P. Lamb, M. Saul, A.E. Winter-Nelson, Meanings of Environmental Terms, J. Environ. Qual., 26 (1997) 581-589.

[2] H.N. Dang, D.T. Tran, V.H. Dinh, T.K.A. Nguyen, M.L. Nguyen, D.K. Nguyen, S.H. Phan, M.H. Nguyen, T.D. Pham, T.B.T. Lai, The sedimentary processes on tidal flats in the North of Vietnam: initial results and implication future, Proceedings of VAST – IRD Symposium on Marine Science, (2013) 164-178.

[3] W.H. McAnally, A.J. Mehta, Collisional aggregation of fine estuarial sediment, Proceedings in Marine Science, Elsevier, 2000, pp. 19-39.

[4] T.D. Pham, T.N.M. Pham, T.A.H. Nguyen, T.K. Hoang, Simultaneous determination of impurities metals in pure Tungsten powder by ICP-MS, Journal of Analytical Sciences, 17 (2012) 22-27.

[5] E. Jackson Peter, D. Thomas, K. Chassaniol, Environmental Analysis of Inorganic Anions and Perchlorate by Ion Chromatography, Environmental Impact of Fertilizer on Soil and Water, American Chemical Society, 2003, pp. 3-15.

[6] Milton J. Rosen, Joy T. Kunjappu, Surfactants and Interfacial Phenomena 4th Edition, John Wiley&Sons, USA, 2012.

[7] M.R. Bohmer, PhD Thesis: Adsorption and Micellization of Surfactants: comparison of theory and experiment, Wageningen Agricultural Univerisy, 1991.

[8] D.A. Sabatini, R.C. Knox, Transport and Remediation of Subsurface Contaminants, American Chemical Society, Washington DC, USA, 1992.

[9] S. Paria, K.C. Khilar, A review on experimental studies of surfactant adsorption at the hydrophilic solid–water interface, Advances in Colloid and Interface Science, 110 (2004) 75-95.

[10] R. Atkin, V.S.J. Craig, E.J. Wanless, S. Biggs, Mechanism of cationic surfactant adsorption at the solid–aqueous interface, Advances in Colloid and Interface Science, 103 (2003) 219-304.

[11] K. Esumi, Y. Yamanaka, Interaction between Sodium Dodecyl Poly(oxyethylene) Sulfate and Alumina Surface in Aqueous Solution, Journal of Colloid and Interface Science, 172 (1995) 116-120.

[12] T.P. Goloub, L.K. Koopal, Adsorption of Cationic Surfactants on Silica. Comparison of Experiment and Theory, Langmuir, 13 (1997) 673-681.

[13] E.M. Lee, L.K. Koopal, Adsorption of Cationic and Anionic Surfactants on Metal Oxide Surfaces: Surface Charge Adjustment and Competition Effects, Journal of Colloid and Interface Science, 177 (1996) 478-489.

[14] S. Paria, Surfactant-enhanced remediation of organic contaminated soil and water, Advances in Colloid and Interface Science, 138 (2008) 24-58.

[15] R. Zhang, P. Somasundaran, Advances in adsorption of surfactants and their mixtures at solid/solution interfaces, Advances in Colloid and Interface Science, 123–126 (2006) 213-229.

[16] A. Adak, M. Bandyopadhyay, A. Pal, Removal of crystal violet dye from wastewater by surfactant-modified alumina, Separation and Purification Technology, 44 (2005) 139-144.

[17] A. Adak, M. Bandyopadhyay, A. Pal, Fixed bed column study for the removal of crystal violet (C. I. Basic Violet 3) dye from aquatic environment by surfactant-modified alumina, Dyes and Pigments, 69 (2006) 245-251.

[18] F. Aloulou, S. Boufi, N. Belgacem, A. Gandini, Adsorption of cationic surfactants and subsequent adsolubilization of organic compounds onto cellulose fibers, Colloid Polym Sci, 283 (2004) 344-350.

[19] F. Aloulou, S. Boufi, M. Chakchouk, Adsorption of octadecyltrimethylammonium chloride and adsolubilization on to cellulosic fibers, Colloid Polym Sci, 282 (2004) 699-707.

[20] S. Chatterjee, D.S. Lee, M.W. Lee, S.H. Woo, Enhanced adsorption of congo red from aqueous solutions by chitosan hydrogel beads impregnated with cetyl trimethyl ammonium bromide, Bioresource Technology, 100 (2009) 2803-2809.

[21] Y.G. Mishael, P.L. Dubin, Toluene Solubilization Induces Different Modes of Mixed Micelle Growth†, Langmuir, 21 (2005) 9803-9808.

[22] Y.G. Mishael, T. Undabeytia, G. Rytwo, B. Papahadjopoulos-Sternberg, B. Rubin, S. Nir, Sulfometuron Incorporation in Cationic Micelles Adsorbed on Montmorillonite, Journal of Agricultural and Food Chemistry, 50 (2002) 2856-2863.

[23] A. Özcan, Ç. Ömeroğlu, Y. Erdoğan, A.S. Özcan, Modification of bentonite with a cationic surfactant: An adsorption study of textile dye Reactive Blue 19, Journal of Hazardous Materials, 140 (2007) 173-179.

[24] A.S. Özcan, B. Erdem, A. Özcan, Adsorption of Acid Blue 193 from aqueous solutions onto Na–bentonite and DTMA–bentonite, Journal of Colloid and Interface Science, 280 (2004) 44-54.

[25] Y. Su, B. Zhao, W. Xiao, R. Han, Adsorption behavior of light green anionic dye using cationic surfactant-modified wheat straw in batch and column mode, Environ Sci Pollut Res, 20 (2013) 5558-5568.

[26] B. Zhao, Y. Shang, W. Xiao, C. Dou, R. Han, Adsorption of Congo red from solution using cationic surfactant modified wheat straw in column model, Journal of Environmental Chemical Engineering, 2 (2014) 40-45.

[27] D.W. Fuerstenau, Streaming Potential Studies on Quartz in Solutions of Aminium Acetates in Relation to the Formation of Hemi- micelles at the Quartz-Solution Interface, The Journal of Physical Chemistry, 60 (1956) 981-985.

[28] D.W. Fuerstenau, H.J. Modi, Streaming Potentials of Corundum in Aqueous Organic Electrolyte Solutions, Journal of The Electrochemical Society, 106 (1959) 336-341.

[29] A.M.F. Gaudin, D. W. Fuerstenau, Streaming Potential Studies. Quartz Flotation with Anionic Collectors, Transactions AIME, 202 (1955) 958-962.

[30] P. Somasundaran, T.W. Healy, D.W. Fuerstenau, Surfactant Adsorption at the Solid—Liquid Interface—Dependence of Mechanism on Chain Length, The Journal of Physical Chemistry, 68 (1964) 3562-3566.

[31] T. Wakamatsu, D.W. Fuerstenau, The Effect of Hydrocarbon Chain Length on the Adsorption of Sulfonates at the Solid/Water Interface, Adsorption From Aqueous Solution, American Chemical Society, 1968, pp. 161-172.

[32] D. Bitting, J.H. Harwell, Effects of counterions on surfactant surface aggregates at the alumina/aqueous solution interface, Langmuir, 3 (1987) 500-511.

[33] J.H. Harwell, J.C. Hoskins, R.S. Schechter, W.H. Wade, Pseudophase separation model for surfactant adsorption: isomerically pure surfactants, Langmuir, 1 (1985) 251-262.

[34] M.A. Yeskie, J.H. Harwell, On the structure of aggregates of adsorbed surfactants: the surface charge density at the hemimicelle/admicelle transition, The Journal of Physical Chemistry, 92 (1988) 2346-2352.

[35] B. Bolto, J. Gregory, Organic polyelectrolytes in water treatment, Water Research, 41 (2007) 2301-2324.

[36] A.W.M. de Laat, PhD Thesis: Adsorption of water-soluble polymers onto barium titanate and its effect on colloidal stability, Wageningen Agricultural University, 1995.

[37] Y. Adachi, Dynamic aspects of coagulation and flocculation, Advances in Colloid and Interface Science, 56 (1995) 1-31.

[38] G.J. Fleer, J.M.H.M. Scheutjens, M.A.C. Stuart, Theoretical progress in polymer adsorption, steric stabilization and flocculation, Colloids and Surfaces, 31 (1988) 1-29.

[39] A.M. Blokhus, K. Djurhuus, Adsorption of poly(styrene sulfonate) of different molecular weights on α-alumina: Effect of added sodium dodecyl sulfate, Journal of Colloid and Interface Science, 296 (2006) 64-70.

[40] S. Chatterjee, T. Chatterjee, S.H. Woo, Influence of the polyethyleneimine grafting on the adsorption capacity of chitosan beads for Reactive Black 5 from aqueous solutions, Chemical Engineering Journal, 166 (2011) 168-175.

[41] G. Crini, P.-M. Badot, Application of chitosan, a natural aminopolysaccharide, for dye removal from aqueous solutions by adsorption processes using batch studies: A review of recent literature, Progress in Polymer Science, 33 (2008) 399-447.

[42] E.S. Dragan, Design and applications of interpenetrating polymer network hydrogels. A review, Chemical Engineering Journal, 243 (2014) 572-590.

[43] J.K. Wolterink, L.K. Koopal, M.A.C. Stuart, W.H. Van Riemsdijk, Surface charge regulation upon polyelectrolyte adsorption, hematite, polystyrene sulfonate, surface charge

regulation: Theoretical calculations and hematite-poly(styrene sulfonate) system, Colloids and Surfaces A: Physicochemical and Engineering Aspects, 291 (2006) 13-23.

[44] J.K. Wolterink, PhD Thesis: Polyelectrolyte behavior in solution and at interfaces, Wagenningen University, 2003.

[45] V.K. Gupta, Suhas, Application of low-cost adsorbents for dye removal – A review, Journal of Environmental Management, 90 (2009) 2313-2342.

[46] G. Crini, Non-conventional low-cost adsorbents for dye removal: A review, Bioresource Technology, 97 (2006) 1061-1085.

[47] E. Forgacs, T. Cserháti, G. Oros, Removal of synthetic dyes from wastewaters: a review, Environment International, 30 (2004) 953-971.

[48] C.A.P. Almeida, N.A. Debacher, A.J. Downs, L. Cottet, C.A.D. Mello, Removal of methylene blue from colored effluents by adsorption on montmorillonite clay, Journal of Colloid and Interface Science, 332 (2009) 46-53.

[49] M. Doğan, M. Alkan, A. Türkyilmaz, Y. Özdemir, Kinetics and mechanism of removal of methylene blue by adsorption onto perlite, Journal of Hazardous Materials, 109 (2004) 141-148.

[50] B.H. Hameed, M.I. El-Khaiary, Removal of basic dye from aqueous medium using a novel agricultural waste material: Pumpkin seed hull, Journal of Hazardous Materials, 155 (2008) 601-609.

[51] M.A. Schoonen, J.M.T. Schoonen, Removal of crystal violet from aqueous solutions using coal, Journal of Colloid and Interface Science, 422 (2014) 1-8.

[52] F. Al-Momani, E. Touraud, J.R. Degorce-Dumas, J. Roussy, O. Thomas, Biodegradability enhancement of textile dyes and textile wastewater by VUV photolysis, Journal of Photochemistry and Photobiology A: Chemistry, 153 (2002) 191-197.

[53] S.-F. Kang, C.-H. Liao, S.-T. Po, Decolorization of textile wastewater by photo-fenton oxidation technology, Chemosphere, 41 (2000) 1287-1294.

[54] M. Pérez, F. Torrades, X. Domènech, J. Peral, Fenton and photo-Fenton oxidation of textile effluents, Water Research, 36 (2002) 2703-2710.

[55] N. Mohan, N. Balasubramanian, C.A. Basha, Electrochemical oxidation of textile wastewater and its reuse, Journal of Hazardous Materials, 147 (2007) 644-651.

[56] A.G. Vlyssides, M. Loizidou, P.K. Karlis, A.A. Zorpas, D. Papaioannou, Electrochemical oxidation of a textile dye wastewater using a Pt/Ti electrode, Journal of Hazardous Materials, 70 (1999) 41-52.

[57] S. Papić, N. Koprivanac, A. Lončarić Božić, A. Meteš, Removal of some reactive dyes from synthetic wastewater by combined Al(III) coagulation/carbon adsorption process, Dyes and Pigments, 62 (2004) 291-298.

[58] S. Ledakowicz, M. Solecka, R. Zylla, Biodegradation, decolourisation and detoxification of textile wastewater enhanced by advanced oxidation processes, Journal of Biotechnology, 89 (2001) 175-184.

[59] A. Bhatnagar, A.K. Jain, A comparative adsorption study with different industrial wastes as adsorbents for the removal of cationic dyes from water, Journal of Colloid and Interface Science, 281 (2005) 49-55.

[60] F. Aloulou, S. Boufi, D. Beneventi, Adsorption of organic compounds onto polyelectrolyte immobilized-surfactant aggregates on cellulosic fibers, Journal of Colloid and Interface Science, 280 (2004) 350-358.

[61] Y.G. Mishael, P.L. Dubin, Uptake of Organic Pollutants by Silica−Polycation-Immobilized Micelles for Groundwater Remediation, Environmental Science & Technology, 39 (2005) 8475-8480.

[62] D. Zadaka, A. Radian, Y.G. Mishael, Applying zeta potential measurements to characterize the adsorption on montmorillonite of organic cations as monomers, micelles, or polymers, Journal of Colloid and Interface Science, 352 (2010) 171-177.

[63] Y. Wang, J. Banziger, P.L. Dubin, G. Filippelli, N. Nuraje, Adsorptive Partitioning of an Organic Compound onto Polyelectrolyte-Immobilized Micelles on Porous Glass and Sand, Environmental Science & Technology, 35 (2001) 2608-2611.

[64] D. Zadaka, Y.G. Mishael, T. Polubesova, C. Serban, S. Nir, Modified silicates and porous glass as adsorbents for removal of organic pollutants from water and comparison with activated carbons, Applied Clay Science, 36 (2007) 174-181.

[65] T. Hiemstra, W.H.v. Riemsdijk, M.G.M. Bruggenwert, Proton adsorption mechanism at the gibbsite and aluminium oxide solid/solution interface, Netherlands Journal of Agricultural Science, 35 (1987) 281-294.

[66] L. Pauling, The Principles Determining The Structure of Complex Ionic Crystals, Journal of the American Chemical Society, 51 (1929) 1010-1026.

[67] T. Hiemstra, PhD Thesis: Surface complexation at mineral interfaces: Multisite and Charge Distribution approach, Wagenningen University, 2010.

[68] T. Hiemstra, J.C.M. De Wit, W.H. Van Riemsdijk, Multisite proton adsorption modeling at the solid/solution interface of (hydr)oxides: A new approach: II. Application to various important (hydr)oxides, Journal of Colloid and Interface Science, 133 (1989) 105-117.

[69] T. Hiemstra, W.H. Van Riemsdijk, G.H. Bolt, Multisite proton adsorption modeling at the solid/solution interface of (hydr)oxides: A new approach: I. Model description and evaluation of intrinsic reaction constants, Journal of Colloid and Interface Science, 133 (1989) 91-104.

[70] G.V. Franks, Y. Gan, Charging Behavior at the Alumina–Water Interface and Implications for Ceramic Processing, Journal of the American Ceramic Society, 90 (2007) 3373-3388.

[71] J.M.H.M. Scheutjens, G.J. Fleer, Statistical theory of the adsorption of interacting chain molecules. 1. Partition function, segment density distribution, and adsorption isotherms, The Journal of Physical Chemistry, 83 (1979) 1619-1635.

[72] J.M.H.M. Scheutjens, G.J. Fleer, Statistical theory of the adsorption of interacting chain molecules. 2. Train, loop, and tail size distribution, The Journal of Physical Chemistry, 84 (1980) 178-190.

[73] F.A.M. Leermakers, J.M.H.M. Scheutjens, Statistical thermodynamics of association colloids: V. critical micelle concentration, micellar size and shape, Journal of Colloid and Interface Science, 136 (1990) 231-241.

[74] M.A.C. Stuart, G.J. Fleer, J. Lyklema, W. Norde, J.M.H.M. Scheutjens, Adsorption of Ions, Polyelectrolytes and Proteins, Advances in Colloid and Interface Science, 34 (1991) 477-535.

[75] A. Fan, P. Somasundaran, N.J. Turro, Adsorption of Alkyltrimethylammonium Bromides on Negatively Charged Alumina, Langmuir, 13 (1997) 506-510.

[76] B.-Y. Zhu, T. Gu, Surfactant adsorption at solid-liquid interfaces, Advances in Colloid and Interface Science, 37 (1991) 1-32.

[77] V. Shubin, P. Linse, Self-Consistent-Field Modeling of Polyelectrolyte Adsorption on Charge-Regulating Surfaces, Macromolecules, 30 (1997) 5944-5952.

[78] B.-Y. Zhu, T. Gu, General isotherm equation for adsorption of surfactants at solid/liquid interfaces. Part 1. Theoretical, Journal of the Chemical Society, Faraday Transactions 1: Physical Chemistry in Condensed Phases, 85 (1989) 3813-3817.

[79] M.R. Bohmer, L.K. Koopal, Adsorption of ionic surfactants on variable-charge surfaces. 1. Charge effects and structure of the adsorbed layer, Langmuir, 8 (1992) 2649-2659.

[80] T.P. Goloub, L.K. Koopal, B.H. Bijsterbosch, M.P. Sidorova, Adsorption of Cationic Surfactants on Silica. Surface Charge Effects, Langmuir, 12 (1996) 3188-3194.

[81] R. Ndong, W. Russel, Linear viscoelasticity of ZrO2 nanoparticle dispersions with associative polymers, Rheol Acta, 51 (2012) 771-782.

[82] I. Hoffmann, C. Oppel, U. Gernert, P. Barreleiro, W. von Rybinski, M. Gradzielski, Adsorption Isotherms of Cellulose-Based Polymers onto Cotton Fibers Determined by Means of a Direct Method of Fluorescence Spectroscopy, Langmuir, 28 (2012) 7695-7703.

[83] F. Doulati Ardejani, K. Badii, N.Y. Limaee, S.Z. Shafaei, A.R. Mirhabibi, Adsorption of Direct Red 80 dye from aqueous solution onto almond shells: Effect of pH, initial concentration and shell type, Journal of Hazardous Materials, 151 (2008) 730-737.

[84] A. Kamari, W.S.W. Ngah, M.Y. Chong, M.L. Cheah, Sorption of acid dyes onto GLA and H2SO4 cross-linked chitosan beads, Desalination, 249 (2009) 1180-1189.

[85] J.S. Piccin, C.S. Gomes, L.A. Feris, M. Gutterres, Kinetics and isotherms of leather dye adsorption by tannery solid waste, Chemical Engineering Journal, 183 (2012) 30-38.

[86] J. Wang, C.P. Huang, H.E. Allen, D.K. Cha, D.-W. Kim, Adsorption Characteristics of Dye onto Sludge Particulates, Journal of Colloid and Interface Science, 208 (1998) 518-528.

Chapter 2. Interfacial characterization of α-alumina with small surface area by streaming potential and chromatography

2.1. Introduction

An understanding interfacial proprieties of various oxides is of great importance to study adsorption and transport of solutes and colloids in soil and water environments [1]. Alumina has been widely investigated in industrial chemistry and environmental applications. Aluminum oxides exist in many different forms, namely α, β, ϒ, η, θ, κ and χ phases [2]. The most thermodynamically stable form is α-Al_2O_3 [3, 4]. So far, a lot of experiments on the electric surface charge of alumina materials have been reported [2, 5]. However, little studies have been conducted simultaneously on both electrokinetic potential and charge density of α-Al_2O_3 [5]. It can be realized by the combination of streaming potential with chromatographic method [6, 7]. Both methods are applicable for the interface with low specific surface area.

Similar to the amphoteric metal oxides, the surface hydroxyl groups of alumina react with acid and base at low and high pH to form positive and negative charge, respectively. The charging behavior of alumina surface depends on protonation and hydroxylation of aluminum hydroxyl surface. The properties of alumina surface therefore strongly depend on pH. There is a pH known as the point zero charge (PZC) of alumina where surface sites are neutral (Al-OH) and the net charge on the surface is zero [8]. Because of a formation layer of immobile ions and water molecules on the surface of alumina, it is not straight forward to directly determine the surface potential of alumina particles. Instead, a closely related potential known as the ζ potential is obtained from electrokinetic phenomena. The value of pH where the ζ potential is zero is denoted as isoelectric point (IEP) [8, 9]. There are some experimental methods to determine the PZC/IEP of alumina materials, which are described using the following abbreviations: 1. Potentiometric titration with different electrolyte concentrations is employed to obtain surface charge and to identify common intersection point (CIP). 2. The ζ potential is determined by electrophoretic mobility or electroosmosis method or electroacoustic measurements [5, 10-15]. Among them, streaming potential measurement has become, the most commonly used tool for determining the ζ potential of macroscopic solid surfaces of various alumina shapes [8, 16-18]. Streaming potential is induced when an electrolyte solution moves tangentially by a hydrodynamic pressure gradient to the charged surface. The difference of streaming potential U_{str} [19, 20] can be measured between two

electrodes located upstream and downstream in the liquid flowing through the packed bed of alumina particles or narrow gap between alumina surface, connected via a high input impedance voltmeter. In this case, streaming potential is the slope of the straight line [16, 18, 21] given by U_{str}= f(ΔP).

Streaming potential does not directly provide charge density of materials. Furthermore, charging behavior of alumina surface charge is complicated, the surface net charge is not only influenced by pH of solution but also dependent on structure, ion binding and hydrogen bonding [13, 22, 23]. The charged condition can be acquired when the oxide has been equilibrated with electrolyte solution at a certain value of pH by acid–base titration. While the potentiometric acid-base titration is most often used method, unfortunately the interpretation of experimental data had been extended beyond the limitation of this method, for example, the effect of impurity or dissolution of solid phase [24]. In case the sorbent has a low surface area with insufficient number of sites for the measurement of charge density, the acid-base titration is not applicable. In this case, Burgisser et al. was successful by using chromatographic method to evaluate charge density of materials quite easily for silica sand and goethite-coated sand with low surface area 0.08 m^2/g and 0.25 m^2/g [6], respectively. The nonlinear chromatography also appears to be well adapted to obtain the number of proton exchange sites for TiO_2 grains with specific surface area 7.80 m^2/g [7]. Furthermore, the modeling of the primary charging behavior of materials may indicate the extensive data sets of materials about the potentials, sites density, capacitance or the effect of dissolution in surface charge determination. As for describing charging behavior on the surface of alumina, the 1-pK model can provide a sufficiently accurate description of the titration behavior of the interface [25]. A 1-pK adsorption model with a Stern electrostatic double layer is used to describe proton adsorption. The 1-pK Stern model could predict the surface charge well [26], except for very high concentration electrolyte or the case of the dissolution of material.

Due to specific surface charging, the adsorption of surfactant on alumina has attracted intense studies [10, 22, 27-32]. The adsorption of anionic surfactant has modified the surface of alumina so that the zeta potential and charge density of alumina materials can be changed. In addition, there are two kinds of sphere complex interactions including outer and inner links such as sodium dodecyl sulfate (SDS) and sodium dodecyl phosphate (SDP) [22]. Thus, SDS can be easily removed with various number of washing (desorption) steps. The effect of SDS on the surface of alumina material needs to be compared in the absence of SDS and with the treatment of SDS adsorption followed by desorption steps. Also, it is practically interesting to find out how to recover the interfacial properties of α-Al_2O_3 after surfactant treatment.

The aim of study in this chapter is to investigate interfacial properties of α-Al_2O_3 with low surface area modified with NaOH, thermal treatment at 550 ^{0}C and adsorption by anionic surfactant SDS. We used streaming potential and chromatographic method to compare zeta potentials and charge density of α-Al_2O_3 treated by different methods. The combination of chromatography and the 1-pK Stern model was used to evaluate surface charge density and the influence of dissolution of α-Al_2O_3 in the absence of SDS on α-Al_2O_3. The effect of SDS after adsorption followed by washing and the recovery of α-Al_2O_3 after cleaning by NaOH followed by reheating was evaluated by streaming potential and chromatographic charge density.

2.2. Experimental

2.2.1. Materials

High purity (99.5 %), alpha alumina beads with an average diameter of 300 ± 12 μm and a density of 3.82 g/cm^3 were purchased from Hiraceramics, Japan and were used in the present study. X-ray diffraction (XRD) was collected on a Bruker D8 Advance X-ray diffractometer, operated at 40 kV and 40 mA, with Cu-target tube and a graphite monochromator. Intensity for the diffraction peaks was recorded in the 20- 70 ^{0} (2θ) range with a step size of 0.03 ^{0}. The analyses confirmed that the alumina beads contain mainly α-phase (Fig. 2.1). The specific surface area was determined by BET method using a surface area analyzer (Micromeritics, Gemini VII 2390) and found to be 0.0041 ± 0.0016 m^2/g. The specific surface area is comparable to that by geometric consideration.

Sodium dodecyl sulfate, SDS (with purity higher than 95 %) from Wako Pure Chemical Industries was used. The critical micelle concentration (CMC) of this surfactant in water at 22 ^{0}C was experimentally determined to be 6 mM. Ionic strength and pH were adjusted by the addition of NaCl (Wako Pure Chemical Industries), HCl and NaOH (volumetric analysis grade, Wako Pure Chemical Industries). Other chemicals were obtained from Wako Pure Chemical Industries. Ultra pure water, produced from Elix Advantage 5 (Millipore) with electric conductivity around 0.6 μS/cm was used in preparing solutions and in all measurements.

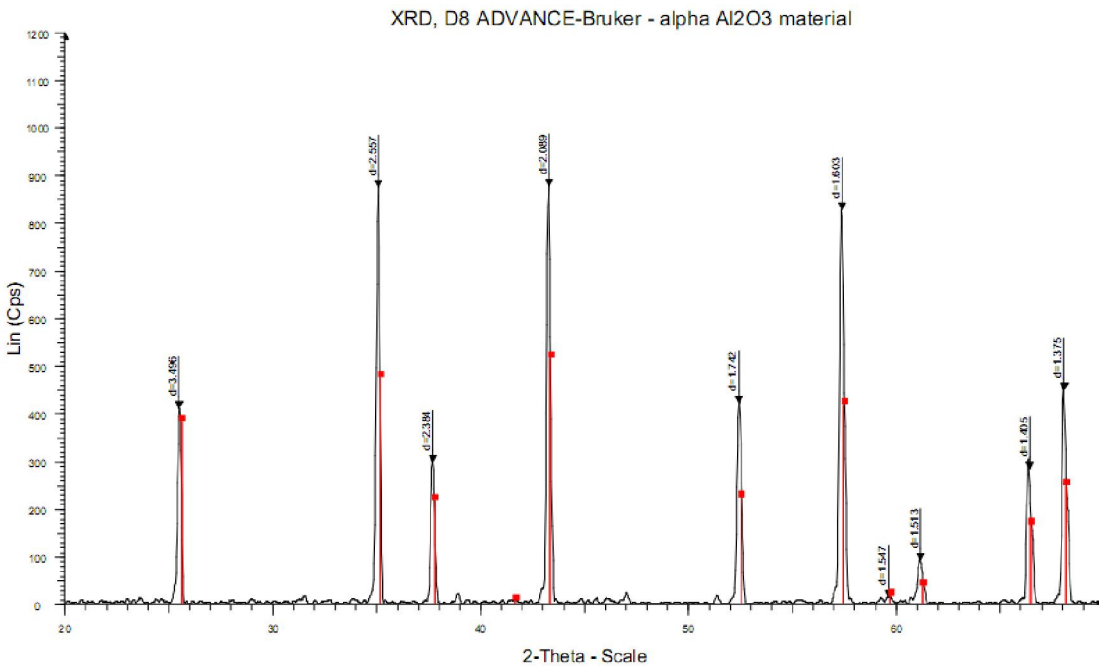

Fig. 2.1. XRD diagram of α-Al_2O_3 material

2.2.2. Modification of α-Al_2O_3 materials

The alpha alumina was modified by several procedures before measurements.

The original α-Al_2O_3 (M0) is the material without any treatment.

M0 was washed many times with 0.1 M NaOH before rinsing by ultra pure water to reach neutral pH. After that, sample was dried at 110 ^{0}C and cooled in a desiccator at room temperature to obtain M1 material. M1 was reactivated by thermal treatment at 550 ^{0}C for 2 hours to form M2 material.

M2 was used to carry out batch SDS adsorption as follows:

A solution of 50 mL SDS 2×10^{-3} M was mixed thoroughly with 50 g α-Al_2O_3 in 0.001 M NaCl at pH 5.0 with a shaker for 24 hours. After the equilibration, the solution was estimated by potentiometric measurement using a surfactant ionic selective electrode. As a sequel, α-Al_2O_3 materials were washed with pure water numerous of times until the conductivity of solution became lower than 1.0 µS/cm. The material was dried at 110 ^{0}C and cooled in a desiccator at room temperature to form M3.

M3 was treated with 1.0 M NaOH (around 8 times), then washed by pure water to neutral pH, dried at 110 ^{0}C and preheated at 550 ^{0}C for 2 hours then cooled down to room temperature in a desiccator, thus M4 was obtained.

2.2.3. Streaming potential measurements

The theory behind streaming potential and zeta potential calculation is described in the literature [19, 33]. Briefly, the ζ potential is related to the slope in the streaming potential versus pressure line using Helmholtz – Smoluchowski's equation (HS) [19]:

$$\zeta = \frac{U_{str}}{\Delta P} \times \frac{\eta K_L}{\varepsilon \varepsilon_0} \quad (2.1)$$

where ζ is the zeta potential (mV), U_{str} the difference of potential (mV), ΔP the pressure difference (mbar), η the viscosity of the solution (mPa.s), K_L the conductivity of the solution (mS/cm), ε the relative dielectric constant of the liquid and ε_0 is the electric permittivity of vacuum (8.854×10^{-12} F/m).

A Zeta CAD (CAD Instrument, France) was used in this study. The measurement was taken in two flow directions to remove the effect of any asymmetrical potential. In this instrument, the liquid is forced through the capillary using the nitrogen gas pressure. The measurement was made over the sequence of increasing pressure in order to determine the slope of U_{str} against ΔP. A pair of Ag/AgCl electrodes at two both sides of the cell is linked to a numeric multimeter to measure the electrical potential difference (U_{str}) along the column. The U_{str} was measured alternatively in the two flow directions for continuously increasing pressure values (from 0 to 500mbar). The streaming potential was determined from the slope of the plot U_{str} versus ΔP. This equipment also measures the temperature, the conductivity of solution (K_L), displays the solution viscosity (η), the dielectric constant (ε), and finally calculates the ζ potential by Eq. (2.1).

In all measurements with Zeta CAD, we used a glass column of 50 mm length and 15 mm internal diameter. Amount of 10.0 g α-Al_2O_3 was dry packed in the column. Experiments were carried out at 22 ^{0}C $\pm$ 2 ^{0}C and different pressure gradients with flow in the two directions. Firstly, the experiment for equilibrium sample was conducted by manual mode with constant pressure starting from pressure 2. In this step air bubbles were removed completely by flushing the cell dead space to waste at the rear of the instrument. The values of streaming potential became stable as time proceeded. Then, the streaming potential of samples was measured by applying automatic mode with starting pressure 2 and step pressure 5. At least 480 experimental points (U_{str} vs ΔP) were collected for each run. The correlation coefficient of all linear curves are higher than 0.98.

2.2.4. Chromatographic charge density method

The α-Al_2O_3 materials in pure water were packed into the glass chromatography columns (Omnifit) of 1 cm internal diameter and 10-25 cm in lengths. The feeding solutions were pumped using peristaltic pumps (Eyela) at flow rates between 1.0 and 5.0 mL/min with an injector (for pulse tracer experiments) and two way valve (for step experiments). For tracer experiments the outflow of the columns was monitored by an UV-vis spectrophotometer (UV-1650PC, Shimadzu) and 1cm flow through cell using kinetic mode. The pH was measured by pH electrode (Mettler Toledo Ingold) combining flow cell (U402-611-DPA-P-S7/40) and connected with a pH meter (Metrohm 781 pH/Ion meter). To calibrate electrode, three standard buffer solutions of pH 4.00, 7.00, and 9.00 (Metrohm) were used at the same flow rates. The slope of all linear curves has been within 95 % to 105 % of theoretical one.

Some parameters of columns such as travel velocity v, dispersion coefficient *D*, Peclet number *P*e, kinetic porosity θ and the mass of sorbent per unit pore volume ρ were determined by means of pulse experiments with conservative tracers. The column was preequilibrated with 0.01 M NaCl. Solutions of 0.001 M $NaNO_3$ were injected with amount of 50–200 μL and measured by kinetic mode at wavelength 220 nm. The determination of columns properties has been performed according to the papers [6, 34]. Because of fast protonation reaction, high travel velocities between $v = 5.0\times10^{-4}$ and $v = 25.0\times10^{-4}$ m/s (corresponding to flow rates of 1.0 to 5.0 mL/min) were used. The columns were carefully packed to achieve the Peclet numbers as high as possible. We have observed that the Peclet numbers increase with increasing the column length and *P*e > 500 when the length of column is higher than 15 cm. The kinematic porosity of $\theta = 0.42 \pm 0.02$ which leads to ρ of 5265 ± 180 g/L, is obtained from the column experiments. By measuring density of the alumina material and the mass of the alumina in the known volume of the column, the porosity is obtained 0.41 ± 0.01 that is in good agreement with the above value. The dispersivities were independent on flow velocity and in the range of $D/v = 0.30 \pm 0.05$ mm.

2.2.5. Potentiometric measurements

Potentiometry was conducted using a Metrohm 781 pH/Ion meter, Switzerland. The pH of NaCl solutions which were used in measuring streaming potential, adsorption isotherm and determination of the concentration of proton in solutions were measured by a glass electrode (Type 6.0258.010, Metrohm). Electrode was previously calibrated with three standard buffers

(Metrohm). The equilibrium concentration of SDS in solution was measured with a surfactant ionic selective electrode (Type 6.0507.120, Metrohm) that is sensitive to ionic surfactants [35, 36]. The electrode potential (E in mV) was measured relative to an Ag/AgCl reference electrode (Type 6.0726.100, Metrohm) equipped with a ceramic plug. The SDS concentration in the samples can be determined from the linear range of the calibration curve, presenting E as the function of the logarithm of SDS concentration [37]. To make standard calibration curve, a series of SDS solutions with the concentrations from 10^{-6} mol/L to 10^{-3} mol/L were prepared at pH 5.0 in 0.1 M acetate buffer. Potentiometric analysis was conducted with above surfactant electrode and reference electrode. The relationship between the potential and log[SDS] should yield a straight line with a correlation coefficient of at least 0.998.

All the measurements were carried out at room temperature, controlled by air conditioner at $22^0C \pm 2^0C$.

2.3. Theory and modeling

2.3.1. Nonlinear chromatography

The calculation of charge density by the present method is briefly summarized below. Details were described in the literatures [6, 34, 38-40].

The concentration c(x,t) of a chemical sorbate at a column depth x and time t follows the one dimensional convection – dispersion equation

$$\frac{\partial c}{\partial t} + \rho \frac{\partial q}{\partial t} = D \frac{\partial^2 c}{\partial x^2} - v \frac{\partial c}{\partial x} \quad (2.2)$$

Here q the amount of the sorbed chemical per unit mass. For a nonsorbing chemical called conservative tracer ($q = 0$), Eq. (2.2) can be used to calculate some parameters of column by a pulse injection of the tracer. The response has a normal distribution shape with the average time $t_0 = L/v$ (L length of column) and a standard deviation σ. The latter quantity can be related to the column Peclet number $Pe = Lv/D$ by $\sigma^2 / t_0^2 = 2/P_e$.

For an adsorbed species in the simplest case of a linear adsorption isotherm $q = K_D.c$ with K_D is the partition coefficient, the breakthrough curve has the same shape in the case of tracer but is delayed in the time by the retention factor $R = 1 + \rho K_D$. Breakthrough fronts may contain diffuse and sharp parts according to the Golden rule [40].

When dispersion effect is negligible ($D = 0$), the diffuse front is used to calculate adsorption isotherm from Eq (2.2). The concentration c is related to a velocity by

$$\left(\frac{\partial x}{\partial t}\right)_c = -\frac{(\partial c/\partial t)_x}{(\partial c/\partial x)_t} = \frac{v}{1+\rho\left(\frac{dq}{dc}\right)} \quad (2.3)$$

The relationship between the concentration and retention time *t(c)* is easily measured at the column outlet and indicates the derivative of adsorption isotherm

$$\frac{t(c)}{t_0} = 1 + \rho\frac{\partial q}{\partial c} \quad (2.4)$$

The experimentally recorded retention time *t(c)* can be integrated to obtain the adsorption isotherm

$$q(C) = q(C_0) + \frac{1}{\rho}\int_{C_0}^{C}\left(\frac{t(c')}{t_0} - 1\right)dC' \quad (2.5)$$

The overall retention factor *R*, which represents the area of normalized breakthrough curve, depends on the input concentration c and equal for the sharp part and the diffuse front

$$R = 1 + \rho\frac{q(C) - q(C_0)}{c - c_0} = \frac{1}{c - c_0}\int_{C_0}^{C}\frac{t(c')}{t_0}dC' \quad (2.6)$$

When column Peclet number is high (typically *P*e > 500), the effect of dispersion on the diffuse part of breakthrough curve is negligible [6, 34].

In the case of proton adsorption isotherm, the development of charge densities with pH can be viewed as acidity adsorption isotherm. With the amphoteric material, the acidity adsorption usually has sigmoidal shape. Thus, it is impossible to calculate the entire adsorption isotherm from single chromatographic experiment. In order to obtain both branches of the adsorption isotherm, it is required to perform two independent experiments to the point of inflection [6]. Because the charge density curves can be transformed from proton adsorption isotherm, the inflection point can be chosen at pH near 7.0 where $c = 0$ [6] or at pH value of PZC where $q(C_0) = 0$ and $c_0 = 0$ [7]. The acidity (at 25^0C) is deduced from pH measurements by the equation

$$c = [H^+] - [OH^-] = 10^{-pH} - \frac{10^{-14}}{10^{-pH}} \quad (2.7)$$

The charge density σ can be calculated from adsorption acidity

$$\sigma = \frac{qF}{A} \quad (2.8)$$

Here *A* is the specific surface area of material per unit mass and *F* is the Faraday constant ($F = 96490$ C/mol).

Breakthrough step experiments have to be performed between solutions of different pH. The columns must be preequilibrated with an unbuffered electrolyte solution, then fed with a solution of pH 7.0. To obtain two branches of acidity adsorption isotherms, two experiments

can be preequilibrated with a high pH and a low pH respectively and flushed with the same electrolyte of pH near 7.0. Experiments are carried out by recording pH of column effluent as the function of time. Using Eq. (2.5), we can obtain two acidity adsorption isotherm curves. As a sequel, by using Eqs. (2.7) and (2.8) the acidity isotherms can be transformed into the charge density curves.

The constant $q(C_0)$ in Eq. (2.5) was obtained by an independent experiment in which column was therefore initially preequilibrated with high pH then flushed with a solution with pH of PZC/IEP. The PZC/IEP of materials can be determined by streaming potential measurement [33]. The retention of this breakthrough gives directly the value of $q(C_0)$.

2.3.2. Surface charge from 1-pK Stern model

The classical 1-pK Stern model is used to evaluate surface charge density and compare experimental data with chromatographic charge density.

This model is based on a single protonation of AlOH surface group [26, 41]

$$AlOH_2^{1/2+} \rightleftharpoons AlOH^{1/2-} + H^+ \quad (2.9)$$

The amphoteric behavior of alumina is described by two surface species $AlOH_2^{1/2+}$ and $AlOH^{1/2-}$, and only one pK value. The equilibrium constant is given by

$$K = \frac{\left[AlOH^{1/2-}\right] a_{H^+} \exp(-e\beta\psi_0)}{\left[AlOH_2^{1/2+}\right]} \quad (2.10)$$

where $a_{H^+}$is activity of proton in mol/L ($pH=-log_{10}\, a_{H^+}$), ψ_0 the surface potential, e the elementary charge and $1/\beta=k_BT$ is the thermal energy, k_B is Boltzmann's constant. We take into account ion pair formation of surface groups of alumina with electrolyte ions [41]. The ion pair formation reactions of alumina in NaCl background electrolyte are defined as

$$AlOH^{1/2-}.Na^+ \rightleftharpoons AlOH^{1/2-} + Na^+ \quad (2.11)$$

$$AlOH_2^{1/2+}.Cl^- \rightleftharpoons AlOH_2^{1/2+} + Cl^- \quad (2.12)$$

$$K_c = \frac{\left[AlOH^{1/2-}\right] a_{Na^+} \exp\left(-e\beta\psi_d\right)}{\left[AlOH^{1/2-}.Na^+\right]} \quad (2.13)$$

$$K_a = \frac{\left[AlOH_2^{1/2+}\right] a_{Cl^-} \exp\left(+e\beta\psi_d\right)}{\left[AlOH_2^{1/2+}.Cl^-\right]} \quad (2.14)$$

Here K_c and K_a are the ion pair formation constants of cation and anion, ψ_d is the potential at the onset plane of the diffuse layer. The activity coefficients were calculated using the

extended Davies equation. The surface charge density (σ_0) in the plane where the protons adsorb and the charge density in Stern plane (σ_s) are

$$\sigma_0=\frac{eN_A}{2}\left(\left[AlOH_2^{1/2+}\right]+\left[AlOH_2^{1/2+}.Cl^-\right]-\left[AlOH^{1/2-}\right]-\left[AlOH^{1/2-}.\ Na^+\right]\right) \quad (2.15)$$

$$\sigma_s= eN_A\left(\left[AlOH^{1/2-}.\ Na^+\right]-\left[AlOH_2^{1/2+}.Cl^-\right]\right) \quad (2.16)$$

where N_A is Avogadro's number. The charge density in the diffuse layer (σ_d) is given by the charge neutrality condition

$$\sigma_d= -(\sigma_0+\sigma_s) \quad (2.17)$$

According to the surface complexation model, the total surface concentration (Γ_0) of active surface sites density in the interfacial layer is

$$\Gamma_0= \left[AlOH_2^{1/2+}\right]+\left[AlOH_2^{1/2+}.Cl^-\right]+\left[AlOH^{1/2-}\right]+\left[AlOH^{1/2-}.\ Na^+\right] \quad (2.18)$$

The Gouy – Chapman equation shows the relationship between the charge density of the diffuse layer and the potential at the onset of diffuse layer

$$\sigma_d= -\sqrt{8\varepsilon\varepsilon_0 N_A I/\beta}\,\sinh\left(e\beta\psi_d/2\right) \quad (2.19)$$

For the Stern plane a linear relationship is assumed

$$\sigma_0= C_s\left(\psi_0-\psi_d\right) \quad (2.20)$$

where *C*s is the Stern capacitance. Eqs. (2.9) to (2.20) is a set of 9 relations containing 9 variables that can be solved numerically.

2.4. Results and discussion

2.4.1. Streaming potential of α-Al_2O_3 materials

The zeta potential was calculated from measured streaming potential with Eq. (2.1). In Figs. 2.2 and 2.3, the ζ potential of α-Al_2O_3 is demonstrated as a function of pH because the surface net charge and the surface potential change depending on the protonation degree of functional group [18] with the underlying ionic framework [42].

Figure 2.3 indicates the influence of pH on the ζ potential of alpha alumina materials M0, M1 and M2 in background 0.01M NaCl. M1 leads to the increase of its IEP from 5.3 to 6.7. Although the absolute value of ζ potential at high and low pH tends to increase, the effect of heat treatment at 550 ^{0}C after the NaOH treatment (M2) on IEP is not significant. It reveals that thermal treatment only activated the surface behavior of alpha alumina. The organic contaminants which are negatively charged, contained in the original material are presumably

considered to be removed by 0.1 M NaOH washing. The present IEP of α-Al_2O_3 with M2 treatment is about 2.0 units lower than the reported values [2, 8, 43]. Das et al. [44-46] published some papers reporting the same value of IEP of our material. They explained that the reason of low IEP of alumina is because of lesser number of surface hydroxyl groups bound to the aluminum atoms. In these cases, alumina materials have a low pK_a [8, 11] that is equal IEP. Contescu et al. [11, 47] have shown that there are some types of different aluminum hydroxyl sites in which aluminum can exist in octahedral site or tetrahedral site, thus net charge of alumina surface is different. In addition, the proton of the surface hydroxyl group is not bound strongly to the oxygen. Thus, the proton may be easily removed in lower pH range due to the weak electronegativity force of the surface hydroxyl group.

Electrokinetic data with M2-treated alumina shows that lowering concentration of NaCl background electrolyte increases magnitude the ζ potential. Although the ionic strength also influences the ζ potential of α-aluminum oxide, the IEP change is insignificant. Nevertheless, SDS adsorption on α-Al_2O_3 followed by desorption by washing probably caused the effect on zeta potential from pH 5.5 to pH 9.0. Thus, the ζ potential increases dramatically in this pH range (Fig. 2.4). Interestingly, the adsorption of an anionic surfactant SDS on a positively charged α-Al_2O_3 surface after desorption can induce the increase in zeta potential of the alumina material. It indicates that with the presence of SDS in electrolyte background, the proton may be strongly bound to surface site of α-alumina after washing many times or the adsorption of proton upon surfactant adsorption. To confirm this, the influence of proton binding to surface behavior of α-Al_2O_3 treated with SDS (M3) and without SDS (M2) will be evaluated by chromatographic charge density method.

Another outstanding feature is that the ζ potential of M4 treated α-Al_2O_3 is similar to M2 (Fig. 2.4). The charging behavior of α-Al_2O_3 can be recovered by treatment with 1.0 M NaOH and then heating at ignition temperature 550 ^{0}C for 2 hours. Because the ζ potential of α-Al_2O_3 treated by M3 is more positive than M2, it is necessary to use strong base with high concentration such as 1.0 M NaOH to restore interfacial property of α-alumina and activate the surface behavior by heat treatment at 550 ^{0}C for 2 hours. The charge density of α-Al_2O_3 treated by M2 and M4 will also be compared by chromatographic method.

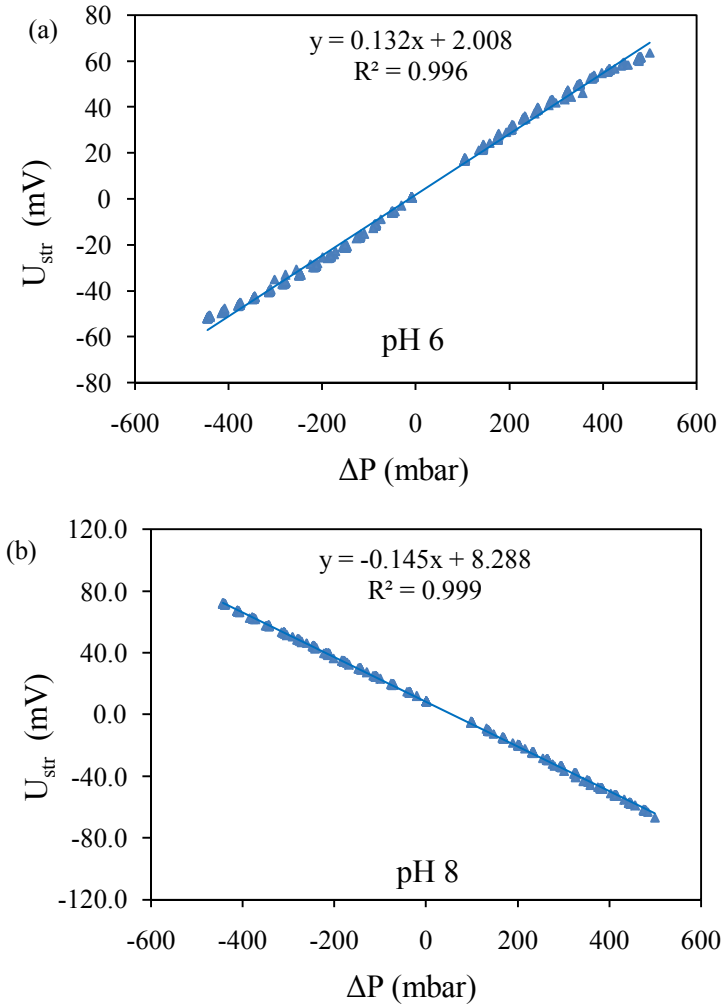

Fig. 2.2. Streaming potential (U_{str}) vs applied pressure difference (ΔP) of M2 treated alpha alumina at pH 6(a) and pH 8(b) in 0.001 M NaCl.

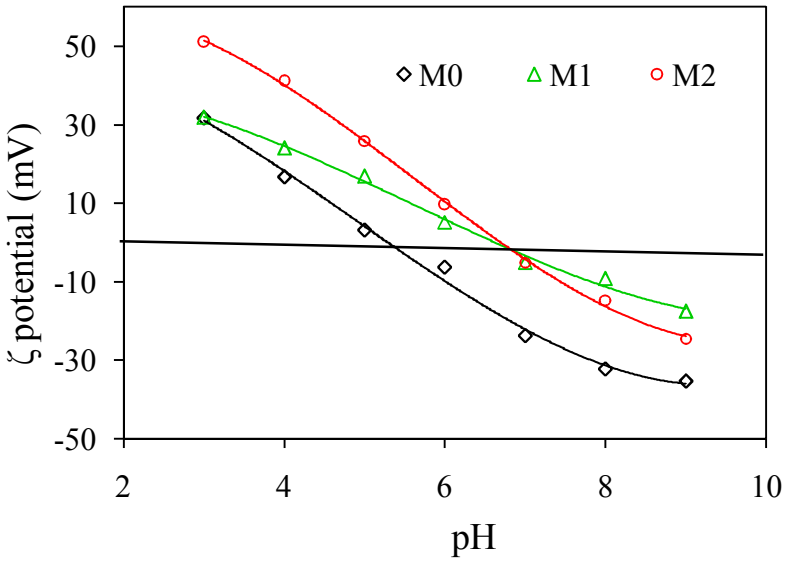

Fig. 2.3. Influence of pH on ζ potential α-Al_2O_3 in 0.01 M NaCl.

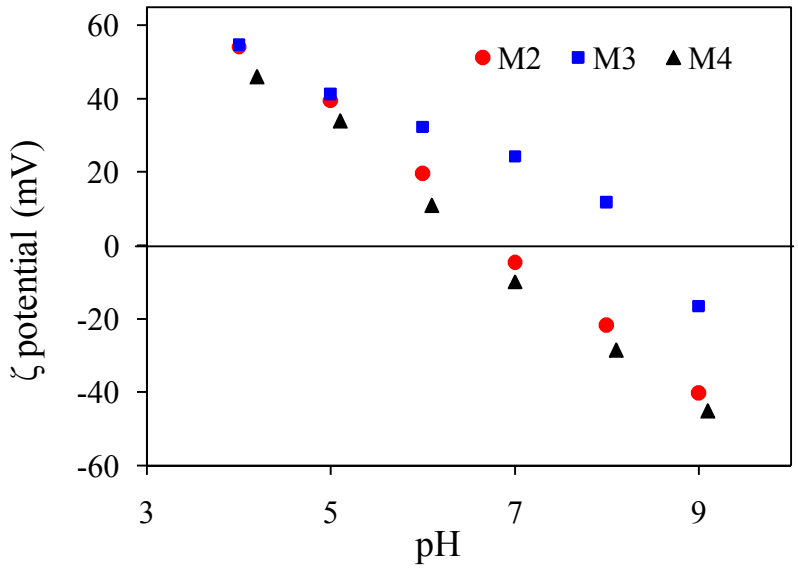

Fig. 2.4. The ζ potential of α-Al_2O_3 materials in 0.001 M NaCl.

2.4.2. Surface charge density from chromatographic method and 1pK-Stern model

2.4.2.1. Surface charge density of M2 treated alpha alumina in the absence of SDS

Firstly, two breakthrough experiments were done with M2 treated α-Al_2O_3 from pH 9.41 to pH 6.70 in 0.01 M NaCl electrolyte and from pH 9.38 to pH 6.70 and in NaCl 0.001M to determine the additive constant $q(C_0)$ in Eq. (2.5). The $q(C_0)$ are 5.31×10^{-12} and 1.00×10^{-12} mol/g with electrolyte background 0.01 and 0.001 M NaCl, respectively. These values seem too small to contribute to adsorption acidity. However, the experiments are performed to pH around 7.0, different from pH of PZC, it is necessary to determine $q(C_0)$ by an independent experiment. In order to obtain two branches of the acidity adsorption isotherm below and above pH 7.0, two experiments were carried out in both electrolyte concentrations.

Figures 2.5a and 2.5b show the experiments performed in 0.001 M NaCl. The experiments have been conducted from pH 9.95 to pH 7.22 (Fig. 2.5a) and from pH 3.87 to pH 7.22 (Fig 2.5b). Two breakthrough curves start with diffuse parts and end with sharp parts. While the column breakthrough in Fig. 2.5a suggests a sorbate obeying a concave isotherm, the breakthrough curve in Fig. 2.5b is indicative for the case of convex isotherm. The experimental data points of the diffuse fronts were used for the calculation with Eq. (2.5) to obtain the adsorption isotherms. The combination of two branches of the acidity isotherms formed a sigmoidal isotherm. The charge density was calculated from the acidity adsorption isotherms by Eq. (2.8). The lower branch of data points of charging curve (open triangle points in Fig. 2.7a) could directly be calculated from the acidity adsorption isotherms from pH 9.95 to pH 7.22. The charging curve was shifted to the value -0.102 C/m^2 at pH 9.95. Nevertheless, the other branch from pH 3.87 to pH 7.22 was again calculated by integration of the diffuse front and shown the upper branch of charging curve (open triangles in Fig. 2.7a). For experimental reasons it is difficult to evaluate the acidity isotherm at pH value near 7.0. Despite two experiments of both branches were flushed with the same electrolyte solutions near pH 7.0, usually the actual pH values of this solution were different at the upper branch. After recalculation, the charging curve was shifted to the charge density of 0.097 C/m^2 at pH 3.87. Several experiments were performed in the pH regions of 10.00 to 6.45 and 3.80 to 6.45, and the resulting charge density were within ± 15 % relative error.

The similar procedure was applied to the experiments in 0.01 M NaCl. The first experiment was carried out from pH 9.42 to pH 7.24 (Fig. 2.6a). From the overall retention,

one calculates a charge density of 0.066 ± 0.005 C/m^2 between these two pH values. By using Eq. (2.5) to calculate the diffuse front and transform to charge density by Eq. (2.8), the lower branch of data points of charging curve (filled circles in Fig. 7b) was shifted to the value of -0.064 C/m^2 at pH 9.42. Fig. 2.6b shows the breakthrough curve which was done from pH 4.75 to pH 7.24. A charge density of 0.032 ± 0.004 C/m^2 was calculated from the retention of the diffuse fronts, which corresponds to the charge density at pH 4.75 after recalculation. It is shown as the upper branch of filled circles of charging curve in Fig. 2.7b.

The surface charge density was shown as the function of pH in the background electrolyte 0.001M NaCl (Fig. 2.7a) and 0.01M NaCl (Fig. 2.7b). In both cases of different ionic strength, the solid lines are results of calculations based on the 1-pK Stern model with parameters from literature [48] with total site density Γ_0 = 1.2sites/nm^2, a Stern layer capacitance C_s = 1.4F/m^2, pair formation constants logK_a = logK_c = 0.2. In the 1-pK Stern model used in the present study, the proton dissociation constant is equal to the point of zero charge, pH_{PZC} = pK= -logK. The IEP coincides with the PZC when there is no specific adsorption [49]. Thus, we assume that pK ≈IEP = 6.7. The data points are calculated from chromatographic charge density method. By performing some experiments in the different pH ranges, a good agreement between the data obtained from the column breakthrough curves and the 1-pK Stern model was obtained. Only at very high and very low pH, the predictions of model for the surface charge deteriorate probably because of the effect of dissolution. The dissolution reactions can be represented as follows [50]:

$$Al_2O_3+2H_3O^++4H^+ \rightleftharpoons 2Al^{3+}+5H_2O \quad (2.21)$$

$$Al_2O_3+2OH^- \rightleftharpoons 2AlO_2^-+H_2O \quad (2.22)$$

In Fig. 2.7, the filled circles show the surface charge calculated from column breakthrough experiments performed in the pH range without dissolution, whereas the open triangles show the experiments affected by dissolution at high and low pH. It can be seen that the dissolution of aluminum oxide becomes significant below pH 4.7 and above pH 9.4 as demonstrated from the difference between model calculations and experimental data. The absolute of calculated values from 1-pK Stern model are smaller than the measured ones from chromatographic charge density method because of the presence of Al^{3+} and AlO_2^- at very low and very high pH, respectively. These findings are close to the results from the previously published paper [50] in which dissolution studies were carried out by agitating the α-alumina suspension for a desired pH in the range 3.0–11.0. In the paper [50], the dissolved concentration of aluminum

species in 0.001 M KNO_3 was determined using inductively couple plasma optical emission spectroscopy ICP-OES, and it was evident that the dissolution of alumina is greater at highly acidic and alkaline pH values while in the pH range 5.0–9.0 there is not much dissolution. In the case of γ-Al_2O_3, direct determination of aluminum in solution 0.1 M $NaNO_3$ in batch dissolution measurements (ICP-OES) and a dissolution rate model in continuous titration experiments indicated that there is a large effect of dissolution on surface charge determination for pH > 10.0 and pH < 4.5 [51]. With δ-Al_2O_3, the assumption of alumina dissolution below pH~5.0 and above pH~9.5 seemed to be evident where the measured total aluminum concentration by means of ICP method is different with FITEQL calculation [24]. The conclusion of this short review about the dissolution of alumina is that the 1-pK Stern model combined with chromatographic charge density method can predict pH regions of dissolution effect of alumina materials.

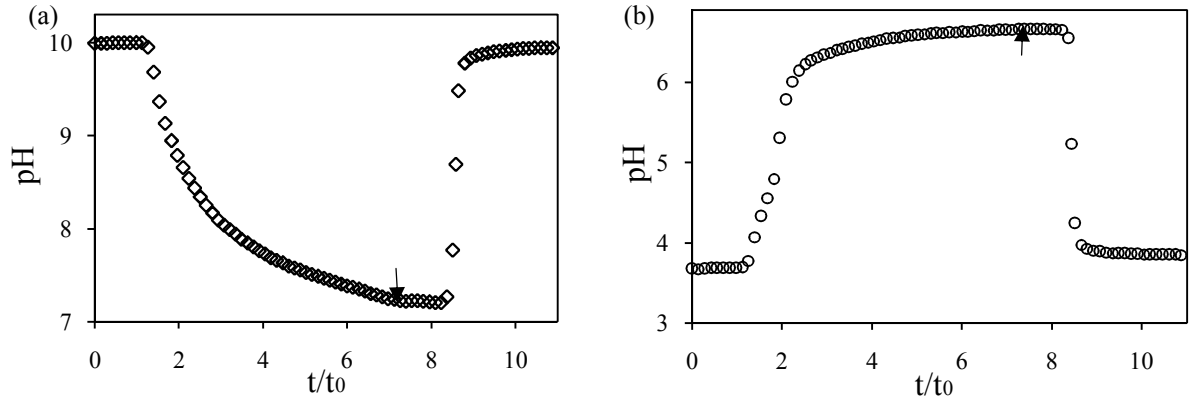

Fig. 2.5. Breakthrough curve through a column packed with α-Al_2O_3 (M2) in 0.001 M NaCl from pH 9.95 to pH 7.22 (a) and from pH 3.87 to pH 7.22 (b).

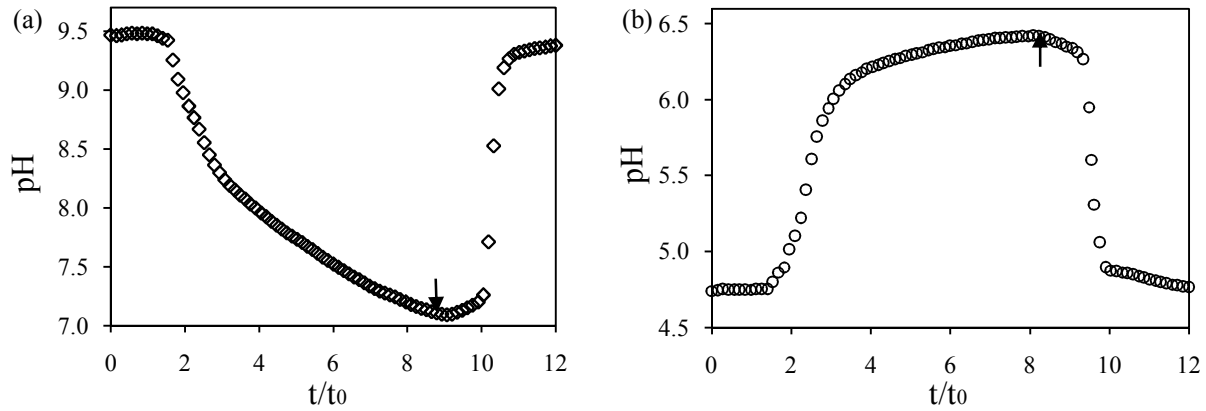

Fig. 2.6. Breakthrough curve through a column packed with α-Al_2O_3 (M2) in 0.01 M NaCl from pH 9.42 to pH 7.24 (a) and from pH 4.75 to pH 7.24 (b).

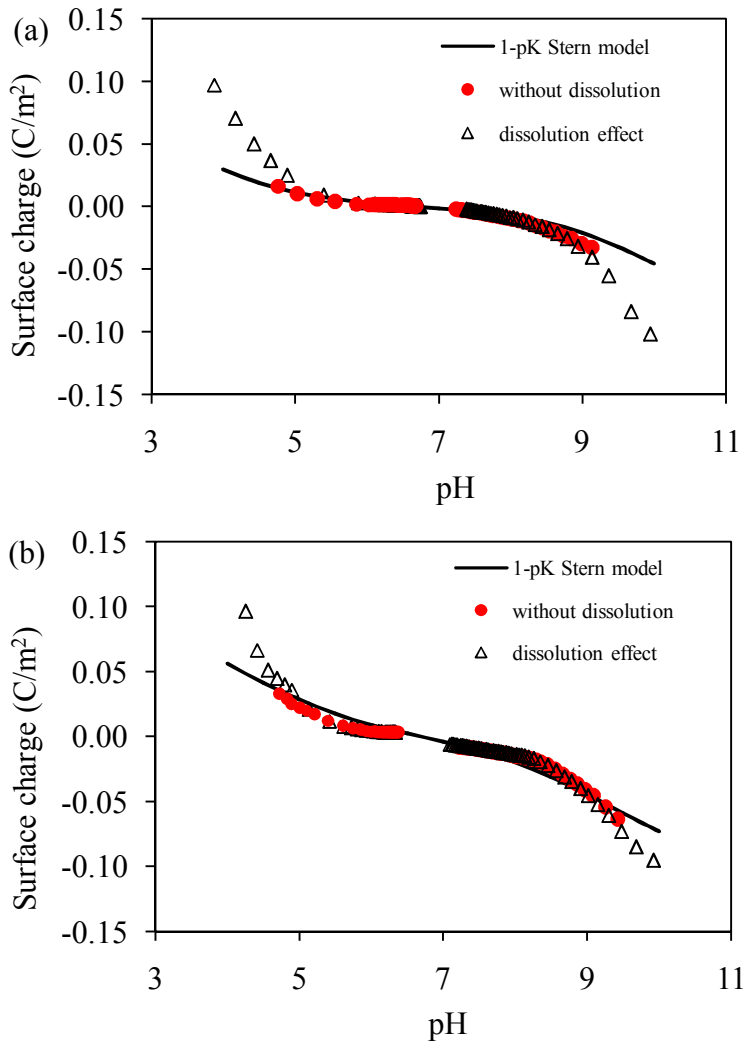

Fig. 2.7. Surface charge α-Al_2O_3 (M2) as the function of pH in 0.001 M (a) and 0.01 M NaCl (b): The solid lines are the results of 1-pK Stern model with 1.2 sites/nm^2, a Stern layer capacitance Cs = 1.4 F/m^2, pair formation constants logKa = logKc = 0.2 and pK = 6.7, while data points are calculated from chromatographic charge density experiments.

2.4.2.2. Surface charge density of M3 treated alpha alumina affected by SDS

Chromatographic method was used to evaluate the surface charge density of α-Al_2O_3 prepared by M3 treatment using SDS and compared with material M2 in the absence of SDS.

In order to compare surface charge density of M3 treated alumina with M2 treated one, several column experiments were performed in 0.01M NaCl background electrolyte at the same pH of the input solutions in which the dissolution of alumina was negligible. We used the same parameters of M2 treated alumina including $q(C_0)= 5.31\times10^{-12}$ mol/g and PZC = 6.7 to calculate surface charge density of M3 treated one in 0.01 M NaCl. The results of surface charge of alumina treated by M2 and M3 are compared in Fig. 2.8. As can be seen, the difference between the upper branches of two curves was not significant while the lower branches had small difference. The lower branch of charging curve of M3 treated by SDS appeared the inflection point at pH ~ 8.3 that should be close to the point of zero charge of M3. In this case, SDS adsorbed at the surface of alumina seems to be completely ineffective after washing. And there is no specific adsorption, the IEP and the PZC are the same [49]. Thus, the data of surface charge density of M3 material was again calculated with its parameters $q(C_0)= 1.67 \times 10^{-11}$ mol/g (this value was determined by an independent breakthrough curve experiment: not shown here) and PZC = 8.3 and revealed in Fig. 2.9. A small range for the charging curve of M2 but the large one of M3 cannot be evaluated. The PZC = 6.7 for M2 is near pH 7.0 where c = 0 while PZC of M3 equal 8.3 that is 1.6 pH unit higher. As the result, the upper branch of charging curve of M2 can be evaluated near pH 6.5 while another of M3 can only be obtained near pH 5.9. The results of M3 are similar to the case of the surface charge density of goethite-coated sand in which the lower branch obtained from pH 9.61 to pH 7.5 (PZC goethite-coated sand around 7.5) and the upper branch evaluated from pH 3.62 to pH 5.8 [6]. Because the nonlinear chromatographic method is not so well adapted to obtain charge density data just around pH_{PZC} value, the charging curve of TiO_2 grains (PZC around 4.5) using 0.1 M NaCl as background electrolyte can only be evaluated below pH 4.5 and above pH 8.5 [7]. Nevertheless, surface charge of M3 is much higher than that of M2 from pH 5.5 to pH 5.9 and the negative charge is less than that of M2 over pH 8.3 where the proton consumed in the presence of SDS is greater than in the absence of SDS. Above pH 5.5, there was a large difference between proton consumption in the absence of and treatment with SDS, indicating that there was more proton binding with the addition of anionic surfactant SDS in washing process. These findings are in good agreement with the results of streaming potential measurements for M3 (see section 2.4.1).

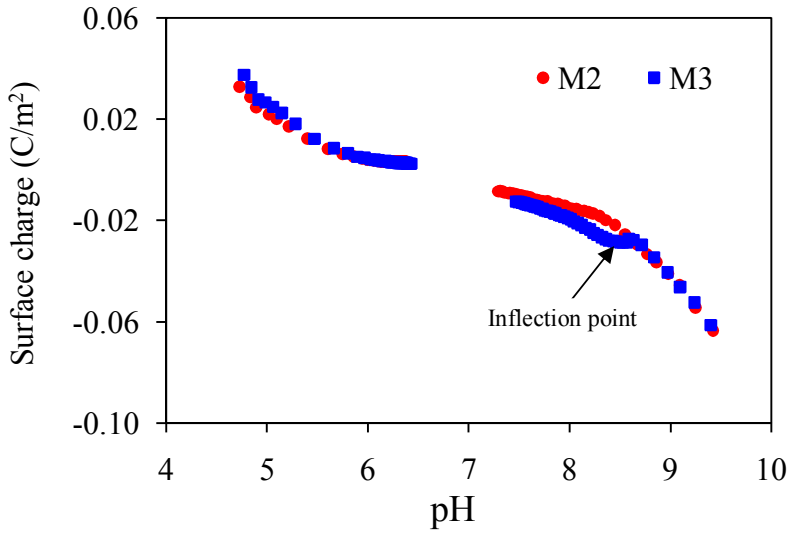

Fig. 2.8. Surface charge of M2 (circles) and M3 (squares) are calculated using the same parameters of $q(C_0)= 5.31\times10^{-12}$ mol/g and PZC = 6.7.

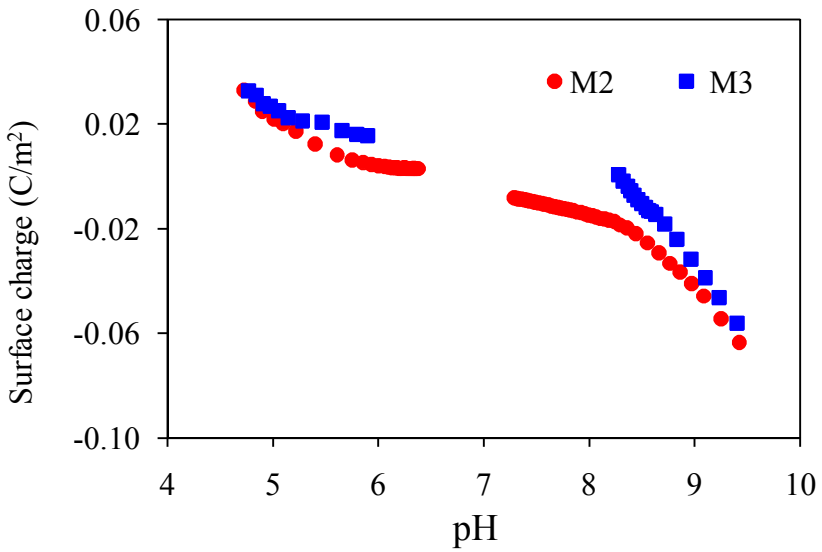

Fig. 2.9. Comparison of the surface charge of M2 (circles) and M3 (squares). The results of M2 are calculated with the parameters $q(C_0) = 5.31\times10^{-12}$ mol/g and PZC = 6.7 while the results of M3 are calculated with $q(C_0) = 1.67\times10^{-11}$ mol/g and PZC = 8.3.

2.4.2.3. Surface charge density of M4 treated alpha alumina

Chromatography was also used to compare surface charge density of M4 treated α-Al_2O_3 with SDS desorption followed by recovering procedure and M2 in the absence of SDS.

Several column pH breakthrough experiments were performed in 0.001 M NaCl with the same electrolyte solutions. In Fig. 2.10, the surface charge of α-Al_2O_3 treated by M2 and M4 are calculated using the same parameters of $q(C_0) = 1.00 \times 10^{-12}$ mol/g and PZC = 6.7. Although the charge density of M2 and M4 has the minor difference above pH 8.10 and below pH 5.50, the difference of charging curves is not significant. And there is not a strong inflection point in the lower branch of charging curve of M4. Thus, the PZC of α-Al_2O_3 with M4 treatment should be around 6.7. The charging behavior of α-Al_2O_3 can be restored by 1.0 M NaOH cleaning and reheating at high temperature 550 ^{0}C.

The amount of SDS adsorbed on α-Al_2O_3 was not too high in the present study. However, this concentration is higher than hemimicelle concentration in which the adsorption increases dramatically [52]. Although the used concentration of SDS is limited (2×10^{-3} M), it is enough to modify alumina surface. SDS was plausibly desorbed by washing many times with pure water because of weak outer sphere complex [22]. Work of Koopal and co-workers on rutile has revealed that the proton is adsorbed due to surfactant adsorption and surfactant ions screen the surface charge [53, 54]. In our study the increase of surface charge in SDS adsorption at pH 5.0 and 2×10^{-3} M SDS in 0.001 M NaCl is not significant when the difference of pH of solution before and after SDS adsorption is quite small. Also, in the present study, only initial pH of solutions is controlled. For the SDS adsorption on α-Al_2O_3, pH is not adjusted. In addition, we observed that SDS was almost completely removed within four rising cycles (data not shown). During desorption step, proton adsorption on α-Al_2O_3 increases significantly and it induces the difference of zeta potential and surface charge. As the results, the increase of zeta potential and surface charge of M3 is higher than M2 above pH 5.5. We used NaOH with different concentrations from 0.1 M to 1.2 M combining with heat treatment at 550 ^{0}C to examine the recovery of surface property of α-Al_2O_3 after SDS desorption. The zeta potential and surface charge of α-Al_2O_3 were restored by NaOH at concentration higher than 1.0 M [55]. Thus, interfacial properties of α-Al_2O_3 after SDS adsorption followed by desorption can be recovered by 1.0 M NaOH washing and heating at high temperature 550 ^{0}C.

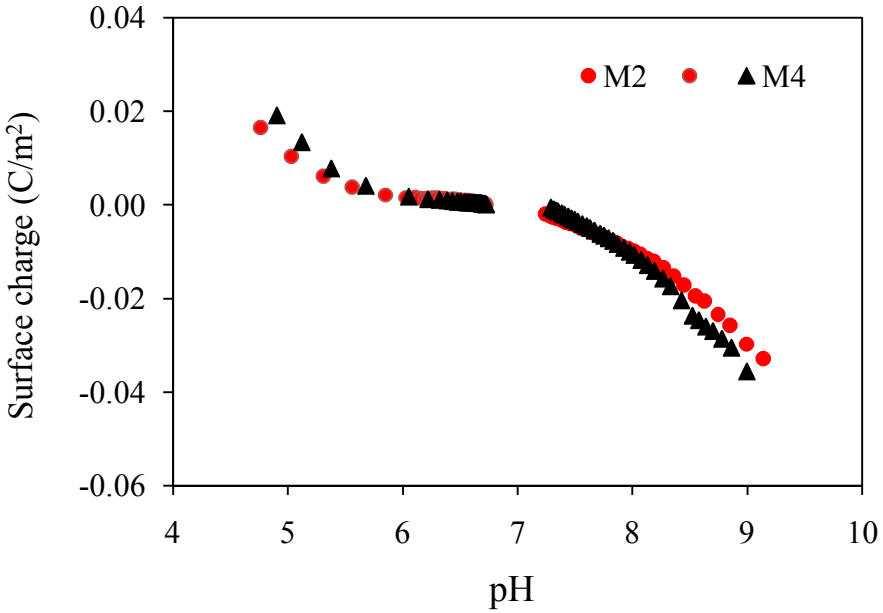

Fig. 2.10. Comparison of surface charge of M2 (circles) and M4 (triangles). The results of M2 and M4 are calculated using the same parameters of $q(C_0) = 1.00\times10^{-12}$ mol/g and PZC = 6.7.

2.4.3. Comparison of zeta potential with diffuse layer potential

Streaming potential is useful method to characterize electrokinetic property of materials with large diameter such as alpha alumina beads in this paper. The IEP of materials determined by streaming potential is necessary for the calculation of surface charge density from chromatographic method. The combination of chromatographic method and 1-pK Stern model can evaluate the pH region where the dissolution of α-Al_2O_3 is significant. In addition, 1-pK Stern model can calculate the diffuse layer potential ψ_d that is related to the zeta potential from streaming potential measurements. Let us discuss these comparisons in more detail.

The experimental values of zeta potential or electrophoretic mobility (EPM) of various colloidal particles reasonably agree with theoretical ones by using surface or diffuse layer potential calculated from surface charge density or 1-pK model. In the case of positively charged amidine latex [56], Borkovec et al. have shown that the mobility is in good agreement with standard electrokinetic model, that includes double layer relaxation and the Poisson – Boltzmann model, by introducing the distance to the slipping plane from the surface x_s. Similar results are obtained for the case of polystyrene sulfate latex spheres with negative charge in the presence of divalent ions [57]. The standard electrokinetic model was also used to evaluate the EPM of the silica particles [58, 59], where the ψ_d was calculated using the 1-pK basic Stern model with the same parameters describing surface charge density. The calculated EPM of silica from the model agree well with experimental EPM when assuming that the distances of slipping plane x_s from the surface are 0.25 nm and 0.5 nm for different colloidal silica particles. The sub-nanometer order of x_s is reasonable because it is comparable to the size of hydrated ion. In all cases, it is possible to use the same parameters for 1-pK model to predict both surface charge density and zeta potential from ψ_d. With hematite particles, Schudel et al. [60] indicated that 1-pK Stern model with the same parameters could describe surface charge density and the zeta potential at the plane of origin of diffuse layer potential ($x_s = 0$).

In this study, however, there was a large difference between the ψ_d obtained from 1-pK Stern model and the ζ potential from streaming potential measurements when the same parameters found from surface charge density were used. Thus, we tried to get the good fit between measured zeta potential and calculated zeta potential by tuning x_s. As the results, we need to assume the very large xs and the dependence of x_s on ionic strength. The best fit of

the ζ potential from ψ_d is obtained when the values of x_s are 3 nm and 7 nm for electrolyte concentrations of 0.01 M and 0.001 M, respectively (Fig. 2.11). Although these values are very close to the plane shear of aluminum oxide at different NaCl concentration [61], they seem to be much larger than above ones (about 12 times higher) and unrealistic as the thickness of immobile fluid layer adjacent to the surface. The reason is probably because of shortcoming of electrokinetic theory for packed bed of large beads. In order to obtain good predictions of diffuse layer potential by 1-pK Stern model comparable to the zeta potential from streaming potential, we have to use very different parameters from the surface charge fit. These results are similar to the case for the description of surface adsorption behavior of γ-Al_2O_3 nanofiltration membrane using 1-pK basic Stern model [26]. They may be induced by the lack of knowledge about the physical and chemical properties in site binding or complex structures of alumina materials.

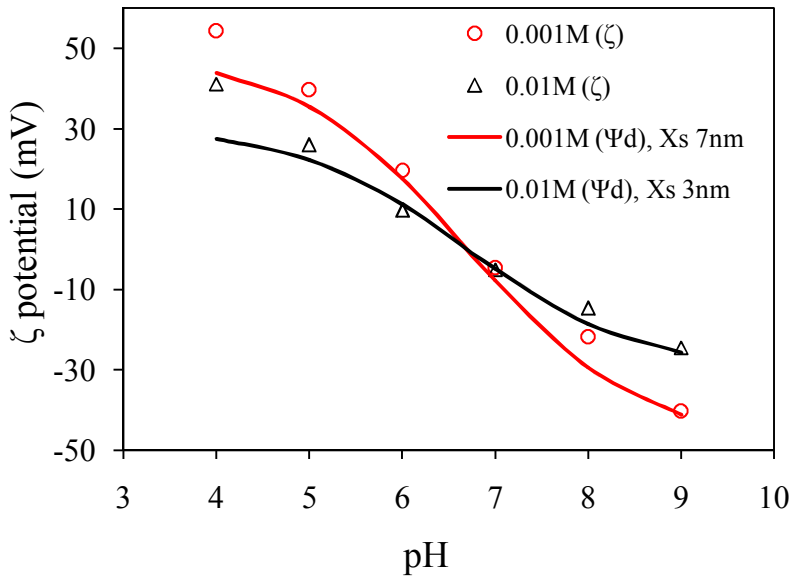

Fig. 2.11. Comparison of zeta potential with diffuse layer potential. The points represent experimental data of ζ potential while solid lines correspond to calculated curves of diffuse layer potential ψ_d with the slipping plane 3 nm and 7 nm for electrolyte concentrations of 0.01 M and 0.001 M, respectively.

2.5. Conclusions

The interfacial properties of α-Al_2O_3 materials with low surface area were studied by streaming potential and chromatographic charge density, combined with 1-pK Stern model. It has been demonstrated experimentally that the zeta potential of α-Al_2O_3 materials are the function of pH and the IEP increase in the order M0 < M1 ~ M2 ~ M4 < M3. The chromatography which was performed in 0.001 M and 0.01 M NaCl background electrolytes, provided the surface charge density of M2. Chromatographic method and 1-pK Stern model were applied successfully to evaluate surface charging behavior and the dissolution effect. The influence of dissolution on surface charge of α-Al_2O_3 seemed to be significant above pH 9.4 and bellow pH 4.7. The SDS adsorption followed by desorption by washing increased the proton consumption on α-Al_2O_3 surface as found from both of zeta potential data and surface charge density of alumina in the absence and treatment by SDS. The recovery of interfacial property of α-Al_2O_3 indicates that we can utilize the above mentioned preparation procedure washing with NaOH and heat treatment at 550 ^{0}C of porous media when using α-Al_2O_3 beads as a reference material.

References

[1] M. Kobayashi, H. Nanaumi, Y. Muto, Initial deposition rate of latex particles in the packed bed of zirconia beads, Colloids and Surfaces A: Physicochemical and Engineering Aspects, 347 (2009) 2-7.

[2] B. Kasprzyk-Hordern, Chemistry of alumina, reactions in aqueous solution and its application in water treatment, Advances in Colloid and Interface Science, 110 (2004) 19-48.

[3] I. Levin, D. Brandon, Metastable Alumina Polymorphs: Crystal Structures and Transition Sequences, Journal of the American Ceramic Society, 81 (1998) 1995-2012.

[4] P.F. Yan, K. Du, M.L. Sui, α- to γ-Al2O3 martensitic transformation induced by pulsed laser irradiation, Acta Materialia, 58 (2010) 3867-3876.

[5] M. Kosmulski, The pH-dependent surface charging and points of zero charge: V. Update, Journal of Colloid and Interface Science, 353 (2011) 1-15.

[6] C.S. Buergisser, A.M. Scheidegger, M. Borkovec, H. Sticher, Chromatographic Charge Density Determination of Materials with Low Surface Area, Langmuir, 10 (1994) 855-860.

[7] L. Svecova, S. Cremel, C. Sirguey, M.-O. Simonnot, M. Sardin, M. Dossot, F. Mercier-Bion, Comparison between batch and column experiments to determine the surface charge properties of rutile TiO2 powder, Journal of Colloid and Interface Science, 325 (2008) 363-370.
[8] G.V. Franks, L. Meagher, The isoelectric points of sapphire crystals and alpha-alumina powder, Colloids and Surfaces A: Physicochemical and Engineering Aspects, 214 (2003) 99-110.
[9] G.V. Franks, Y. Gan, Charging Behavior at the Alumina–Water Interface and Implications for Ceramic Processing, Journal of the American Ceramic Society, 90 (2007) 3373-3388.
[10] M. Colic, D.W. Fuerstenau, Influence of the Dielectric Constant of the Media on Oxide Stability in Surfactant Solutions, Langmuir, 13 (1997) 6644-6649.
[11] C. Contescu, J. Jagiello, J.A. Schwarz, Heterogeneity of proton binding sites at the oxide/solution interface, Langmuir, 9 (1993) 1754-1765.
[12] A.L. Costa, C. Galassi, R. Greenwood, α-Alumina–H2O Interface Analysis by Electroacoustic Measurements, Journal of Colloid and Interface Science, 212 (1999) 350-356.
[13] S.B. Johnson, P.J. Scales, T.W. Healy, The Binding of Monovalent Electrolyte Ions on α-Alumina. I. Electroacoustic Studies at High Electrolyte Concentrations, Langmuir, 15 (1999) 2836-2843.
[14] E.J. Teh, Y.K. Leong, Y. Liu, B.C. Ong, C.C. Berndt, S.B. Chen, Yield stress and zeta potential of washed and highly spherical oxide dispersions — Critical zeta potential and Hamaker constant, Powder Technology, 198 (2010) 114-119.
[15] W.J. Tseng, C.H. Wu, Sedimentation, rheology and particle-packing structure of aqueous Al2O3 suspensions, Ceramics International, 29 (2003) 821-828.
[16] R.J. Kershner, J.W. Bullard, M.J. Cima, Zeta Potential Orientation Dependence of Sapphire Substrates, Langmuir, 20 (2004) 4101-4108.
[17] R. Wäsche, M. Naito, V.A. Hackley, Experimental study on zeta potential and streaming potential of advanced ceramic powders, Powder Technology, 123 (2002) 275-281.
[18] J. Zhou, X. Zhang, Y. Wang, X. Hu, A. Larbot, M. Persin, Electrokinetic characterization of the Al2O3 ceramic MF membrane by streaming potential measurements, Desalination, 235 (2009) 102-109.
[19] A.V. Delgado, F. González-Caballero, R.J. Hunter, L.K. Koopal, J. Lyklema, Measurement and interpretation of electrokinetic phenomena, Journal of Colloid and Interface Science, 309 (2007) 194-224.
[20] W. Staffan, The history of electrokinetic phenomena, Current Opinion in Colloid & Interface Science, 15 (2010) 119-124.

[21] A. Szymczyk, P. Fievet, M. Mullet, J.C. Reggiani, J. Pagetti, Comparison of two electrokinetic methods – electroosmosis and streaming potential – to determine the zeta-potential of plane ceramic membranes, Journal of Membrane Science, 143 (1998) 189-195.

[22] P.M. Karlsson, A.E.C. Palmqvist, K. Holmberg, Adsorption of Sodium Dodecyl Sulfate and Sodium Dodecyl Phosphate on Aluminum, Studied by QCM-D, XPS, and AAS, Langmuir, 24 (2008) 13414-13419.

[23] K.-S. Khoo, E.J. Teh, Y.-K. Leong, B.C. Ong, Hydrogen Bonding and Interparticle Forces in Platelet α-Al2O3 Dispersions: Yield Stress and Zeta Potential, Langmuir, 25 (2009) 3418-3424.

[24] E. Tombácz, M. Szekeres, Interfacial Acid−Base Reactions of Aluminum Oxide Dispersed in Aqueous Electrolyte Solutions. 1. Potentiometric Study on the Effect of Impurity and Dissolution of Solid Phase, Langmuir, 17 (2001) 1411-1419.

[25] M. Borkovec, Origin of 1-pK and 2-pK Models for Ionizable Water−Solid Interfaces, Langmuir, 13 (1997) 2608-2613.

[26] W.B.S. de Lint, N.E. Benes, A.P. Higler, H. Verweij, Derivation of adsorption parameters for nanofiltration membranes using a 1-pK Basic Stern model, Desalination, 145 (2002) 87-95.

[27] C. Attaphong, E. Asnachinda, A. Charoensaeng, D.A. Sabatini, S. Khaodhiar, Adsorption and adsolubilization of polymerizable surfactants on aluminum oxide, Journal of Colloid and Interface Science, 344 (2010) 126-131.

[28] A. Charoensaeng, D. Sabatini, S. Khaodhiar, Solubilization and Adsolubilization of Polar and Nonpolar Organic Solutes by Linker Molecules and Extended Surfactants, Journal of Surfactants and Detergents, 12 (2009) 209-217.

[29] J.J. Lopata, K.M. Werts, J.F. Scamehorn, J.H. Harwell, B.P. Grady, Thermodynamics of mixed anionic/nonionic surfactant adsorption on alumina, Journal of Colloid and Interface Science, 342 (2010) 415-426.

[30] R.P. Sperline, Y. Song, H. Freiser, Temperature Dependent Structure of Adsorbed Sodium Dodecyl Sulfate at the Al2O3/Water Interface, Langmuir, 13 (1997) 3727-3732.

[31] A. Upadhyaya, E. Acosta, J. Scamehorn, D. Sabatini, Adsorption of Anionic–Cationic Surfactant Mixtures on Metal oxide Surfaces, Journal of Surfactants and Detergents, 10 (2007) 269-277.

[32] L. Yang, K. Du, X.S. Zhang, B. Cheng, Preparation and stability of Al2O3 nano-particle suspension of ammonia–water solution, Applied Thermal Engineering, 31 (2011) 3643-3647.

[33] R. J. Hunter, Zeta potential in Colloid Science, Academic Press, London, 1981.

[34] C.S. Buergisser, M. Cernik, M. Borkovec, H. Sticher, Determination of nonlinear adsorption isotherms from column experiments: an alternative to batch studies, Environmental Science & Technology, 27 (1993) 943-948.

[35] D.O. Hummel, Handbook of Surfactant Analysis, John Wiley&Sons, New York, USA, 2000.

[36] L.K. Koopal, T.P. Goloub, T.A. Davis, Binding of ionic surfactants to purified humic acid, Journal of Colloid and Interface Science, 275 (2004) 360-367.

[37] G. Nizri, S. Lagerge, A. Kamyshny, D.T. Major, S. Magdassi, Polymer–surfactant interactions: Binding mechanism of sodium dodecyl sulfate to poly(diallyldimethylammonium chloride), Journal of Colloid and Interface Science, 320 (2008) 74-81.

[38] C.T. Miller, W.J. Weber Jr, Modeling the sorption of hydrophobic contaminants by aquifer materials—II. Column reactor systems, Water Research, 22 (1988) 465-474.

[39] M. Sardin, D. Schweich, F.J. Leij, M.T. van Genuchten, Modeling the Nonequilibrium Transport of Linearly Interacting Solutes in Porous Media: A Review, Water Resour. Res., 27 (1991) 2287-2307.

[40] D. Schweich, M. Sardin, Adsorption, partition, ion exchange and chemical reaction in batch reactors or in columns — A review, Journal of Hydrology, 50 (1981) 1-33.

[41] T. Hiemstra, J.C.M. De Wit, W.H. Van Riemsdijk, Multisite proton adsorption modeling at the solid/solution interface of (hydr)oxides: A new approach: II. Application to various important (hydr)oxides, Journal of Colloid and Interface Science, 133 (1989) 105-117.

[42] J.N. Ryan, M. Elimelech, Colloid mobilization and transport in groundwater, Colloids and Surfaces A: Physicochemical and Engineering Aspects, 107 (1996) 1-56.

[43] M. Kosmulski, IEP as a parameter characterizing the pH-dependent surface charging of materials other than metal oxides, Advances in Colloid and Interface Science, 171–172 (2012) 77-86.

[44] M.R. Das, J.M. Borah, W. Kunz, B.W. Ninham, S. Mahiuddin, Ion specificity of the zeta potential of α-alumina, and of the adsorption of p-hydroxybenzoate at the α-alumina–water interface, Journal of Colloid and Interface Science, 344 (2010) 482-491.

[45] M.R. Das, S. Mahiuddin, Kinetics and adsorption behaviour of benzoate and phthalate at the α-alumina–water interface: Influence of functionality, Colloids and Surfaces A: Physicochemical and Engineering Aspects, 264 (2005) 90-100.

[46] M.R. Das, O.P. Sahu, P.C. Borthakur, S. Mahiuddin, Kinetics and adsorption behaviour of salicylate on α-alumina in aqueous medium, Colloids and Surfaces A: Physicochemical and Engineering Aspects, 237 (2004) 23-31.

[47] C. Contescu, A. Contescu, J.A. Schwarz, Thermodynamics of Proton Binding at the Alumina/Aqueous Solution Interface. A Phenomenological Approach, The Journal of Physical Chemistry, 98 (1994) 4327-4335.

[48] T. Hiemstra, W.H.v. Riemsdijk, M.G.M. Bruggenwert, Proton adsorption mechanism at the gibbsite and aluminium oxide solid/solution interface, Netherlands Journal of Agricultural Science, 35 (1987) 281-294.

[49] W.B.S. de Lint, N.E. Benes, J. Lyklema, H.J.M. Bouwmeester, A.J. van der Linde, M. Wessling, Ion Adsorption Parameters Determined from Zeta Potential and Titration Data for a γ-Alumina Nanofiltration Membrane, Langmuir, 19 (2003) 5861-5868.

[50] D. Santhiya, S. Subramanian, K.A. Natarajan, S.G. Malghan, Surface chemical studies on alumina suspensions using ammonium poly(methacrylate), Colloids and Surfaces A: Physicochemical and Engineering Aspects, 164 (2000) 143-154.

[51] G. Lefèvre, M. Duc, M. Fédoroff, Effect of solubility on the determination of the protonable surface site density of oxyhydroxides, Journal of Colloid and Interface Science, 269 (2004) 274-282.

[52] B.-Y. Zhu, T. Gu, Surfactant adsorption at solid-liquid interfaces, Advances in Colloid and Interface Science, 37 (1991) 1-32.

[53] M.R. Bohmer, L.K. Koopal, Adsorption of ionic surfactants on variable-charge surfaces. 1. Charge effects and structure of the adsorbed layer, Langmuir, 8 (1992) 2649-2659.

[54] L.K. Koopal, E.M. Lee, M.R. Böhmer, Adsorption of Cationic and Anionic Surfactants on Charged Metal Oxide Surfaces, Journal of Colloid and Interface Science, 170 (1995) 85-97.

[55] A. Adak, M. Bandyopadhyay, A. Pal, Removal of crystal violet dye from wastewater by surfactant-modified alumina, Separation and Purification Technology, 44 (2005) 139-144.

[56] M. Borkovec, S.H. Behrens, M. Semmler, Observation of the Mobility Maximum Predicted by the Standard Electrokinetic Model for Highly Charged Amidine Latex Particles, Langmuir, 16 (2000) 5209-5212.

[57] M. Kobayashi, Electrophoretic mobility of latex spheres in the presence of divalent ions: experiments and modeling, Colloid Polym Sci, 286 (2008) 935-940.

[58] M. Kobayashi, F. Juillerat, P. Galletto, P. Bowen, M. Borkovec, Aggregation and Charging of Colloidal Silica Particles: Effect of Particle Size, Langmuir, 21 (2005) 5761-5769.

[59] M. Kobayashi, M. Skarba, P. Galletto, D. Cakara, M. Borkovec, Effects of heat treatment on the aggregation and charging of Stöber-type silica, Journal of Colloid and Interface Science, 292 (2005) 139-147.

[60] M. Schudel, S.H. Behrens, H. Holthoff, R. Kretzschmar, M. Borkovec, Absolute Aggregation Rate Constants of Hematite Particles in Aqueous Suspensions: A Comparison of Two Different Surface Morphologies, Journal of Colloid and Interface Science, 196 (1997) 241-253.

[61] T. Hiemstra, H. Yong, W.H. Van Riemsdijk, Interfacial Charging Phenomena of Aluminum (Hydr)oxides†, Langmuir, 15 (1999) 5942-5955.

Chapter 3. Adsorption of anionic surfactant sodium dodecyl sulfate onto alpha alumina with small surface area

3.1. Introduction

Adsorption of surfactant from aqueous solution on solid surface has been a topic of a lot of research. While many scientific papers reported on the adsorption of surfactant onto colloidal particles, not so many studies have been conducted on surfactant adsorption onto large metal oxide beads [1-7]. It is preferable to study an analysis using relatively large beads that can be directly used to analysis of transport phenomena of colloids [8]. Many surfactants are charged and the charge on the solid–liquid interface plays an important role in surfactant adsorption on metal oxide. The charging behavior influences the shape of the adsorption isotherm and the way of organization of adsorbed surfactant molecules [9]. There are several proposed concepts for the structure of adsorbed layer. Among them, the concepts of hemimicelle and admicelle are often discussed. The concept of hemimicelle was firstly proposed by Gaudin and Fuerstenau [10]. Then, the group of Fuerstenau used the hemimicelle concept to investigate adsorption of ionic surfactants on the charged surface [11-14]. In the hemimicelle, the surfactants are oriented with their charged head groups toward the solid surface while the hydrophobic hydrocarbon chains protrude into aqueous phase [15, 16]. Subsequently, Harwell et al. [17] proposed a local bilayer of surfactant, admicelles, were assumed to be the only surfactant aggregates formed at the solid–liquid interface and their isotherm may not allow for the possibility of hemimicelle formation [18, 19].

While two-step adsorption model [1, 20] suggests the hemimicelles on a linear–linear scale plot, the four-region isotherm is indicative for the case of both hemimicelles and admicelles on a log–log scale [1, 7, 18, 21, 22]. According to two-step model, the adsorption of the surfactant shows a two-step characteristic. In the first step, individual surfactant monomers adsorb on the solid surface at low concentrations: That is no aggregates form. In the second step, the adsorption increases dramatically due to the formation of hemimicelles (Fig. 3.1a). On the basis of two-step adsorption model, a general adsorption isotherm equation can be derived. This equation has been successfully applied to various types of surfactant adsorption isotherms for numerous systems [20, 23]. The equations of hemimicelle concentration (HMC) can also be derived in the cases of S-shape and Langmuir-S (LS)-type isotherms.

When the adsorption isotherms are plotted on a log–log scale, four regions can be found [1, 21, 24, 25]. Region I adsorption occurs at low equilibrium surfactant concentrations and low levels of adsorption. Region I is similar to the first step of two-step adsorption model. Region II can be recognized indicated by an increase of the slope of the adsorption isotherm with increasing equilibrium surfactant concentration. The concentration at which the first change of slope occurs is HMC. However, the slope of region II sometimes decreases when surfactants adsorb onto the porous materials with small specific surface area [26-28]. In these cases, the HMC cannot occur on the I/II transition. In the hemimicelle, the surfactants are oriented with their charged head groups toward the solid surface while the hydrophobic hydrocarbon chains protrude into aqueous phase [15, 16]. In the region III, the slope of the isotherm is reduced because of the electrostatic repulsion between oncoming ions and the similarly charged solid [25]. In region IV, the adsorption can be completed while the surfactant concentration in solution reaches to critical micelle concentration (CMC) (Fig. 3.1b). The region where the adsorption amount remains nearly constant is called the plateau adsorption region [18, 24]. However, the shapes of four regions in some cases are different depending on the sorbent types [27, 28], the ionic surfactant types or effect of ionic strength [1, 3, 6].

Many studies have focused on surfactant adsorbed layer on solid by fluorescence, Raman, and electrospin resonance (ESR) [7, 29-31]. Nevertheless, information about hemimicelle and admicelle of the adsorbed layer of ionic surfactants on metal oxide is still inadequate. Koopal and coworkers [3, 32-35] used the modern self-consistent field lattice theory (SCFA theory) for surfactant adsorption and association to study surface charge effects, structure of the adsorbed layer, and the influence of ionic surfactant chain length. Results obtained with the SCFA theory show the shape of surfactant adsorption isotherms to be complex and different for constant charge and constant potential (variable charge) surfaces [32-34]. Accordingly, SCFA theory indicates that the two-step adsorption and four-region isotherm models coexist and are valid under different conditions depending on the charging properties of solid surface [21]. The adsorption behavior of anionic and cationic surfactants on oppositely charged rutile (TiO_2) consisted of four regions [35]. The adsorption of anionic surfactant on the positively charged TiO_2 at different pH values suggests the forming of hemimicelles [32, 36]. For silica, the adsorption of cationic surfactant corresponds with two steps and four regions, but the shape of isotherms at high salt concentration differs from that at low salt concentrations [3, 37]. Although SCFA theory was used to describe the effects of charged surface, chain length, and branching well, it could not confirm the local aggregates. Fortunately, by measuring total adsorbed amount at plateau of isotherm and the amount of surfactant with head group toward

the surface that is equal to a surface charge adjustment upon surfactant adsorption, one can estimate the amount of surfactant with head groups toward solution [32, 37]. It indicates that charge regulation induced by surfactant adsorption is of great importance to study adsorption of ionic surfactant [9] and predict the structure of adsorbed layer on the surface of sorbent.

Alumina is often used as a substrate for adsorption of anionic surfactants [2, 15, 16, 18, 19, 22, 25, 38-40]. The change in pH upon adsorption of surfactant on alumina has been reported [18, 41], indicating a change in surface charge. Nevertheless, the interplay between the pristine surface charge of alumina due to proton adsorption and the adsorption of anionic surfactant sodium dodecyl sulfate (SDS) is too complex to be explained within a simple model [42]. The adsorption of SDS onto alumina is more difficult when this sorbent has large diameter with low surface area. In a previous work, we showed that the interfacial properties of alpha alumina with small surface area in the absence and the presence of SDS can be evaluated by using streaming potential and chromatographic methods [43].

The purpose of this chapter is to analyze adsorption isotherm of SDS onto large beads of α-Al_2O_3 with variably charged surfaces. The SDS adsorption and surface charge isotherms at various NaCl concentrations and pH values have been experimentally studied to clarify the applicability of both the two-step and four-region models. To our best knowledge, we succeeded for the first time in SDS/alumina system to relate proton adsorption upon surfactant uptake with two-step model. With this approach, charge effects and the presence of hemimicelle and admicelle are discussed in depth.

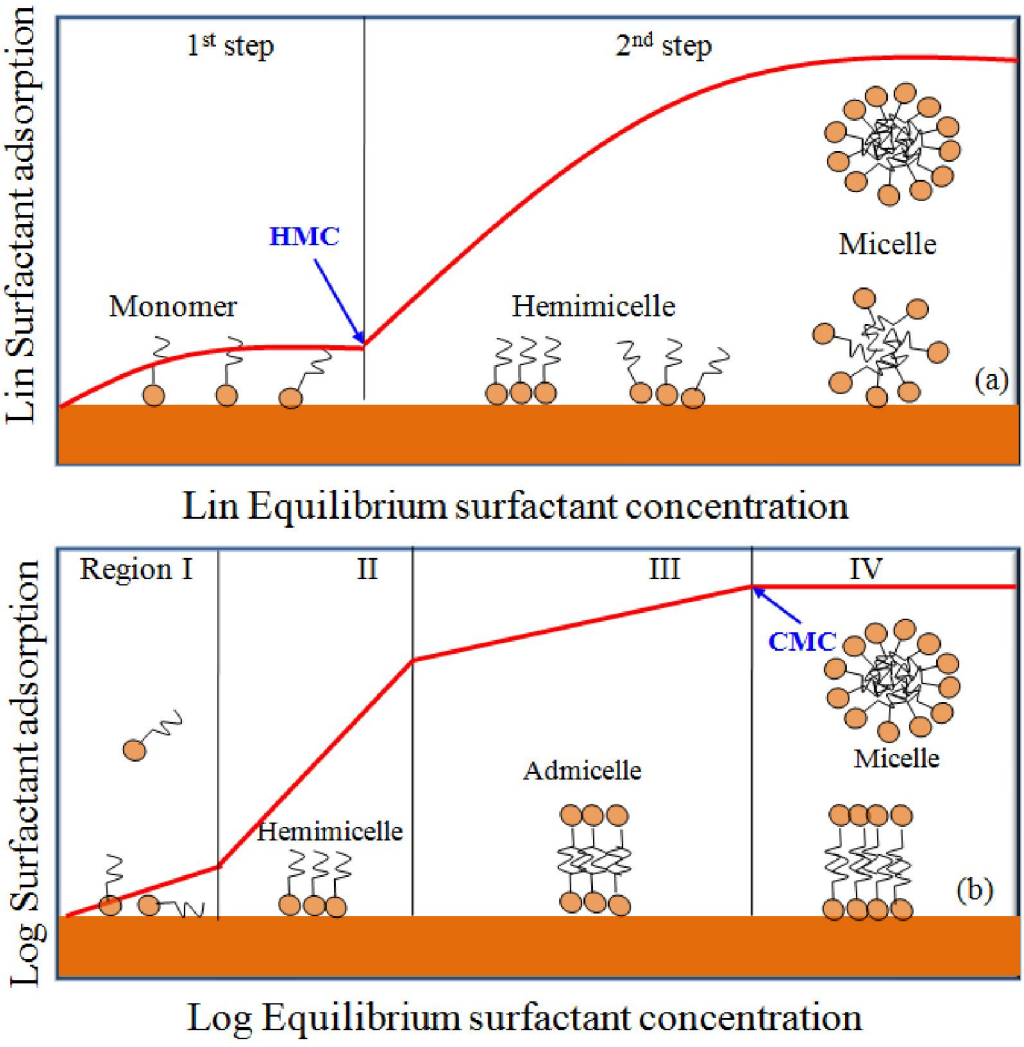

Fig. 3.1. Schematic representation of ionic surfactant adsorption isotherm on hydrophilic surface from aqueous solution.

3.2. Experimental

3.2.1. Materials

High-purity (99.5 %), alpha alumina beads with an average diameter of 300 ± 12 μm and a density of 3.82 g/cm^3 were purchased from Hiraceramics, Japan, and were used in the present study. X-ray diffraction (XRD) was collected on a Bruker D8 Advance X-ray diffractometer. The analyses confirmed that the alumina beads contain mainly α-phase (detail shown in chapter 2). The specific surface area was determined by Brunauer-Emmett-Teller (BET) method using a surface area analyzer (Micromeritics, Gemini 2390) and found to be 0.0041 ± 0.0016 m^2/g. The alpha alumina was treated before measurements. The original α-Al_2O_3 was washed many times with 0.1 M NaOH before rinsing by ultrapure water to reach neutral pH. After that, α-Al_2O_3 was dried at 110 ^{0}C and was reactivated by thermal treatment at 550 ^{0}C for 2 h. Finally, the treated material was cooled in a desiccator at room temperature and stored in polyethylene container. The treated α-Al_2O_3 has a point of zero charge (PZC) of about 6.7 [43].

Sodium dodecyl sulfate (SDS, with purity higher than 95 %) from Wako Pure Chemical Industries was used. The structure of SDS is shown in Fig. 3.2. The critical micelle concentration (CMC) of SDS at 22 ^{0}C was experimentally determined by conductometric and potentiometric measurements and shown in Table 3.1. Cationic dye, methylene blue (with purity higher 98.5 %) and organic solvent chloroform ($CHCl_3$, GC grade, purity higher 99 %) from Wako Pure Chemical Industries were used to determine concentration of SDS by colorimetric method. Ionic strength and pH were adjusted by the addition of NaCl (Wako Pure Chemical Industries), HCl, and NaOH (volumetric analysis grade, Wako Pure Chemical Industries). Other chemicals were obtained from Wako. Ultrapure water, produced from Elix Advantage 5 (Millipore) with electric conductivity around 0.6 μS/cm, was used in preparing solutions and in all measurements.

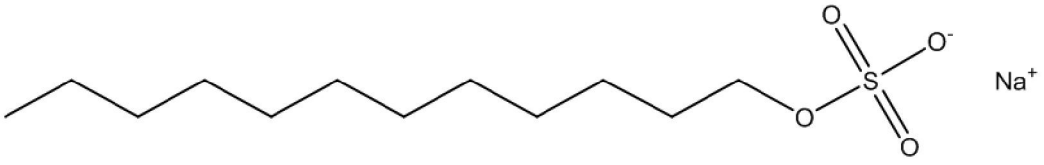

Fig. 3.2. The structure of anionic surfactant, sodium dodecyl sulfate (SDS).

3.2.2. Adsorption isotherms

Adsorption isotherms were obtained in 100-mL Erlenmeyer flask at room temperature, controlled by air conditioner (22 $\pm$ 2 ^{0}C), using a depletion method. For SDS adsorption studies, 0.5 g of treated α-Al_2O_3 was mixed with 25 mL of NaCl aqueous solutions at different concentrations by a shaker for 1 h. Then, SDS with concentrations from 10^{-5} M to 10^{-2} M was prepared and pH was adjusted to original value. After mixing alumina and SDS and shaking for 3 h, the pH was measured again and if necessary, readjusted by 0.01 M HCl or 0.1 M HCl and 0.1 M NaOH using a Socorex Acura 825 micro pipette with minimum volume of 1 μL. More than 12 h later, the samples were equilibrated by vigorous shaking. Then, the pH was checked and, if necessary, readjusted again. This procedure was repeated until no further changes in pH were attained. When equilibrium process was achieved, the α-Al_2O_3 was separated from the solutions. The adsorption density of SDS onto α-Al_2O_3 was determined by the difference in the concentration of SDS solutions before and after adsorption by colorimetric method using the following equation:

$$\Gamma_{\mathrm{SDS}} = \frac{(C_{\mathrm{i}} - C_{\mathrm{e}})V}{mA} \quad (3.1)$$

where Γ_{SDS} is the SDS adsorption density (mmol/m^2), C_{i} is the initial SDS concentration (mmol/L), C_{e} is the equilibrium SDS concentration (mmol/L), V is the volume of sample (L), m the mass of α-Al_2O_3 (g), and A is the specific surface area of α-Al_2O_3 (m^2/g).

By recording the added amount of HCl or NaOH to keep the pH constant after SDS addition, the surface charge adjustment of alpha alumina has been obtained. The surface charge adjustment was combined with initial surface charge of alpha alumina by chromatographic method [43] to calculate the equilibrium surface charge expressed as $\Gamma_0 = \sigma(0)/F$ with F is the Faraday constant. For example, at 0.01M NaCl and pH 5, the initial surface charge of α-Al_2O_3 is 0.01×10^{-4} mmol/g. Total added volume of 0.01M HCl to keep constant pH after SDS addition is 0.025 mL. Thus, the adjusted one is 5×10^{-4} mmol/g (for 0.5 g α-Al_2O_3 at the plateau adsorption of SDS). Therefore, equilibrium adsorption density of proton is 5.01×10^{-4} mmol/g that is equal 0.122 mmol/m^2.

3.2.3. Colorimetric method

The concentration of anionic surfactant SDS was determined by colorimetric method using chloroform as the organic solvent and methylene blue as cationic dye. Measurements of samples and standard solutions or blanks were carried out simultaneously according to the

papers [44, 45]. To make a standard calibration curve for each NaCl concentration, a series of SDS solutions with the concentrations from 5×10^{-7} to $1.5\times10\text{-}^{5}$ mol/L was prepared in glass tubes in different electrolyte concentrations. Methylene blue stock solution (10^{-2} M) was diluted 100 times with 10 mM acetate buffer, pH 5.5, and then 1 mL of the diluted solution was added to each tube. A 2 mL of $CHCl_3$ was added per tube and mixed by hand. Then, the same volume of $CHCl_3$ was added to each tube (two or three times), followed by vigorous mixing. The aqueous and chloroform phases were separated by a centrifuge (H-103N, Kokusan) at 2000 rpm for 10 min at room temperature. The absorbance of chloroform phase was measured at wavelength 655 nm by an UV-vis spectrophotometer (UV-1650PC, Shimadzu) with closed quartz cuvette with 1-cm optical path length. The relationship between the absorbance and concentrations of SDS of standard calibration curves in different electrolyte concentrations and pH should yield a straight line with a correlation coefficient of at least 0.999. In every experiment done with different salt concentrations, samples and blanks were appropriately diluted with the same dilution factors before measuring the absorbance to quantify SDS concentrations by different standard calibration curves. In this way, by always keeping the same amounts of salt in each sample as in blanks and standard samples, the concentration of SDS could be accurately determined.

3.2.4. Potentiometric method

Potentiometry was conducted using a Metrohm 781 pH/Ion meter, Switzerland. The pH of NaCl solutions used in adsorption isotherm and determination of the concentration of proton in solutions was measured by a glass combination electrode (Type 6.0258.010 Metrohm). The electrode was previously calibrated with three standard buffers (Metrohm). The CMC of SDS in different electrolyte concentrations was determined with a surfactant ion selective electrode (Type 6.0507.120 Metrohm) that is sensitive to ionic surfactants [46, 47]. The electrode potential (E in mV) was measured relative to an Ag/AgCl reference electrode (Type 6.0726.100 Metrohm) equipped with a ceramic plug. The CMC of SDS in pure water and NaCl background solutions can be obtained from the inflection point after the linear range of the curve, presenting E as the function of the logarithm of SDS concentration [48]. The CMC of SDS was compared with that by conductometric method by an electrical conductivity meter (EC Meter Toa CM-30G). All measurements were carried out at 22 ± 2 ^{0}C. The

difference in the CMC of SDS determined via the conductometric and potentiometric methods did not exceed 10 %. The values of CMC are listed in Table 3.1.

Table 3.1 Critical micelle concentration (CMC) of SDS at 22 ^{0}C

NaCl (M)	CMC (mM)
0	6.0
0.001	5.5
0.01	5.0
0.05	2.5
0.1	2.0
0.2	1.0

3.3. Two-step adsorption model

3.3.1. Theory and modeling

Two-step adsorption model assumes that the adsorption of surfactants on solid-liquid interface occurs in two steps [20]. In the first step, surfactant monomers adsorb on the solid surface through electrostatic attraction (in case of ionic surfactants) at low concentration below critical aggregation concentration (CAC) or hemimicelle concentration (HMC); thus, no aggregates form [7]:

Site + Monomer ⇄ Adsorbed Monomer (3.2)

The equilibrium constant is given by

$$k_1 = \frac{a_1}{a_s a} \quad (3.3)$$

Here a is the activity of surfactant monomers in solutions, and a_1 and a_s are the activities of adsorbed monomers and surface sites, respectively.

In the second step, the adsorption increases significantly because of the presence of hemimicelle:

(n – 1) Monomers + Adsorbed Monomers ⇄ Hemimicelle (3.4)

The equilibrium constant is

$$k_2 = \frac{a_{hm}}{a_1 a^{n-1}} \quad (3.5)$$

where a_{hm} is the activity of hemimicelle and n is the aggregation number of hemimicelle.

As an approximation for dilute solutions, one can use $a = C$ (C is surfactant monomer concentration), the amount of adsorbed monomer Γ_1, the amount of hemimicelle Γ_{hm}, and the number of sites Γ_s instead of a_1, a_{hm} and a_s, respectively. Thus, Eqs. (3.3) and (3.5) become

$$k_1 = \frac{\Gamma_1}{\Gamma_s C} \quad (3.6)$$

and

$$k_2 = \frac{\Gamma_{hm}}{\Gamma_s C^{n-1}} \quad (3.7)$$

The amount of surfactant adsorbed Γ and the maximum adsorption Γ_∞ are

$$\Gamma = \Gamma_1 + n\Gamma_{hm} \quad (3.8)$$

and

$$\Gamma_\infty = n(\Gamma_s + \Gamma_1 + \Gamma_{hm}) \quad (3.9)$$

The general expression for the two-step model can be derived by the combination of Eqs. (3.6), (3.7), (3.8), and (3.9). The general isotherm equation is

$$\Gamma = \frac{\Gamma_\infty k_1 C \left(\frac{1}{n} + k_2 C^{n-1}\right)}{1 + k_1 C(1 + k_2 C^{n-1})} \quad (3.10)$$

If $k_2 \to 0$ and $n \to 1$, Eq. (3.10) reduces to Langmuir equation:

$$\Gamma = \frac{\Gamma_\infty k_1 C}{1 + k_1 C} \quad (3.11)$$

If $n > 1$, there are two limiting cases. When $k_2 C^{n-1} \gg 1/n$, Eq. (3.10) again becomes a Langmuir – type equation:

$$\Gamma = \frac{(\Gamma_\infty / n) k_1 C}{1 + k_1 C} \quad (3.12)$$

except the monolayer adsorption Γ_∞ / n. If $k_2 C^{n-1} \gg 1$ or $k_1 C \ll 1$ and $k_1 C \ll k_2 C^n$, the adsorption isotherm would have S-type shape and Eq. (3.10) could be reduced to

$$\Gamma = \frac{\Gamma_\infty k_1 k_2 C^n}{1 + k_1 k_2 C^n} = \frac{\Gamma_\infty K C^n}{1 + K C^n} \quad (3.13)$$

When the value of k_1 is high enough, the two-plateau isotherm (LS-type) can be obtained.

The hemimicelle concentration (HMC) in the two-step model, is concentration where the straight line with the maximum $\partial\Gamma/\partial C$ on the adsorption isotherm intersects the line of $\Gamma = 0$ or $\Gamma - (\Gamma_\infty / n) = 0$ [20]. Thus, HMC can be determined by equations as follows:

$$HMC = \left(\frac{n-1}{n+1}\right)^{\frac{n+1}{n}} K^{\frac{-1}{n}} \quad (3.14)$$

and

$$HMC = \left(\frac{n-2}{n}\right)^{\frac{n}{n-1}} K^{\frac{-1}{n-1}} \quad (3.15)$$

for S-type and LS-type isotherms, respectively.

3.3.2. Fitting procedure

The selected fitting parameters are described in the following in the following: (a) Γ_∞ can be obtained from adsorption data at high concentrations. (b) The values of k_1 can be predicted from the adsorption data at low concentrations by a limiting Langmuir equation. (c) By using reasonable guesses for k_1 in step (b) and k_2 (with fixed one value of n), the calculation of the adsorption density Γ_{cal} for SDS or proton by Eq. (3.10) was calculated from experimental data points. (d) Procedure was repeated with 0.1 step change. (e) We use trial and error to find the minimum sum of square of residuals for every isotherm, $\mathrm{SS_{residuals}} = \sum(\Gamma_{cal} - \Gamma_{exp})^2$, where Γ_{exp} is the experimental adsorption density of SDS or proton. (f) The minimum $\mathrm{SS_{residuals}}$ was chosen to find the appropriate values for parameters k_1, k_2 and n.

3.4. Results and discussion

3.4.1. Surface charge and surfactant isotherms by two-step adsorption model

The effect of pH and ionic strength on SDS adsorption to the alumina surface is well known and demonstrated in the isotherms. In the linear–linear plot, the presented isotherms show two steps (Fig. 3.3) at different pH and ionic strength. The calculated curves by two-step adsorption model shown as the solid lines in Fig. 3.3 can reasonably represent experimental data by using the fit parameters in Table 3.2. This model assumes that all adsorbed surfactant molecules exist as the form of monomers or hemimicelles. From the fitting procedure, the values of n are chosen about 10 (Table 3.2). Although the values of n obtained from this model are much smaller than measured aggregation number using spectroscopic methods [7, 40], the two-step model is useful to evaluate the influence of pH and ionic strength. As can be seen from Fig. 3.3, the adsorption density is strongly dependent on pH in different electrolyte concentrations. Because the CMC is independent of pH [25] and our CMC is close to the result from Thongngam et al. [49], the association between SDS

molecules and protons can be neglected. Figure 3.3 demonstrates that the adsorption density of SDS on alumina reaches constant around the CMC in different pH, except for high ionic strength. In 0.1 M NaCl, the adsorption plateau is not observed near the CMC. These trends are in good agreement with previously published papers [2, 18, 40]. The increase of adsorbed amount with surfactant concentration after the CMC can be explained by a dramatic decrease of CMC in high ionic strength [32] (see Table 3.1) and the adsorption characteristics of surfactant onto porous materials [27, 28].

Table 3.2 The fit parameters for SDS adsorption, which are maximum adsorbed amount Γ_∞, the equilibrium constants k_1, k_2 for first step and second step, respectively, n the aggregation number of hemimicelle and HMC the hemimicelle concentration

C salt (M NaCl)	pH	Γ_∞ (mmol/m^2)	k_1 (m^2/mmol)	k_2 (m^2/mmol)$^{n-1}$	n	HMC (mM) (Eq. (3.14))	HMC (mM) (Eq. (3.15))
0.001	4	1.20	6×10^3	1×10^{24}	9.8	1.17	1.45
0.001	5	0.95	6×10^3	6×10^{23}	9.8	1.23	1.54
0.001	6	0.52	6×10^3	5×10^{23}	9.8	1.25	1.57
0.01	4	1.55	4×10^3	8×10^{23}	9.8	1.25	1.49
0.01	5	1.10	4×10^3	7×10^{23}	9.8	1.26	1.51
0.01	6	0.65	4×10^3	6×10^{23}	9.9	1.37	2.66
0.1	4	1.67	1×10^3	6×10^{22}	10.1	2.25	2.46
0.1	5	1.40	1×10^3	5×10^{22}	10.1	2.29	2.51
0.1	6	0.77	1×10^3	4×10^{22}	10.1	2.35	2.57

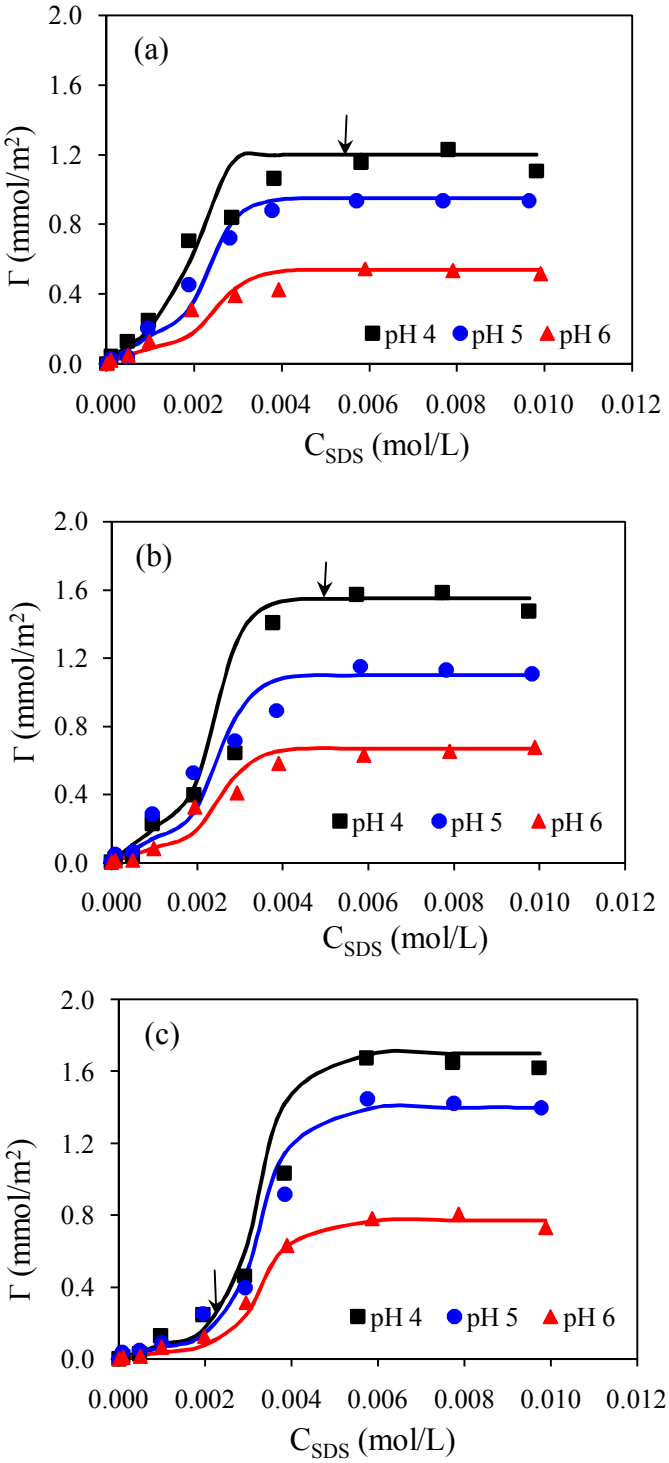

Fig. 3.3. Adsorption isotherms of SDS onto α-Al_2O_3 in 0.001 M NaCl (a), 0.01 M NaCl (b), and 0.1 M NaCl (c) as a function of pH. C_{SDS} is the equilibrium SDS concentration. While the points are experimental data, the solid lines are the results of two-step adsorption model. The arrows show the CMC value.

At different salt concentrations, the maximum adsorption density increases with decreasing pH due to the difference in equilibrium surface charge isotherms. As shown in Fig. 3.3 and Table 3.2, for the higher k_2, the second step on the isotherm is steeper [20, 50] and the lower HMC is obtained. The values of k_1 can be used to evaluate the effect of salt concentrations. The values of k_1 are 6×10^3, 4×10^3 and 10^3 for 0.001, 0.01 and 0.1 M NaCl, respectively. The higher k_1 values are observed for the lower salt concentration in which the higher adsorption density in the first step is obtained. Adsorption density at low SDS concentration decreases with increasing salt concentration because the electrostatic attraction between the negatively charged SDS head groups and positively charged surface sites is screened by increasing salt concentrations. However, at high surfactant concentration, adsorption density increases with increasing the salt concentration by screening of repulsive force between negatively charged DS^- ions. The groups of Bohmer [32] and Goloub [37] indicated that the surfactant ions effectively screen the surface charge of metal oxides so that the charge can change upon surfactant adsorption. While Bohmer et al. [32] has revealed that in the plateau of the surfactant adsorption, surface charge does not depend on the salt concentration, Goloub et al. [37] has shown that the maximum change in surface charge occurs at low surfactant and low salt concentrations. In our case, the surface charge changes more significantly in low salt concentrations (0.001 and 0.01 M NaCl) and at pH 4 and pH 5. The change in surface charge increases dramatically in the region ranging from HMC to CMC. The charge adjusting at pH 4 and pH 5 shown in Figs. 3.4 and 3.5 demonstrates that the proton adsorption upon SDS adsorption increases with increasing the concentration of SDS. The maximum adsorption density of proton is observed at the plateau of SDS adsorption.

At pH 6, it is too difficult to evaluate the change in surface charge (data not shown) due to very low concentration of proton in solutions. Also, at high salt concentration (0.1 M NaCl), this change is not significant. It should be noted that the relative error between experimental points and predicted curves by two-step model without charge adjustment is smaller than that for significant change in surface charge. This result implies that the fitting parameters depend on the degree of charge adjustment. Table 3.2 and Fig. 3.3 indicate that when the change of surface charge is significant, the HMC is much lower (higher k_2) because charge adjustment enhances the formation of hemimicelles or vice versa.

It is interesting to note that the change in surface charge of α-Al_2O_3 induced by SDS adsorption can also be represented by two-step model. To study the surface charge effects in more detail, the experiments were carried out at pH 4 and pH 5 in 0.001 and 0.01 M NaCl. In

Figs. 3.4 and 3.5, the points are experimental data and the solid lines are the results of two-step adsorption model for adsorption isotherms of SDS and equilibrium surface charge. Here the equilibrium surface charge, Γ_0 and the adsorption density of SDS, Γ_{SDS} are both expressed in mmol/m^2. The expressed unit of the adsorbed amount of surfactant is large compared with surfactant adsorption [1, 6, 7] and proton adsorption upon adsorbing surfactant [32, 37]. However, the plateau adsorption density in our research is rather similar to the published papers [28, 51]. The maximum adsorption density of SDS onto neutral alumina (mean particle size 130 μm) in 0.043 M NaCl at pH 4.4 is about 4.3 mmol/m^2 [51]. When anionic surfactants adsorb onto poly-dimethyldiallyammonium chloride (PDMAC) treated cellulosic fibers at pH 6.5 – 7, the highest adsorption density is around 0.4 mmol/m^2 [28]. These values are due to highly porous material and/or low surface area.

Another outstanding feature is that we are able to use almost the same fitting parameters (k_1 and k_2) from two-step model for SDS adsorption on α-Al_2O_3 to describe adsorption of proton upon surfactant adsorption. Figures 3.4 and 3.5 show that two-step adsorption model represents proton adsorption as well as SDS adsorption isotherms. The values of aggregation number for proton adsorption (n = 10. 6 for pH 4 and n = 10.8 for pH 5) are slightly higher than those of the hemimicelle of SDS ($n \approx 10$). The amount of the proton adsorption due to adsorbing SDS molecules is much smaller below the HMC than above the HMC (Figs. 3.4 and 3.5). In 0.001 M NaCl, the maximum values of Γ_{SDS} are equal to 1.20, 0.95, and 0.52 mmol/m^2 for pH 4, pH 5 and pH 6, respectively. On one hand, in 0.01 M NaCl, these values are 1.55, 1.10, and 0.65 mmol/m^2. The maximum adsorption density of both SDS and proton has been reached around the CMC, except for the case of high ionic strength (0.1 M NaCl).

At low salt concentrations, the adsorption amount of SDS is larger than that of proton, but the proton adsorption or the change in surface charge is significant. The screening by SDS molecules is of great importance to induce the proton adsorption. The influence of pH in proton adsorption is significant when surfactant molecules adsorb with head groups screening the surface. On the other hand, if their head groups are toward solution, the effect on the change of surface charge is small. In addition, the net charge at the surface site of the bilayer is very low and the screening of any remaining net charge in hydrophobic core is limited [32]. These findings reveal that the adsorption isotherms of SDS onto α-Al_2O_3 at low ionic strength are in accordance with the hemimicelle concept. For high ionic strength, although the adsorption isotherms of SDS onto α-Al_2O_3 at different pH were fitted well by two-step model,

the adsorption of proton was not significant so that only the hemimicelles could not be supportable.

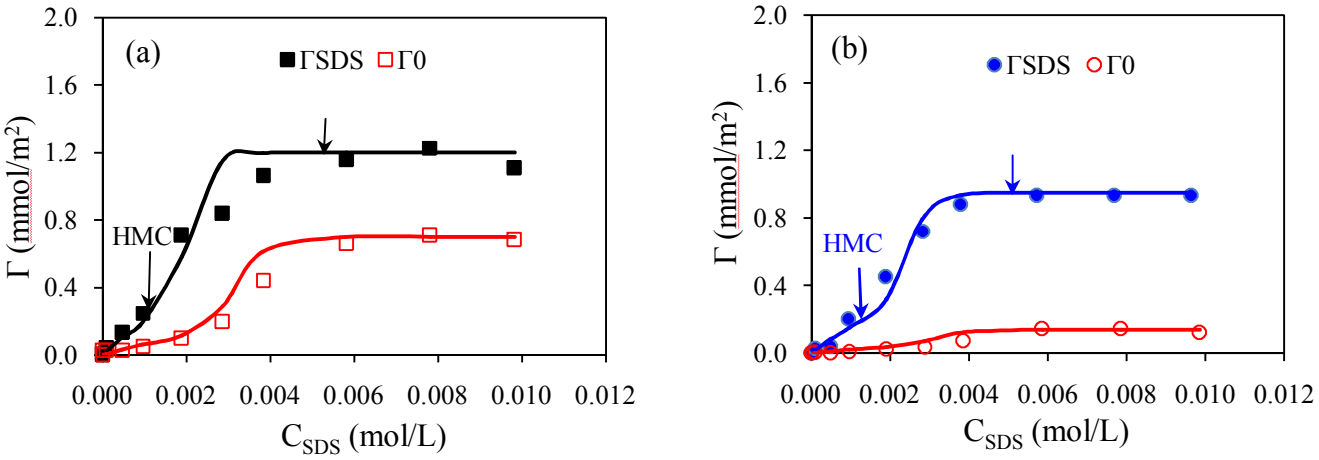

Fig. 3.4. Adsorption isotherms of SDS (Γ_{SDS}) and proton (Γ_0) onto α-Al_2O_3 as a function of the equilibrium SDS concentration at pH 4 (a) and pH 5 (b) in 0.001 M NaCl. The points are experimental data while the solid lines are the results of two-step adsorption model. The above arrows indicate the CMC.

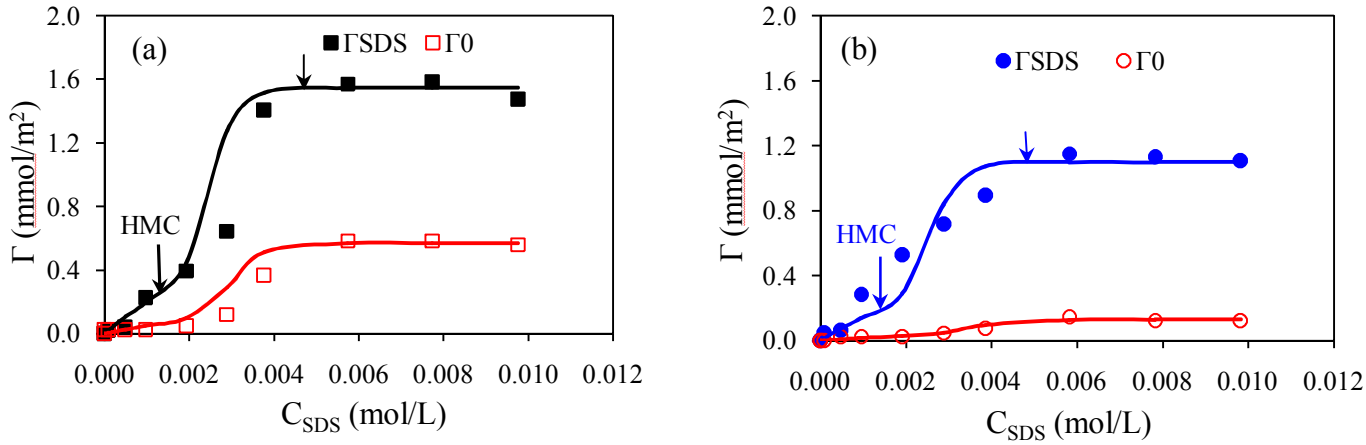

Fig. 3.5. Adsorption isotherms of SDS (Γ_{SDS}) and proton (Γ_0) onto α-Al_2O_3 as a function of the equilibrium SDS concentration at pH 4 (a) and pH 5 (b) in 0.01 M NaCl. The points are experimental data while the solid lines are the results of two-step adsorption model. The above arrows indicate the CMC.

3.4.2. Surfactant adsorption isotherm using four-region model

The adsorption isotherms of SDS onto α-Al_2O_3 measured at different pH and three salt concentrations in log–log plots are shown in Fig. 3.6. Generally, four regions can be clearly distinguished in the isotherm [1, 3, 6, 7, 32, 33, 35, 37, 39] as mentioned in the "Introduction" section. In this work, the shapes of isotherms are close to those in reported paper [28] in which the adsorption of ionic surfactants onto porous cellulosic fibers reveals different shapes in four regions. As shown in Fig. 3.6, the first region appears in the equilibrium SDS concentration ranging from 10^{-5} to 10^{-4} mol/L. The slope of the plot in region I is approximately close to unity, corresponding a constant affinity [3].

The region II which appears in the SDS concentration from 10^{-4} to 10^{-3} mol/L corresponds to the growth of aggregates (hemimicelles) already formed [28]. The slope in this region is less than unity because of the electrostatic repulsion between the charged SDS head groups and interaction of hydrophobic cores. Otherwise, the decrease in the slope of region II can be realized by the structure of porous metal oxides. The adsorption of SDS molecules into porous sites seems more difficult than adsorption on the surface sites. SDS molecules can adsorb onto α-Al_2O_3 with the head groups toward the surface and porous sites. However, the surfactant molecules are not enough to influence the surface charge of α-Al_2O_3. In regions I and II from pH 4 to pH 6, the higher salt concentration is, the lower adsorption density of SDS is. This is due to the screening of attractive electrostatic force at low surfactant concentration.

With increasing the concentration of SDS, the amounts of adsorption increase significantly in region III [3, 28]. It can be explained by the presence of hemimicelle with head groups toward surface at low salt concentration or the appearance of admicelle with the head groups pointing toward solution at high salt concentration. The groups of Harwell [18, 19, 22] showed that the presence of admicelle in region III reduced the slope of adsorption isotherm because of a change in the sign of surface charge or from the distribution of patch adsorption energies. Nevertheless, the generation of local bilayer structure probably reduces contact area between hydrophobic tail and the surrounding water molecules in the present research [28]. As can be seen in Fig. 3.6, the increase of slopes of adsorption isotherm in region III is significant for 0.1 M NaCl, but it is not so clear for 0.001 M NaCl. The differences of these slopes suggest that only hemimicelles for low salt concentration and both hemimicelle and admicelles for 0.1 M NaCl are formed.

At different pH, the isotherms show a common intersection point (CIP) in which the electrostatic contribution to the free energy of adsorption vanishes and the salt effect disappears. For SDS, the adsorption decreases with increasing electrolyte concentration below CIP because of screening of attractive force and competition between electrolyte counter-ions (anions) and surfactant monomers. Above the CIP, the salt effect is reversed so that adsorption density at high salt concentration is enhanced due to reduced electrostatics repulsions between the SDS head groups [1, 3, 32]. In our experiments, the locations of CIP are in region III and higher than CMC of SDS in 0.1 M NaCl. It seems to be different with previous studies [3, 18, 32, 35] in which the CIP is lower than CMC. The occurrence of CIP at high amount of SDS adsorption can be explained by two reasons. First, SDS was adsorbed on both surface sites and into the porous structures of α-Al_2O_3. The adsorption occurs onto the surface before the porous sites at very low surfactant concentration, but it can take place simultaneously onto both surface and porous sites at high surfactant concentration. Second, the specific property of dodecyl sulfate surfactant which has a small head group area (about 25 $Å^2$) [21] could promote adsorption into porous sites.

Further increase in SDS concentration leads to region IV; a maximum adsorption is observed (Fig. 3.6). In 0.001 and 0.01 M NaCl, the adsorption amount starts to saturate at solution concentrations near the CMC as seen in Ref. [52]. In 0.1 M NaCl, the maximum adsorption is reached at a concentration higher than the CMC. The value of CMC is decreased dramatically in high ionic strength, but the proton adsorption due to SDS adsorption is not significant. Because the proton adsorption is negligible, there is no competitive adsorption onto α-Al_2O_3 between SDS molecule and hydroxide (proton). The adsorption of SDS is not completed at the CMC at high ionic strength, and the adsorption density of SDS still increases after passing the CMC. The maximum adsorption is only obtained after passing the CIP that is followed by the CMC. As shown in Fig. 3.6, at high salt concentration, the plateau adsorption is located at high adsorption density where SDS equilibrium concentration is about 5.0×10^{-3} mol/L. It is also indicated that admicelles appear on the surface of α-Al_2O_3 beads when SDS concentration in bulk solutions reaches over the CMC.

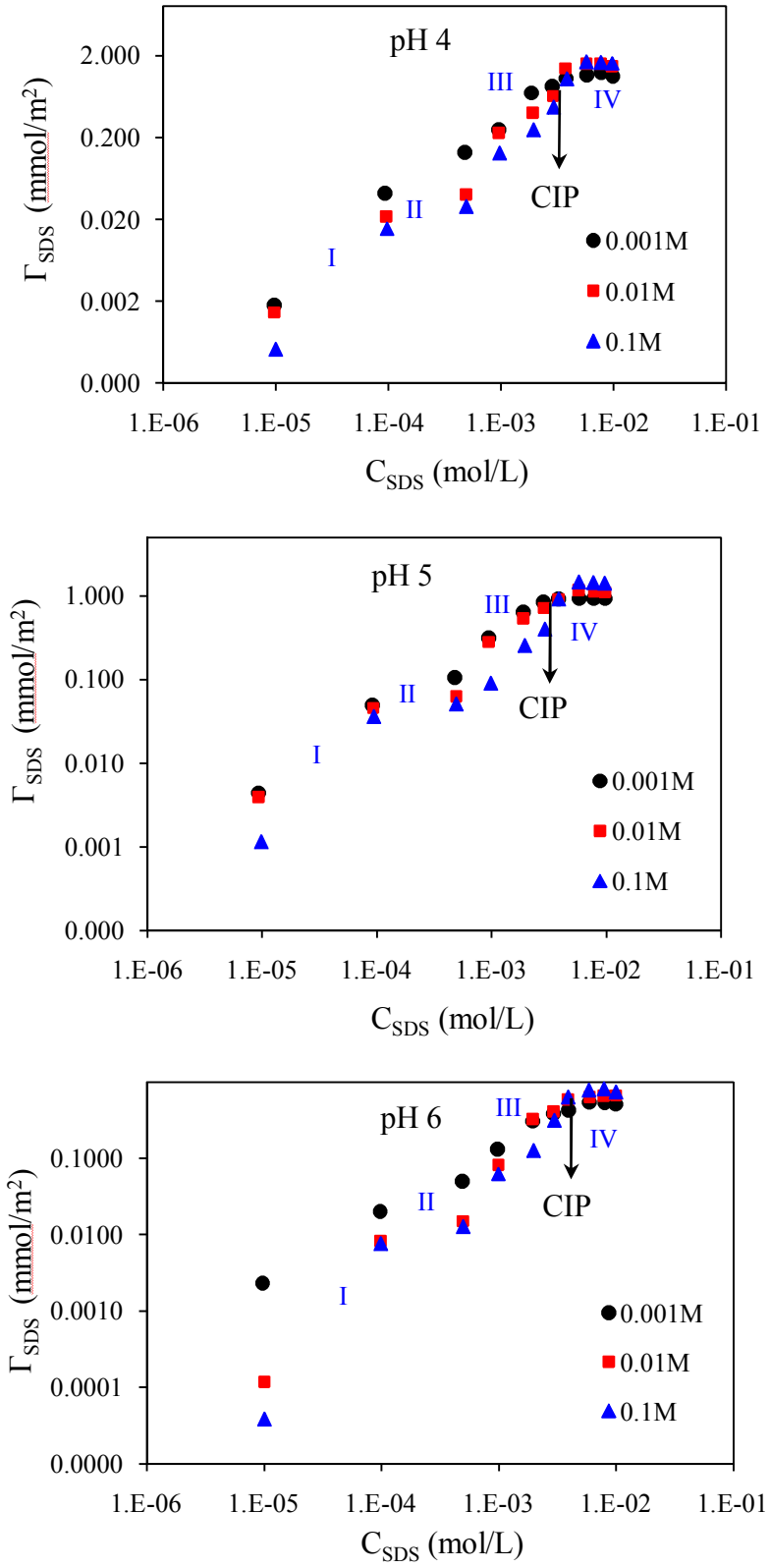

Fig. 3.6. Adsorption isotherm of SDS onto α-Al_2O_3 on log–log scales at three pH and three salt concentrations. C_{SDS} is the equilibrium SDS concentration.

3.4.3. Structure of adsorbed layer

When the adsorption isotherms of both SDS and proton only occur on the surface of α-Al_2O_3, the structure of adsorbed layer can be examined by adsorbed amount of surfactant in the plateau region (Γ_∞) and the amount of adsorbed surfactant with the head groups toward the surface Γ_1 that is equal to the equilibrium surface charge Γ_0 [32]. As a consequence, the amount of surfactant adsorbed with the head groups toward the solution Γ_2 can also be determined [37]. The values of calculated amounts of head groups toward the surface and toward the solution over CMC are presented in Table 3.3. It can be observed that Γ_1 decreases with an increase of pH. This amount seems too small to contribute to total adsorbed amount at pH 6 (Γ_1 < 0.01 mmol/m^2). In 0.1 M NaCl, the head-on to the surface is not significant compared with head-out to solution. When salt concentration increases, SDS head groups toward the α-Al_2O_3 surface decreases, but SDS head groups toward solution increases. Therefore, the values which are given in Table 3 can support for both admicelle and hemimicelle concepts.

Table 3.3 Adsorbed amount of surfactant with head groups toward the surface (Γ_1) and toward solution (Γ_2) at the plateau adsorbed amount (Γ_∞)

C salt (M NaCl)	pH	Γ_∞ (mmol/m^2)	Γ_1 (mmol/m^2)	Γ_2 (mmol/m^2)
0.001	4	1.20	0.70	0.50
0.001	5	0.95	0.14	0.81
0.001	6	0.52	< 0.01	> 0.51
0.01	4	1.55	0.57	0.98
0.01	5	1.10	0.13	0.97
0.01	6	0.65	< 0.01	> 0.64
0.1	4	1.67	0.03	1.64
0.1	5	1.40	0.03	1.37
0.1	6	0.77	< 0.01	> 0.76

As mentioned in sections above, the adsorption isotherms of SDS and proton occurred onto both surface and porous sites of α-Al_2O_3. Basically, it is extremely difficult to form macropores in pure α-Al_2O_3. Nevertheless, Ayeme et al. [53] reported a several pure α-Al_2O_3 crystal particles with macropores of 0.1–3.8 μm in diameter that is in good agreement with α-Al_2O_3 material in our study. The average pore width of our α-Al_2O_3 which was determined by using the Barrett–Joyner–Halenda (BJH) model [54] to the N_2 desorption branch of isotherm was about 0.11 μm. Although the pores in α-Al_2O_3 are difficult to be detected by N_2–BET

(BJH) method, this result can support one explanation for adsorption behavior of SDS and proton into pores of α-Al_2O_3.

In Fig. 3.7, the adsorption of proton expressed by Γ_0 is plotted as a function of the adsorbed amount of surfactant Γ_{SDS} at different pH and salt concentrations. In 0.001 and 0.01 M NaCl, the slopes of all isotherm curves still increase after passing the CIP, which are located at SDS adsorption density around 0.8 and 1.1 mmol/m^2 for pH 5 and pH 4, respectively. It suggests that beyond the CIP the surfactant molecules keep their head groups toward the surface of α-Al_2O_3. The change in proton adsorption still occurs beyond the CIP, demonstrating that the head-on is not completed at the CIP. In addition, the adsorption of SDS and proton could be described well by the two-step model with almost same fit parameters (only small difference in aggregation number), indicating that adsorbing SDS molecules adsorbed protons. In other words, all SDS molecules have their head groups close to the surface than to the solution. Figure 3.8a shows a cartoon representation for SDS adsorption onto α-Al_2O_3 [55] at low salt concentrations. We support for the hemimicelle concept than admicelle concept at low salt concentration. These finding are in good agreement with the published paper [32] in which the adsorption of anionic surfactant SNBS on variable charge surface of TiO_2 is presented by the hemimicelle concept. The presence of admicelles in these cases only appears after the CMC.

At high salt concentration (0.1 M NaCl), SDS adsorption isotherms onto α-Al_2O_3 are predicted well by two-step adsorption model. The proton adsorption is too small to apply this model with the same fit parameters. The proton adsorption can be emphasized by the relationship between adsorption density of proton and SDS onto α-Al_2O_3. Nevertheless, in this case, the slopes of the curves are much less than unity and decrease after the CIP (not shown in detail). From the results of two-step model (Table 3.2), the HMC at high ionic strength is higher than that at low ionic strength but surfactant molecules can form hemimicelles before the CIP (Fig. 3.7). The plateau adsorption is not observed near the CMC because CMC decreases dramatically in 0.1M NaCl. Above the CMC, admicelles can appear in region III when the surface charge is neutralized by adsorbed surfactant ions and micelles appear in solutions. The value of CMC is also smaller than the CIP. Therefore, it suggests that the CIP reveals the formation of local bilayer. After the CIP, the electrostatic attraction between charged surface and SDS head groups is negligible and only lateral hydrophobic attraction and the repulsions of head groups remain [37]. In Fig. 3.8b, a cartoon of the adsorbed admicelles of SDS onto α-Al_2O_3 is represented. The surfactant molecules absorbed onto both porous sites and surface where SDS molecules are oriented with head groups toward solution and the SDS

bilayer [56] on the surface of α-Al_2O_3 is formed. Thus, at high ionic strength, it could argue that admicelles are supported than hemimicelles.

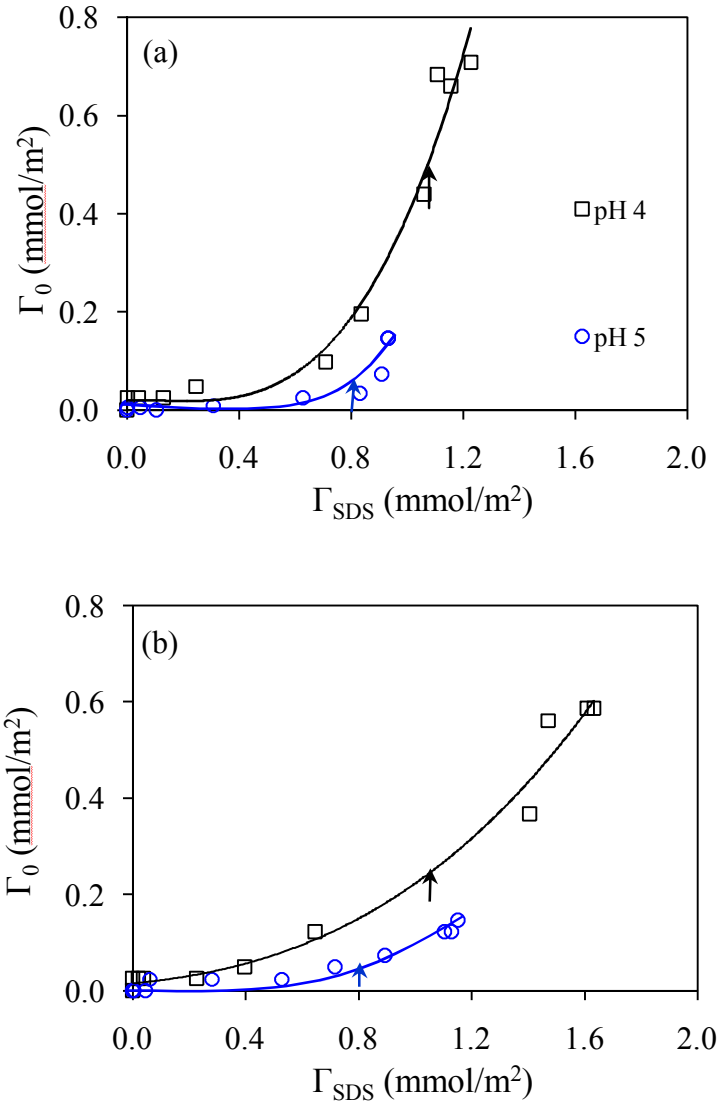

Fig. 3.7. Proton adsorption (Γ_0) as a function of the adsorbed amount of SDS (Γ_{SDS}) onto α-Al_2O_3 at pH 4 and pH 5 in 0.001 M NaCl (a) and 0.01 M NaCl (b). The arrows indicate the CIP. The lines are guides to the eye.

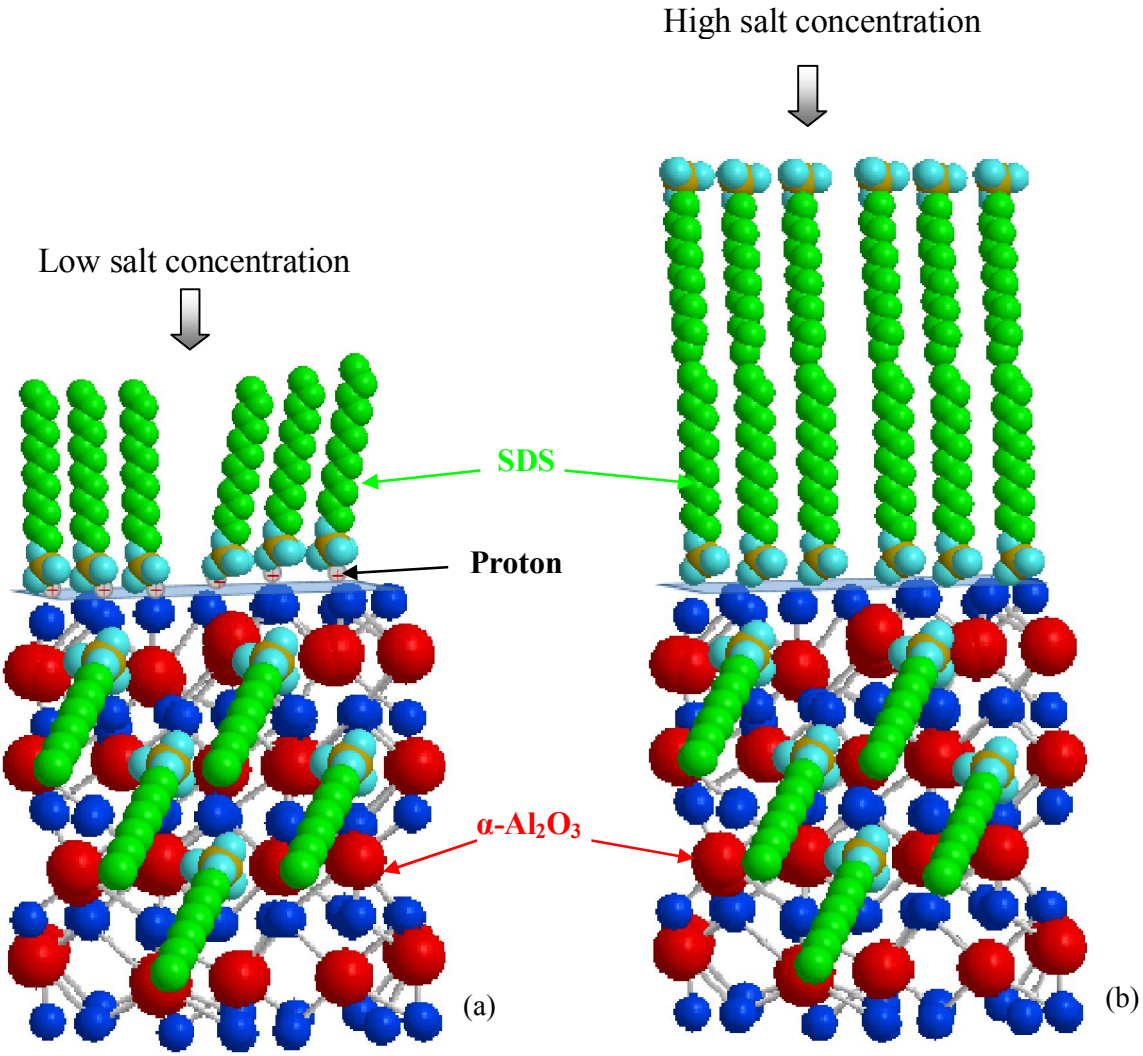

Fig. 3.8. Cartoon showing the adsorbed hemimicelles of SDS (a) and admicelles of SDS (b) onto α-Al_2O_3. Blue spheres represent oxygen atoms, red spheres represent aluminum atoms, and grey spheres represent proton.

3.5. Conclusions

We have studied adsorption of SDS onto large α-Al_2O_3 beads with low specific surface area as functions of pH and NaCl concentration. The adsorption isotherms are in accordance with two-step and four-region models. Four regions of isotherms can be more clearly distinguished for 0.1 M NaCl than that at low salt concentrations due to the presence of admicelles at high salt concentration. With varying pH and salt concentrations, two-step model can reasonably represent adsorption isotherms of SDS onto α-Al_2O_3. At low salt concentrations, the proton adsorption upon SDS adsorption can be fitted by two-step model with almost the same parameters of surfactant adsorption. The proton adsorption amount as a function of SDS adsorption shows that hemimicelle concept is plausible for the case of low ionic strength. At high ionic strength, the increase in the proton adsorption is not significant, indicating that admicelles are presented rather than hemimicelles.

References

[1] R. Atkin, V.S.J. Craig, E.J. Wanless, S. Biggs, Mechanism of cationic surfactant adsorption at the solid–aqueous interface, Advances in Colloid and Interface Science, 103 (2003) 219-304.

[2] K. Esumi, Y. Yamanaka, Interaction between Sodium Dodecyl Poly(oxyethylene) Sulfate and Alumina Surface in Aqueous Solution, Journal of Colloid and Interface Science, 172 (1995) 116-120.

[3] T.P. Goloub, L.K. Koopal, Adsorption of Cationic Surfactants on Silica. Comparison of Experiment and Theory, Langmuir, 13 (1997) 673-681.

[4] E.M. Lee, L.K. Koopal, Adsorption of Cationic and Anionic Surfactants on Metal Oxide Surfaces: Surface Charge Adjustment and Competition Effects, Journal of Colloid and Interface Science, 177 (1996) 478-489.

[5] S. Paria, Surfactant-enhanced remediation of organic contaminated soil and water, Advances in Colloid and Interface Science, 138 (2008) 24-58.

[6] S. Paria, K.C. Khilar, A review on experimental studies of surfactant adsorption at the hydrophilic solid–water interface, Advances in Colloid and Interface Science, 110 (2004) 75-95.

[7] R. Zhang, P. Somasundaran, Advances in adsorption of surfactants and their mixtures at solid/solution interfaces, Advances in Colloid and Interface Science, 123–126 (2006) 213-229.

[8] M. Kobayashi, H. Nanaumi, Y. Muto, Initial deposition rate of latex particles in the packed bed of zirconia beads, Colloids and Surfaces A: Physicochemical and Engineering Aspects, 347 (2009) 2-7.

[9] A. Tulpar, W.A. Ducker, Surfactant Adsorption at Solid−Aqueous Interfaces Containing Fixed Charges: Experiments Revealing the Role of Surface Charge Density and Surface Charge Regulation, The Journal of Physical Chemistry B, 108 (2004) 1667-1676.

[10] A.M.F. Gaudin, D.W. Fuerstenau, Streaming Potential Studies. Quartz Flotation with Anionic Collectors, Transactions AIME, 202 (1955) 958-962.

[11] D.W. Fuerstenau, Streaming Potential Studies on Quartz in Solutions of Aminium Acetates in Relation to the Formation of Hemi- micelles at the Quartz-Solution Interface, The Journal of Physical Chemistry, 60 (1956) 981-985.

[12] D.W. Fuerstenau, H.J. Modi, Streaming Potentials of Corundum in Aqueous Organic Electrolyte Solutions, Journal of The Electrochemical Society, 106 (1959) 336-341.

[13] D.W. Fuerstenau, T. Wakamatsu, Effect of pH on the adsorption of sodium dodecane-sulphonate at the alumina/water interface, Faraday Discussions of the Chemical Society, 59 (1975) 157-168.

[14] T. Wakamatsu, D.W. Fuerstenau, The Effect of Hydrocarbon Chain Length on the Adsorption of Sulfonates at the Solid/Water Interface, Adsorption From Aqueous Solution, American Chemical Society, 1968, pp. 161-172.

[15] P. Somasundaran, D.W. Fuerstenau, Mechanisms of Alkyl Sulfonate Adsorption at the Alumina-Water Interface, The Journal of Physical Chemistry, 70 (1966) 90-96.

[16] P. Somasundaran, T.W. Healy, D.W. Fuerstenau, Surfactant Adsorption at the Solid—Liquid Interface—Dependence of Mechanism on Chain Length, The Journal of Physical Chemistry, 68 (1964) 3562-3566.

[17] J.H. Harwell, J.C. Hoskins, R.S. Schechter, W.H. Wade, Pseudophase separation model for surfactant adsorption: isomerically pure surfactants, Langmuir, 1 (1985) 251-262.

[18] D. Bitting, J.H. Harwell, Effects of counterions on surfactant surface aggregates at the alumina/aqueous solution interface, Langmuir, 3 (1987) 500-511.

[19] M.A. Yeskie, J.H. Harwell, On the structure of aggregates of adsorbed surfactants: the surface charge density at the hemimicelle/admicelle transition, The Journal of Physical Chemistry, 92 (1988) 2346-2352.

[20] B.-Y. Zhu, T. Gu, Surfactant adsorption at solid-liquid interfaces, Advances in Colloid and Interface Science, 37 (1991) 1-32.

[21] A. Fan, P. Somasundaran, N.J. Turro, Adsorption of Alkyltrimethylammonium Bromides on Negatively Charged Alumina, Langmuir, 13 (1997) 506-510.

[22] N.P. Hankins, J.H. O'Have, J.H. Harwell, Modeling Effects of pH and Counterions on Surfactant Adsorption at the Oxide/Water Interface, Industrial & Engineering Chemistry Research, 35 (1996) 2844-2855.

[23] T. Gu, B.-Y. Zhu, The S-type isotherm equation for adsorption of nonionic surfactants at the silica gel—water interface, Colloids and Surfaces, 44 (1990) 81-87.

[24] D.A. Sabatini, R.C. Knox, Transport and Remediation of Subsurface Contaminants, American Chemical Society, Washington DC, USA,1992.

[25] Milton J. Rosen, Joy T. Kunjappu, Surfactants and Interfacial Phenomena 4th Edition, John Wiley&Sons, USA, 2012.

[26] S. Alila, F. Aloulou, D. Beneventi, S. Boufi, Self-Aggregation of Cationic Surfactants onto Oxidized Cellulose Fibers and Coadsorption of Organic Compounds, Langmuir, 23 (2007) 3723-3731.

[27] S. Alila, S. Boufi, M.N. Belgacem, D. Beneventi, Adsorption of a Cationic Surfactant onto Cellulosic Fibers I. Surface Charge Effects, Langmuir, 21 (2005) 8106-8113.

[28] F. Aloulou, S. Boufi, D. Beneventi, Adsorption of organic compounds onto polyelectrolyte immobilized-surfactant aggregates on cellulosic fibers, Journal of Colloid and Interface Science, 280 (2004) 350-358.

[29] P. Chandar, P. Somasundaran, N.J. Turro, Fluorescence probe studies on the structure of the adsorbed layer of dodecyl sulfate at the alumina—water interface, Journal of Colloid and Interface Science, 117 (1987) 31-46.

[30] K. Esumi, T. Nagahama, K. Meguro, Characterization of cationic surfactant adsorbed layer on silica, Colloids and Surfaces, 57 (1991) 149-160.

[31] K. Esumi, H. Otsuka, K. Meguro, Adsorption of binary mixtures of hydrocarbon and fluorocarbon surfactants on alumina, Journal of Colloid and Interface Science, 142 (1991) 582-588.

[32] M.R. Bohmer, L.K. Koopal, Adsorption of ionic surfactants on variable-charge surfaces. 1. Charge effects and structure of the adsorbed layer, Langmuir, 8 (1992) 2649-2659.

[33] M.R. Bohmer, L.K. Koopal, Adsorption of ionic surfactants on variable-charge surfaces. 2. Molecular architecture and structure of the adsorbed layer, Langmuir, 8 (1992) 2660-2665.
[34] M.R. Bohmer, L.K. Koopal, Adsorption of ionic surfactants on constant charge surfaces. Analysis based on a self-consistent field lattice model, Langmuir, 8 (1992) 1594-1602.
[35] L.K. Koopal, E.M. Lee, M.R. Böhmer, Adsorption of Cationic and Anionic Surfactants on Charged Metal Oxide Surfaces, Journal of Colloid and Interface Science, 170 (1995) 85-97.
[36] D.W. Fuerstenau, H.M. Jang, On the nature of alkylsulfonate adsorption at the rutile/water interface, Langmuir, 7 (1991) 3138-3143.
[37] T.P. Goloub, L.K. Koopal, B.H. Bijsterbosch, M.P. Sidorova, Adsorption of Cationic Surfactants on Silica. Surface Charge Effects, Langmuir, 12 (1996) 3188-3194.
[38] C. Attaphong, E. Asnachinda, A. Charoensaeng, D.A. Sabatini, S. Khaodhiar, Adsorption and adsolubilization of polymerizable surfactants on aluminum oxide, Journal of Colloid and Interface Science, 344 (2010) 126-131.
[39] J.J. Lopata, K.M. Werts, J.F. Scamehorn, J.H. Harwell, B.P. Grady, Thermodynamics of mixed anionic/nonionic surfactant adsorption on alumina, Journal of Colloid and Interface Science, 342 (2010) 415-426.
[40] P. Somasundaran, J.T. Kunjappu, In-situ investigation of adsorbed surfactants and polymers on solids in solution, Colloids and Surfaces, 37 (1989) 245-268.
[41] S. Partyka, W. Rudzinski, B. Brun, J.H. Clint, Calorimetric studies of adsorption of anionic surfactants onto alumina, Langmuir, 5 (1989) 297-304.
[42] E. Mączka, J. Luetzenkirchen, M. Kosmulski, The significance of the solid-to-liquid ratio in the electrokinetic studies of the effect of ionic surfactants on mineral oxides, Journal of Colloid and Interface Science, 393 (2013) 228-233.
[43] T.D. Pham, M. Kobayashi, Y. Adachi, Interfacial characterization of α-alumina with small surface area by streaming potential and chromatography, Colloids and Surfaces A: Physicochemical and Engineering Aspects, 436 (2013) 148-157, This Thesis: Chapter 2.
[44] K. Hayashi, A rapid determination of sodium dodecyl sulfate with methylene blue, Analytical Biochemistry, 67 (1975) 503-506.
[45] P. Mukerjee, Use of Ionic Dyes in Analysis of Ionic Surfactants and Other Ionic Organic Compounds, Analytical Chemistry, 28 (1956) 870-873.
[46] D.O. Hummel, Handbook of Surfactant Analysis, John Wiley&Sons, New York, USA, 2000.
[47] L.K. Koopal, T.P. Goloub, T.A. Davis, Binding of ionic surfactants to purified humic acid, Journal of Colloid and Interface Science, 275 (2004) 360-367.

[48] G. Nizri, S. Lagerge, A. Kamyshny, D.T. Major, S. Magdassi, Polymer–surfactant interactions: Binding mechanism of sodium dodecyl sulfate to poly(diallyldimethyl-ammonium chloride), Journal of Colloid and Interface Science, 320 (2008) 74-81.

[49] M. Thongngam, D.J. McClements, Influence of pH, Ionic Strength, and Temperature on Self-Association and Interactions of Sodium Dodecyl Sulfate in the Absence and Presence of Chitosan, Langmuir, 21 (2004) 79-86.

[50] B.-Y. Zhu, T. Gu, General isotherm equation for adsorption of surfactants at solid/liquid interfaces. Part 1. Theoretical, Journal of the Chemical Society, Faraday Transactions 1: Physical Chemistry in Condensed Phases, 85 (1989) 3813-3817.

[51] A. Adak, A. Pal, M. Bandyopadhyay, Removal of phenol from water environment by surfactant-modified alumina through adsolubilization, Colloids and Surfaces A: Physicochemical and Engineering Aspects, 277 (2006) 63-68.

[52] K. Hu, A.J. Bard, Characterization of Adsorption of Sodium Dodecyl Sulfate on Charge-Regulated Substrates by Atomic Force Microscopy Force Measurements, Langmuir, 13 (1997) 5418-5425.

[53] A. Ayame, Y. Uchida, H. Ono, M. Miyamoto, T. Sato, H. Hayasaka, Epoxidation of ethylene over silver catalysts supported on α-alumina crystal carriers, Applied Catalysis A: General, 244 (2003) 59-70.

[54] E.P. Barrett, L.G. Joyner, P.P. Halenda, The Determination of Pore Volume and Area Distributions in Porous Substances. I. Computations from Nitrogen Isotherms, Journal of the American Chemical Society, 73 (1951) 373-380.

[55] G.V. Franks, Y. Gan, Charging Behavior at the Alumina–Water Interface and Implications for Ceramic Processing, Journal of the American Ceramic Society, 90 (2007) 3373-3388.

[56] S.-H. Song, P. Koelsch, T. Weidner, M.S. Wagner, D.G. Castner, Sodium Dodecyl Sulfate Adsorption onto Positively Charged Surfaces: Monolayer Formation With Opposing Headgroup Orientations, Langmuir, 29 (2013) 12710-12719.

Chapter 4. Adsorption characteristics of anionic surfactant and anionic dye onto large α-alumina beads

4.1. Introduction

The treatment of wastewater is of great importance in environmental remediation. Organic dyes are one of the major constituents of wastewater produced from many industries related to textile, paint, pulp and paper, cosmetic, etc [1]. Many dye wastes are colored and extremely toxic [1, 2]. Various treatment techniques have been reported on the removal of dyes from aquatic environment [3, 4] like adsorption [5-8], photocatalytic degradation [9-11], electrochemical oxidation [12, 13], coagulation/ flocculation [14], biological process [15]. Recently, removal of ionic dyes by adsorption from aqueous solutions using surfactant modified solid surface has attracted intense studies [1, 4, 16-19]. The large bead particles are applicable to remove dyes after surface modification with surfactant adsorption [1, 20, 21]. Another feature is that large beads can be directly used to analyze fixed bed column for the study on transport phenomena [16, 18, 19, 22].

Interfacial properties of large beads are changed after adsorption of ionic surfactant in aqueous solution to enhance the removal efficiency of oppositely charged dyes. Surfactant adsorption on the surface of solid beads can be induced by both electrostatic and hydrophobic interactions [23]. Nevertheless, in order to modify the surface of adsorbents for the efficient removal of ionic dyes, it should be assumed that ionic surfactants and ionic dyes are mainly adsorbed on the charged solid surface by electrostatic force [24]. Surfactants modify solid surface with the formation of micelles-like structure and improve the ability of adsorption/adsolubilization. These micelles-like structures are called hemimicelles [25-29] (head groups of surfactant molecules toward solid surface) and admicelles [30-32] (a local bilayer structure with head groups of outer surfactant toward solution). As a consequence, oppositely charged dyes can be efficiently sorbed at the solid-liquid interface and removed from aqueous solutions. Ozcan et al. [21, 33] indicated that surface of bentonite was changed with cationic surfactant to remove anionic dyes by the ion-exchange mechanism. Anjali Pal and co-workers [1, 16, 34] used anionic surfactant sodium dodecyl sulfate (SDS), to modify surface of alumina and chitosan hydrogel beads which can bear negatively charged surface to enhance adsorption of cationic dye, crystal violet, by batch and column studies.

Systematic investigations on the adsorption of both ionic dyes and surfactants on metal oxide beads become more important because of practical utility. However, adsorption characteristics of ionic surfactants are complex when the surface charge of solid adsorbents such as metal oxides is regulated upon surfactant uptake [35-38]. Also, the adsorption properties of ionic dyes are rather complicated due to the complex structures of adsorbed layers when dye molecules have a number of charged groups [2]. Thus, adsorption isotherms of individual ionic dyes and ionic surfactants with variably charged solid surfaces are still inadequate. It is preferable to study a comparative adsorption between ionic surfactants and ionic dyes with the similar charge (anionic or cationic) on oppositely charged surface of solid beads.

Many studies focused on the individual adsorption properties of ionic surfactants and ionic dyes on metal oxides by combining electrokinetic and spectroscopic measurements with modeling [35, 39-44]. While electrokinetic measurements can provide the information about charging behavior of metal oxides in the absence and presence of ionic surfactants or ionic dyes, spectroscopic methods can show the active groups on the surface of adsorbent after adsorption and evaluate the adsorption capacity of surfactants or dyes. The Fourier transform infrared attenuated total reflection (FTIR-ATR) has been successfully used for in situ adsorption studies of surfactant at the solid-solution interface [43], but it is difficult to apply for adsorption on large beads.

The isotherms fitted by theoretical models are useful to better understand the adsorption mechanism and to explain the interaction on the surface of metal oxides between ionic surfactants and ionic dyes. As for describing adsorption characteristics, Langmuir and Freundlich isotherm models are often discussed. Nevertheless, Langmuir and Freundlich models cannot be applied for S-shape or Langmuir-S (LS)-shape adsorption isotherms. Fortunately, a two-step adsorption model presented by Zhu et al. [45] could describe these curves. On the basis of the two-step model, a general adsorption isotherm equation can be derived. This equation was successfully applied to various types of surfactant adsorption isotherms for numerous systems [45, 46]. The general isotherm equation is not only limited to surfactant adsorption but also applicable for proton uptake upon surfactant adsorption [38]. Recently, adsorption isotherms of some kinds of polymers on ZrO_2 nanoparticle [47] and onto cotton fiber [48] were fitted and interpreted by the general equation. The multilayer model which was introduced by the Brunauer-Emmett-Teller (BET), was used to describe adsorption isotherms of some ionic dyes [49-52]. However, the complex multilayer adsorption of ionic dyes fitted by the general equation has not been reported.

Alumina is often used as a substrate for adsorption of anionic surfactants [23, 30, 32, 53-55] and anionic dyes [56-58]. The surface charge adjustment of alumina upon anionic surfactant adsorption has been recognized [30, 38], while a change in pH of aqueous solutions due to adsorption of anionic dyes on alumina has never been reported. The interplay between the pristine surface charge of alumina due to proton adsorption and the adsorption of anionic surfactant sodium dodecyl sulfate (SDS) is too complex to be explained within a simple model [42]. The adsorption of azo sulfonate dyes on alumina is controlled by bridged bidentate complex [39] while adsorption of cationic dye on alumina and SDS modified alumina is mainly promoted by electrostatic interaction, and probably by hydrophobic interaction [1]. The adsorption properties of SDS and azo dye onto alumina are more complicated when sorbents are large beads with low surface area.

In the current study, we investigated the adsorption characteristics of anionic surfactant, SDS, and anionic dye, new coccine (NC), onto large α-Al_2O_3 beads with variably charged surfaces. The effect of SDS and NC adsorption on the surface charge of α-Al_2O_3 is determined by streaming potential. The adsorption mechanisms with adsorbed structures of SDS and NC molecules onto α-Al_2O_3 are proposed on the basis of adsorption isotherms analyzed, with the two-step adsorption model, the evaluated surface charge effect, and the analysis by FTIR-ATR spectra.

4.2. Experimental

4.2.1. Materials

Alpha alumina beads were used as adsorbents. The specific properties and initial treated procedure for adsorption studies were described in chapters 3.

Anionic surfactant sodium dodecyl sulfate (SDS, with purity higher than 95 %), and anionic dye new coccine (NC, with purity higher than 85%), from Wako Pure Chemical Industries were used as adsorbates in surfactant adsorption and dye adsorption, respectively. The chemical structures of SDS is shown in Fig 3.2 (in chapter 3) while NC is indicated in Fig. 4.1. Cationic dye methylene blue (with purity higher 98.5 %), and organic solvent chloroform $CHCl_3$ (GC grade, purity higher 99 %), from Wako Pure Chemical Industries were used to determine concentration of SDS by colorimetric method. Ionic strength and pH were adjusted by the addition of NaCl (Wako Pure Chemical Industries), HCl, and NaOH (volumetric analysis grade, Wako Pure Chemical Industries). Other chemicals were obtained

from Wako. Ultra pure water, produced from Elix Advantage 5 (Millipore) with electric conductivity around 0.6 μS/cm, was used in preparing solutions and in all measurements.

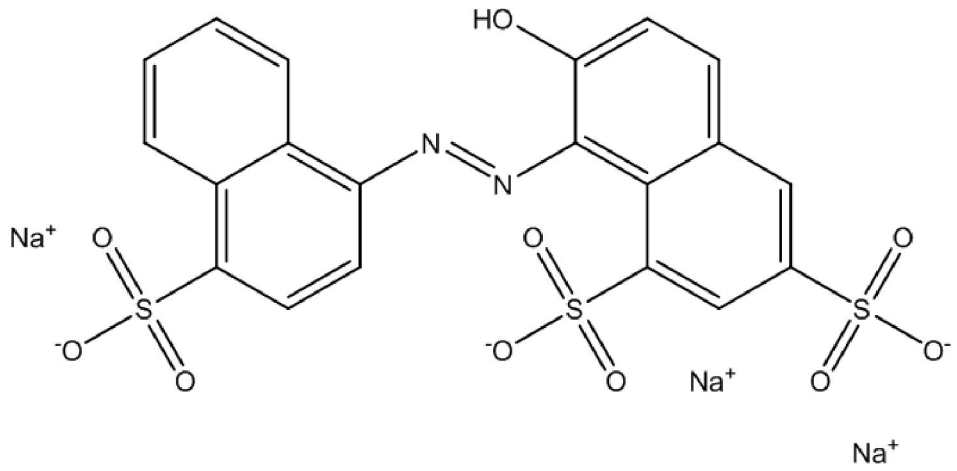

Fig. 4.1. The structure of anionic dye new coccine (NC).

4.2.2. Adsorption isotherms

The batch experiments were carried out in 100-mL Erlenmeyer flask at room temperature, controlled by air conditioner (22 $\pm$ 2 ^{0}C), using a depletion method. To carry out adsorption experiments, 0.5 g of treated α-Al_2O_3 was mixed with 25 mL of NaCl aqueous solutions at different concentrations by a shaker for 1 h.

For NC adsorption studies, the concentration from 10^{-6} M to 10^{-3} M was desired and pH was adjusted to original value. The equilibrium time in dye adsorption was achieved after 3 h while the change in pH of all solutions during adsorption was not significant. The adsorption density of NC (Γ_{NC}) onto α-Al_2O_3 was obtained by the difference in the concentration of NC solutions before and after adsorption by colorimetric method.

To study surfactant adsorption, SDS with concentrations from 10^{-5} M to 10^{-2} M was prepared and pH was also adjusted to original value. The adsorption density of SDS (Γ_{SDS}) and proton adsorption (Γ_0) upon surfactant adsorption onto α-Al_2O_3 was determined according to previous chapter [38].

4.2.3. Colorimetric method

The concentration of anionic dye NC was analyzed by colorimetric method at wavelength 505 nm using an UV-vis spectrophotometer (UV-1650PC, Shimadzu) with a quartz cuvette with a 1-cm optical path length. The relationship between the absorbance and concentrations of NC by standard calibration curves in different electrolyte concentrations and pH should yield a straight line with a correlation coefficient of at least 0.999. Samples were diluted appropriately before measuring the absorbance to quantify NC concentrations by standard calibration curves.

The concentration of anionic surfactant SDS was also determined by colorimetric method using chloroform as the organic solvent and methylene blue as cationic dye. The detail of this procedure was described in elsewhere [38, 59].

4.2.4. Potentiometric method

Potentiometry was conducted using a Metrohm 781 pH/Ion meter, Switzerland. The pH of NaCl solutions used in measuring streaming potential, adsorption isotherm, and determination of the concentration of proton in solutions was measured by a glass combination electrode (Type 6.0258.010 Metrohm). Detail of this method was described in chapter 3 (section 3.2.4). All measurements were carried out at 22 ± 2 ^{0}C. The difference in the CMC of SDS determined via the conductometric and potentiometric methods did not exceed 10 % (section 3.1 in chapter 3). The values of CMC are again listed in Table 4.1.

Table 4.1 Critical micelle concentration (CMC) of SDS at 22^0C

NaCl (M)	CMC (mM)
0	6.0
0.001	5.5
0.01	5.0
0.05	2.5
0.1	2.0
0.2	1.0

4.2.5. Streaming potential measurements

A streaming potential technique was again applied to evaluate the change in surface charge by charactering zeta potential of α-Al_2O_3 before and after adsorption of SDS and NC. The theory behind streaming potential and zeta potential calculation is described in the literature [60, 61]. Briefly, the ζ potential is related to the slope in the streaming potential versus pressure line using Helmholtz – Smoluchowski's equation (HS) [60]:

$$\zeta = \frac{U_{str}}{\Delta P} \times \frac{\eta K_L}{\varepsilon \varepsilon_0} \quad (4.1)$$

where ζ is the zeta potential (mV), U_{str} the difference of potential (mV), ΔP the pressure difference (mbar), η the viscosity of the solution (mPa.s), K_L the conductivity of the solution (mS/cm), ε the relative dielectric constant of the liquid and ε_0 is the electric permittivity of vacuum (8.854×10^{-12} F/m).

A Zeta CAD (CAD Instrument, France) was used in this study. The detail of experimental procedure of streaming potential with Zeta CAD was indicated in section 2.2.3 (chapter 2). Adsorption of SDS and NC onto α-Al_2O_3 was conducted with a solid-to-solution ratio of 200 g/L in 0.01 M NaCl at pH 4.0. The adsorption isotherms were carried out at the concentration of 8×10^{-3} and 10^{-3} M for SDS and NC, respectively. The α-Al_2O_3 beads after adsorption with SDS or NC were separated without washing and dried in air, and then stored in dark container until the measurement of streaming potential.

4.2.6. FTIR-ATR spectroscopy

To confirm surface modification of α-Al_2O_3 and to examine the structures of adsorbed SDS and NC, Fourier transform infrared spectroscopy was taken. The infrared spectra were recorded on a Perkin Elmer GX FT-IR spectrometer equipped with a deuterated glycine sulphate (DTGS) detector. An attenuated total reflection (ATR) attachment with a micro germanium (Ge) crystal was used. The samples used to investigate the effect of SDS and NC adsorption were prepared as follows: The α-Al_2O_3 material (10.0 g) was equilibrated with the concentration of 8×10^{-3} M of SDS or the concentration of 10^{-3} M of NC in 50mL solution of 0.01M NaCl at pH 4 according to adsorption procedure in section 4.2.2. The α-Al_2O_3 samples after adsorption with SDS or NC were separated without rising and dried in air at 70 ^{0}C, and then stored in dark container. The spectrum of SDS and NC powders were obtained without any pretreatment. All samples spectra recorded obtained at room temperature and atmospheric pressure at a resolution of 4 cm^{-1}.

4.3. General isotherm equation

4.3.1. Theory and modeling

The general isotherm equation was derived by assuming that adsorption on solid-liquid interface occurs in two steps [45, 62]. It was originally derived to describe the adsorption of surfactant with hemimicelle formation.

The general isotherm equation is

$$\Gamma = \frac{\Gamma_\infty k_1 C\left(\frac{1}{n} + k_2 C^{n-1}\right)}{1 + k_1 C(1 + k_2 C^{n-1})} \quad (4.2)$$

where Γ is amount of surfactant or dye adsorbed, Γ_∞ is the maximum adsorption, k_1 and k_2 are equilibrium constants for the adsorption of monomers or first layer adsorption, and for clusters of *n* molecules (aggregation number of hemimicelle), or multilayer adsorption, respectively. *C* denotes the concentration of free adsorbates in the bulk solution.

For surfactant adsorption, the hemimicelle concentration (HMC) is rewritten as

$$HMC = \left(\frac{n-1}{n+1}\right)^{\frac{n+1}{n}} K^{\frac{-1}{n}} \quad (4.3)$$

and

$$HMC = \left(\frac{n-2}{n}\right)^{\frac{n}{n-1}} K^{\frac{-1}{n-1}} \quad (4.4)$$

for S-type, and LS-type isotherms, respectively.

In the case of new coccine adsorption, no micelle formation is expected because of its structure [52], but this dye might adsorb in a cooperative fashion; the cooperative structure can be expressed by the parameter *n*.

4.3.2. Fitting procedure

The fitting procedures were described chapter 3 (Section 3.3.2).

4.4. Results and discussion

4.4.1. Streaming potential measurements

Streaming potential was used to monitor the zeta potential at several pH values to identify isoelectric point (IEP) of α-Al_2O_3 before and after adsorption of SDS and NC. The zeta potential was calculated from measured streaming potential with Eq. (4.1). Figure 4.2 indicates the ζ potential of treated α-Al_2O_3 as a function of pH in 0.01 M NaCl. The present IEP of α-Al_2O_3 without SDS and NC (open triangles in Fig. 4.2) which is around 6.7 [63].

Open square points in Fig. 4.2 show that the ζ potential of α-Al_2O_3 increases dramatically in the pH range of 4 – 9 after SDS adsorption. The residual of SDS concentration was above CMC and the maximum adsorption could be reached. Interestingly, the adsorption of an anionic surfactant SDS on a positively charged α-Al_2O_3 surface can induce the increase in zeta potential of the alumina material. The IEP of α-Al_2O_3 after SDS adsorption shifts to 8.7, indicating that after SDS adsorption, the surface charge of α-Al_2O_3 increases by proton adsorption on surface site of α-alumina. Proton binding to α-Al_2O_3 surface after SDS adsorption without washing increased the surface charge upon SDS adsorption on α-Al_2O_3 [38]. In Fig. 4.3a, the schematic representation shows the change in surface charge of α-Al_2O_3 before SDS adsorption, after SDS adsorption and during streaming potential measurement. Surfactant adsorption at low salt concentration with the head group toward the surface induces an increase of surface charge although admicelles can be formed after the CMC. The desorption of SDS molecules is possible in equilibrium step due to a outer-sphere complex between a sulfate group and the Al_2O_3 surface [64]. On one hand, proton adsorption upon SDS adsorption on the Al_2O_3 surface is remaining. As the results, the highly positively charged α-Al_2O_3 surface seems to remain during the measurement of measuring streaming potential.

On the contrary, the zeta potential of α-Al_2O_3 after NC adsorption (open circles in Fig. 4.2) decreases in the range from pH 4 to pH 9, comparing with the treated α-Al_2O_3. The values of ζ potential of α-Al_2O_3 decrease due to the presence of sulfonic groups of azo dye. This trend of ζ potential is close to literatures [24, 40, 65]. Ramesh Kumar and Teli [24] indicated that in the presence of anionic azo dye, CI Direct Yellow 28, the streaming potential of cotton fibers has become more negative than that of raw one. Bourikas et al. [40] has revealed that the magnitude of ζ potential of TiO_2 from pH 2 to pH 8 in 0.01 M $NaNO_3$ reduced significantly in the presence of anionic dye, Acid Orange 7 (AO7) in solutions. The shift of IEP of AO7/TiO_2 suspensions was over 2 pH units. In the present study, the adsorption of dye induces a small

shift of IEP (about 1 pH unit). This precludes a very strong interaction of NC with the surface of α-Al_2O_3. In other word, the inner-sphere complex between sulfonic groups and α-Al_2O_3 surface is not formed. Figure 4.3b shows the illustration of α-Al_2O_3 before and after NC adsorption, at equilibrium and during streaming potential measurement. It shows that the α-Al_2O_3 becomes less positively charged surface after NC adsorption although NC can be partly desorbed in the equilibrium process of streaming potential measurements. Therefore, the adsorption of NC still makes the decrease in surface charge of α-Al_2O_3.

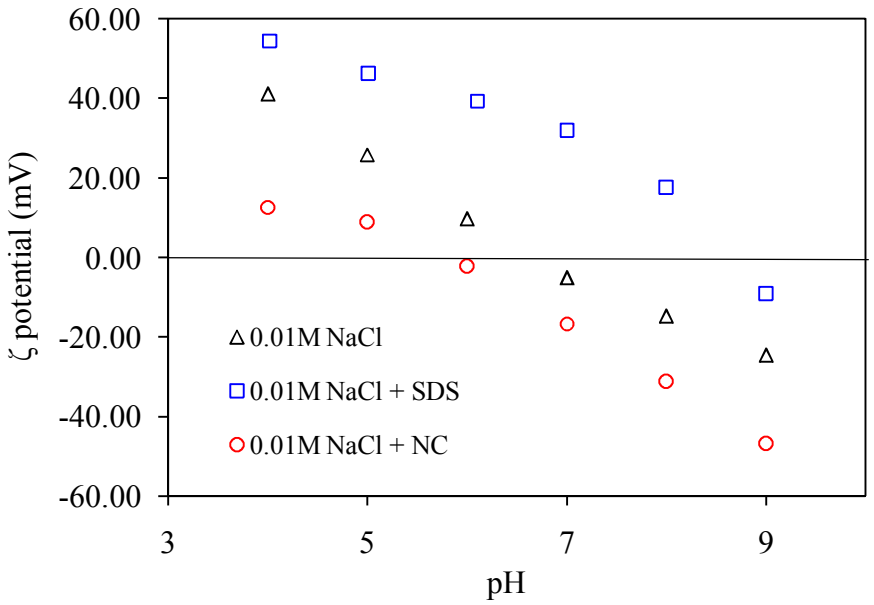

Fig. 4.2. The ζ potential of α-Al_2O_3 without adsorption (open triangles) and after SDS adsorption (open squares) and after NC adsorption (open circles) as the function of pH in 0.01 M NaCl.

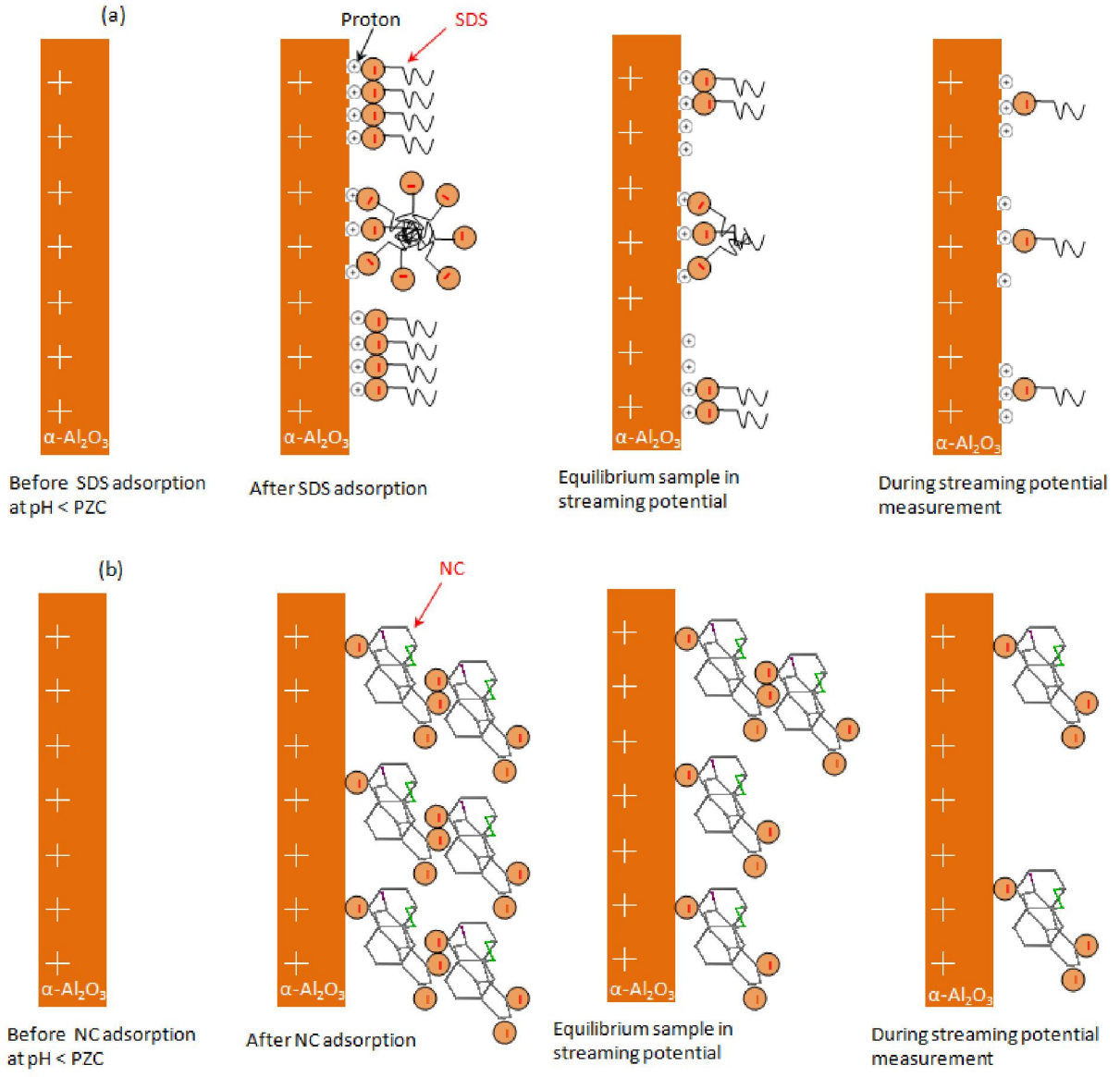

Fig. 4.3. Schematic representations show the change in surface charge of α-Al_2O_3 with the different effect of SDS (a) and NC (b) before adsorption, after adsorption and during streaming potential measurements.

4.4.2. Ex situ FTIR-ATR spectra

The Fourier transform infrared (FTIR) is often used to characterize active groups in the adsorption. FTIR combined with attenuated total reflection for in situ of surface has become one of the powerful tool to explore the solid-liquid interface [66]. The in situ FTIR-ATR was used to investigate the surface excess and molecular orientation of SDS adsorbed at Al_2O_3/ water interface [43]. Nevertheless, in situ technique is not applicable for large particles with small surface area such as α-Al_2O_3 beads in our experiments. Thus, the ex situ FTIR-ATR spectra of α-Al_2O_3 beads without adsorption and after adsorption of SDS (Al_2O_3-SDS), and NC (Al_2O_3-NC) have been assigned in the wavenumber range of 1000 – 2200 cm^{-1} are shown in Fig. 4.4. The FTIR-ATR spectra of SDS and NC powders which have been recorded from 400 cm^{-1} to 4000 cm^{-1} are given in Fig. 4.5.

In Fig. 4.4, the spectra of Al_2O_3-SDS presents a large band near 1618 cm^{-1} that corresponds to the bending vibrations of adsorbed water molecular [67]. This band is much stronger than that of Al_2O_3, indicating that the existence of larger amount of adsorbed water upon SDS adsorption. A weak peak of Al_2O_3-SDS at 1470 cm^{-1} is assigned to the alkyl bending modes of SDS molecules [68]. The asymmetrical deformation vibration of CH_3 at 1468 cm^{-1} can be seen in the FTIR spectra of SDS powder (Fig. 4.5) that is very close to the peak of 1470 cm^{-1} found in spectra of pristine SDS [67]. From the curve of Al_2O_3-SDS compared with the curve of SDS in the wavenumber range of 400 – 4000 cm^{-1}, the relative intensity of asymmetrical and symmetrical stretching of $–CH_2–$ are represented at about 2919 and 2850 cm^{-1} decreases dramatically (not shown in detail). These results suggest that the hydrophobic interaction between hydrocarbon chains can work on the surface of α-Al_2O_3. The adsorption of SDS onto α-Al_2O_3 was conducted at higher concentration than CMC so that admicelle (local bilayer formation) could be formed after the formation of hemimicelle. The characteristic peak of SO_4^{2-} at about 1219 cm^{-1} [43, 67, 68] of Al_2O_3-SDS is similar to this peak of Al_2O_3 (Fig. 4.4) while this peak of SDS powder appears strongly in Fig. 4.5. In addition, Del Nero et al. [69] indicated that the band appeared at around 1216 cm^{-1} due to the FTIR-ATR spectra of pure α-Al_2O_3 coating deposited on Ge crystal in 0.01 M NaCl at pH 3.3. It is demonstrated that SDS with the sulfate head groups contact to the surface of α-Al_2O_3 via the electrostatic attraction. The results of FTIR-ATR spectra of α-Al_2O_3 after SDS adsorption compared with others of SDS powder and α-Al_2O_3 beads suggest that SDS molecules mainly adsorb on the surface of α-Al_2O_3 by electrostatic attraction as well as probably by hydrophobic interaction.

In Fig. 4.4, the large band at around 1612 cm^{-1} appeared in the spectra of Al_2O_3-NC. But the magnitude of this band is similar to another one of Al_2O_3 beads, demonstrating that increased amount of adsorbed water upon NC adsorption is not significant. The spectra of NC powder in Fig. 4.5 indicated that the bands at 1423, 1491, 1570 and 1632 cm^{-1} were assigned to C = C of naphthalene rings or phenyl ring vibration with stretching of the C = N group that corresponded to active groups of azo dye. These bands are in good agreement with the spectra of NC [70]. The appearance and the shifts of the bands were also seen in Fig. 4.4 with wavenumber of 1407, 1514, 1550 cm^{-1} appeared in the spectra of Al_2O_3-NC. Thus, the hydrophobic groups cannot contact the hydrophilic surface of alumina. It should be noted that the strong bands at 1193 and 1047 cm^{-1} corresponded to the vibrations of the O – S – (O_2) group [39, 40] of NC molecules (Fig. 4.5) disappeared in the spectra of Al_2O_3-NC (Fig. 4.4). This result suggests the adsorption of NC molecules on the alumina surface via two oxygen atoms of sulfonic group of the azo dye [39, 40]. The FTIR-ATR spectra of α-Al_2O_3 after adsorption of NC imply that the surface of α-Al_2O_3 is modified by adsorbed NC molecules via sulfonic groups. Therefore, we support that NC molecules mainly adsorb on the surface of α-Al_2O_3 by electrostatic attraction.

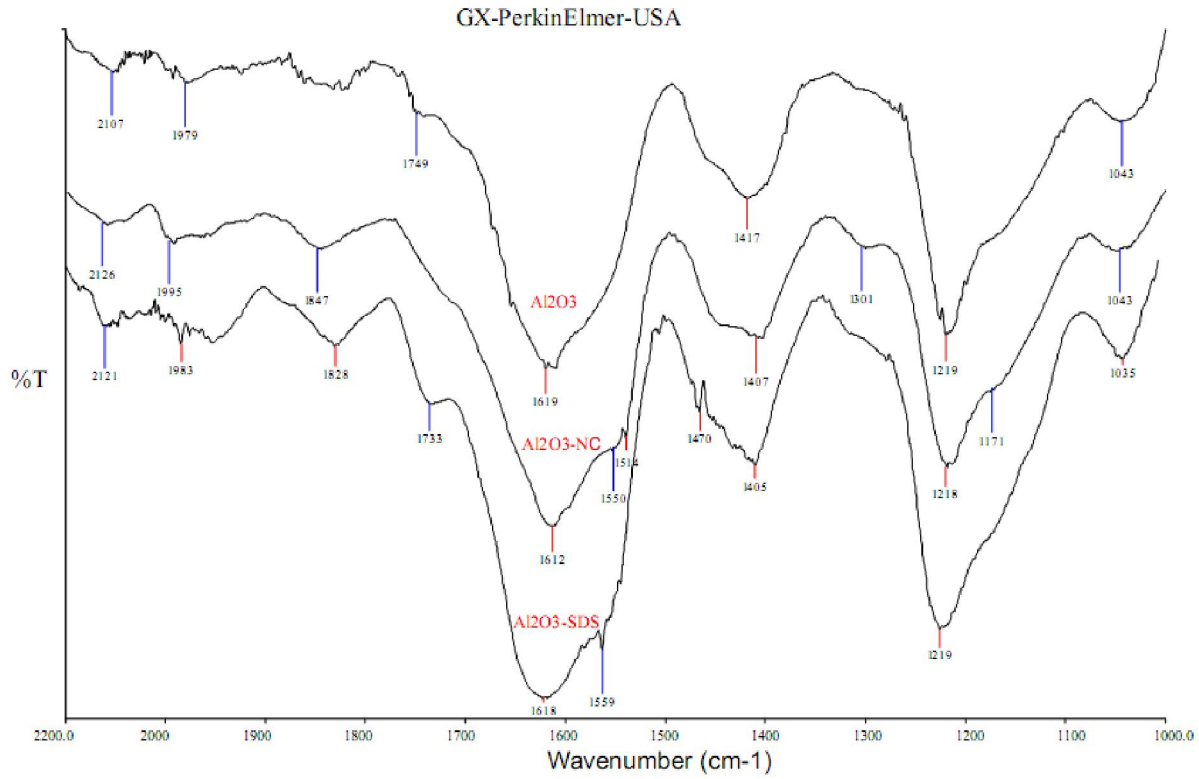

Fig. 4.4. Ex situ FTIR-ATR spectra for α-Al_2O_3 without adsorption and after SDS adsorption and after NC adsorption.

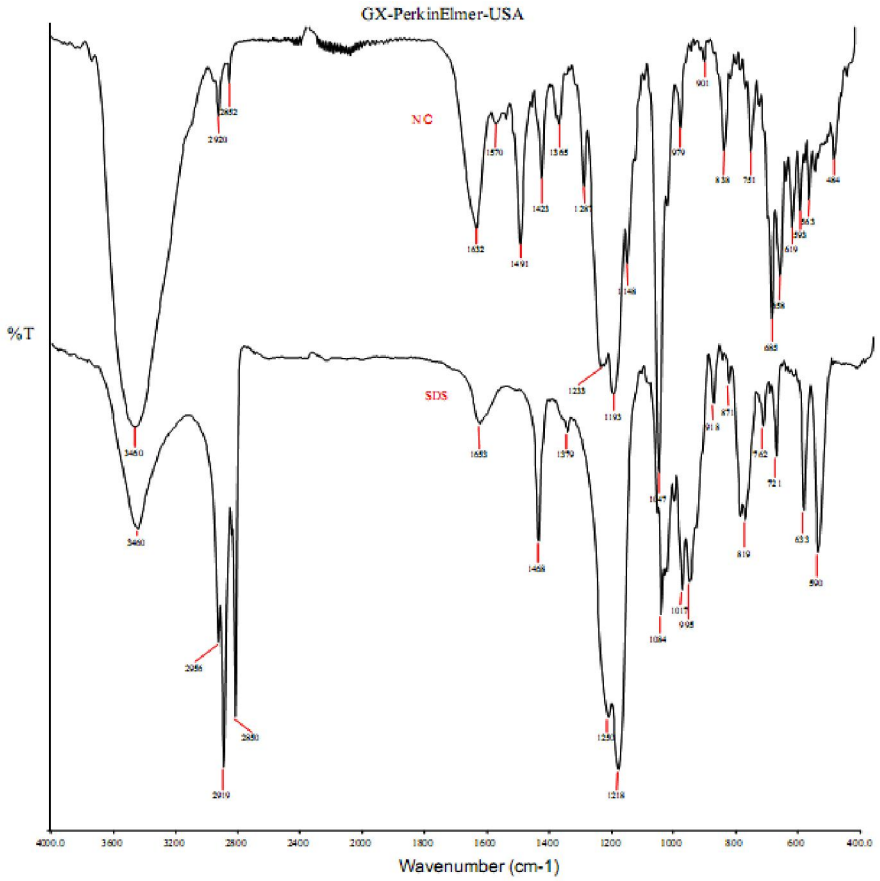

Fig. 4.5. FTIR-ATR spectra of SDS and NC powders in the wavenumber range of 400 – 4000 cm^{-1}

4.4.3. Adsorption isotherms discussed by two-step model

4.4.3.1. Surface charge and surfactant isotherms

The effect of pH and ionic strength on SDS adsorption to α-Al_2O_3 surface is well known and demonstrated in the isotherms. As shown in Fig. 4.6, the calculated curves by two-step adsorption model at different pH and ionic strength (solid lines) can reasonably represent experimental data by using the parameters in Table 4.2. From the fitting procedure (see section 3.3.2), the values of n_{SDS} are chosen about 10. As shown in Fig. 4.6, the adsorption density of SDS onto α-Al_2O_3 reaches constant around the CMC in different pH, except for high ionic strength. In 0.1 M NaCl, the plateau adsorption is not observed near the CMC. These trends are in good agreement with previously published papers [30, 53, 71]. The increase of adsorbed amount with surfactant concentration after the CMC in 0.1 M NaCl can be explained by the dramatic decrease of CMC in high ionic strength [35] (see CMC of SDS in Table 4.1). The micellization takes place in bulk solution at low surfactant concentration in high ionic strength because of the decrease in the thickness of ionic surrounding surfactant head groups [23]. As the result, an increase in concentration of surfactant probably promote the adsorption due to the presence of hemicelles or/ and admicelles [72] on the surface of α-Al_2O_3.

Table 4.2. The fit parameters for SDS adsorption, which are maximum adsorbed amount $\Gamma_{\infty,SDS}$, the equilibrium constants $k_{1,SDS}$ and $k_{2,SDS}$ for first step and second step, respectively, n_{SDS} the aggregation number of hemimicelle and HMC the hemimicelle concentration.

C salt (M NaCl)	pH	$\Gamma_{\infty,SDS}$ (mmol/m^2)	$k_{1,SDS}$ (m^2/mmol)	$k_{2,SDS}$ (m^2/mmol)$^{n-1}$	n_{SDS}	HMC (mM) (Eq. (4.3))	HMC (mM) (Eq. (4.4))
0.001	4	1.20	6×10^3	1×10^{24}	9.8	1.17	1.45
0.001	5	0.95	6×10^3	6×10^{23}	9.8	1.23	1.54
0.001	6	0.52	6×10^3	5×10^{23}	9.8	1.25	1.57
0.01	4	1.55	4×10^3	8×10^{23}	9.8	1.25	1.49
0.01	5	1.10	4×10^3	7×10^{23}	9.8	1.26	1.51
0.01	6	0.65	4×10^3	6×10^{23}	9.9	1.37	2.66
0.1	4	1.67	1×10^3	6×10^{22}	10.1	2.25	2.46
0.1	5	1.40	1×10^3	5×10^{22}	10.1	2.29	2.51
0.1	6	0.77	1×10^3	4×10^{22}	10.1	2.35	2.57

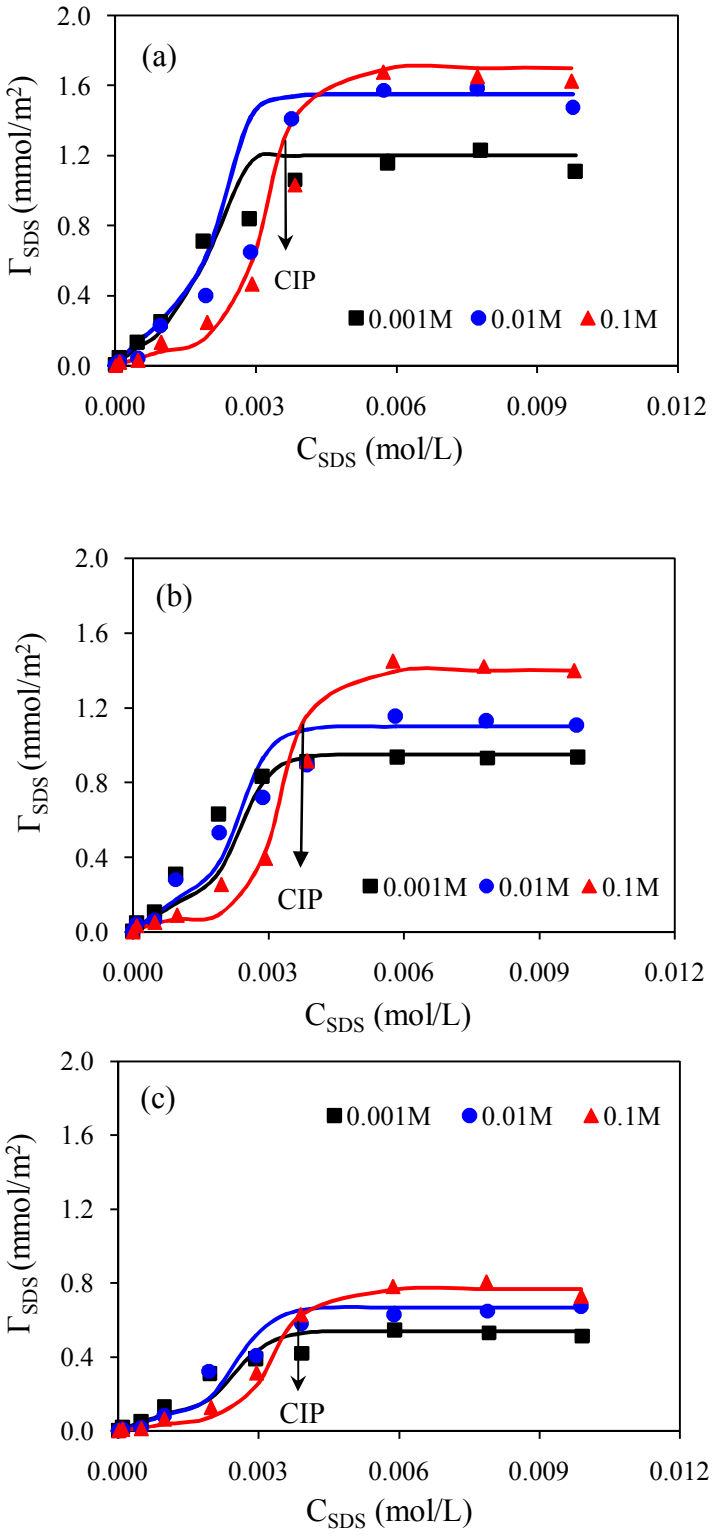

Fig. 4.6. Adsorption isotherms of SDS onto α-Al_2O_3 at pH 4 (a), pH 5 (b), pH 6 (c), and three salt concentrations as a function of the equilibrium SDS concentration. While the points are experimental data, the solid lines are the results of two-step adsorption model.

Figure 4.6 and Table 4.2 show the salt effect and its relation to two steps of isotherms. The values of $k_{1,SDS}$ can be kept as constant and equal to 6×10^3, 4×10^3 and 10^3 for 0.001 M, 0.01 M and 0.1 M NaCl, respectively. Higher $k_{1,SDS}$ values are observed for the lower electrolyte concentration in which the higher adsorption density in the first step is obtained. Adsorption density at low SDS concentration decreases with increasing salt concentration because the electrostatic attraction between the negatively charged SDS head groups and positively charged surface sites is screened by increasing salt concentrations. Nevertheless, an increase of SDS concentration in solutions induces the reversed effect of salt so that the adsorption decreases with increasing electrolyte concentration due to screening of repulsive force between negatively charged DS^- ions. The isotherms show a common intersection point (CIP) at which the electrostatic contribution to the free energy of adsorption vanishes and the salt effect disappears. The CIP is obtained more clearly in the isotherms at log – log scale than linear – linear scale [35, 37, 41]. According to the results of previous work [38], we show here the positions of CIP in the linear – linear scale to demonstrate the different effect of ionic strength in surfactant adsorption compared with the adsorption of anionic azo dye shown in the next section. Above the CIP, adsorption density at high salt concentration is enhanced due to the reduced electrostatic repulsion between the SDS head groups. The isotherms show the CIP which is probably due to the surface charge adjustment upon surfactant adsorption and the effect of hydrophobic interaction between chains in surfactant adsorption above the HMC.

Figure 4.6 shows that the adsorption density is highly affected by pH of solutions at the same salt concentration. The maximum adsorption density decreases with increasing pH due to the difference in equilibrium surface charge isotherms. The surface charge changes more significantly in low salt concentrations and low pH values. The charge adjustment at pH 4 and pH 5 shown in Figs. 4.7 and 4.8 demonstrates that the proton adsorption (Γ_0) upon SDS uptake (Γ_{SDS}) increases with increasing the concentration of SDS. The change in surface charge increases significantly in the region ranging from HMC to CMC. The plateau adsorption density of proton is observed at the maximum of SDS adsorption. At pH 6, it is extremely difficult to evaluate the change in surface charge (data not shown) because of very low proton concentration in solutions. Also, at high salt concentration (0.1 M NaCl), this change is negligible. As can be seen in Table 4.2 and Fig. 4.6, when the change of surface charge is significant, the HMC is much lower (higher $k_{2,SDS}$) because charge adjustment probably enhances the formation of hemimicelles.

In order to study the surface charge effect in more detail, the experiments were conducted at pH 4 and pH 5 in 0.001 and 0.01 M NaCl. In Figs. 4.7 and 4.8, the points are experimental data while the solid lines are the results of two-step adsorption model for adsorption isotherms both of SDS and proton. From Figs. 4.7 and 4.8, the two-step adsorption model can represent proton adsorption as well as SDS adsorption. Another outstanding feature is that we are able to use almost the same fitting parameters ($k_{1,SDS}$ and $k_{2,SDS}$) of two-step model for SDS adsorption onto α-Al_2O_3 to describe adsorption of proton upon surfactant uptake. The values of aggregation number for proton adsorption (n = 10. 6 for pH 4, and n = 10.8 for pH 5) are slightly higher than those of the hemimicelle ($n_{SDS} \approx 10$). The adsorption amount of proton due to adsorbing SDS molecules is much smaller below the HMC than above the HMC. Also, the maximum adsorption density of both SDS and proton has been reached around the CMC.

At low salt concentrations, the amount of proton adsorption is smaller than that for surfactant but the proton uptake or the change in surface charge seems to be significant. The charge adjustment is in good agreement with the results of streaming potential of α-Al_2O_3 after SDS adsorption (section 4.4.1). The screening by SDS molecules is important to induce the proton adsorption. The effect of initial pH in proton adsorption is only significant when surfactant molecules adsorb with head groups toward the surface. Conversely, if their head groups of surfactants are toward solution, the influence on the change of surface charge is negligible. In addition, the net charge at the surface site of the bilayer is very low and the screening of any remaining net charge in hydrophobic core is not significant [35]. These findings indicate that the adsorption isotherms of SDS onto α-Al_2O_3 at low ionic strength are in accordance with the hemimicelle concept. At high salt concentration, the adsorption isotherms of SDS onto α-Al_2O_3 at different pH were fitted well by two-step model but the adsorption of proton was very small so that only the hemimicelles could not be supportable.

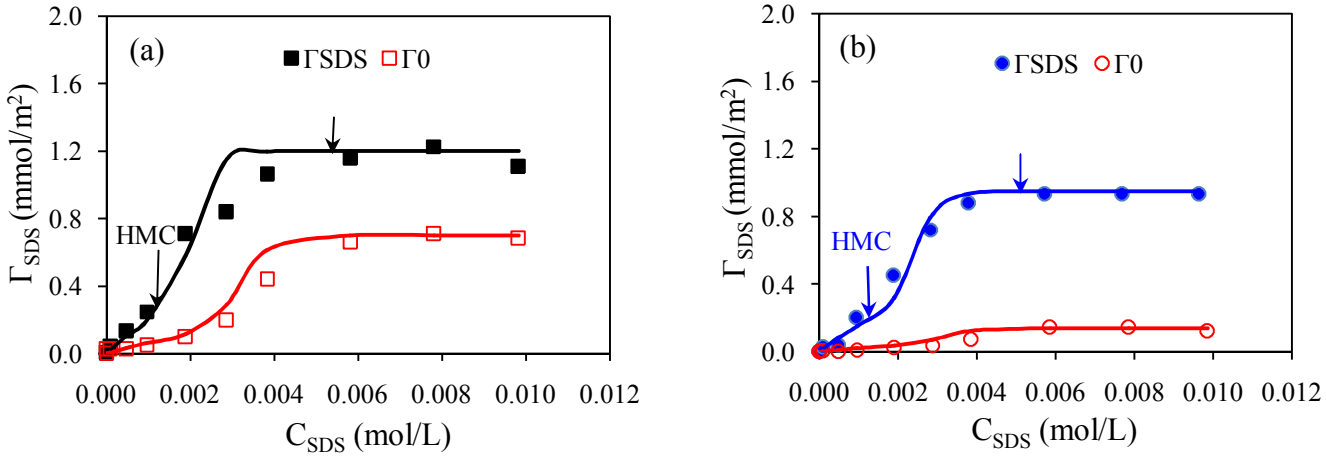

Fig. 4.7. Adsorption isotherms of SDS (Γ_{SDS}) and proton (Γ_0) onto α-Al_2O_3 as a function of the equilibrium SDS concentration at pH 4 (a) and pH 5 (b) in 0.001 M NaCl. The points are experimental data while the solid lines are the results of two-step adsorption model. The above arrows indicate the CMC.

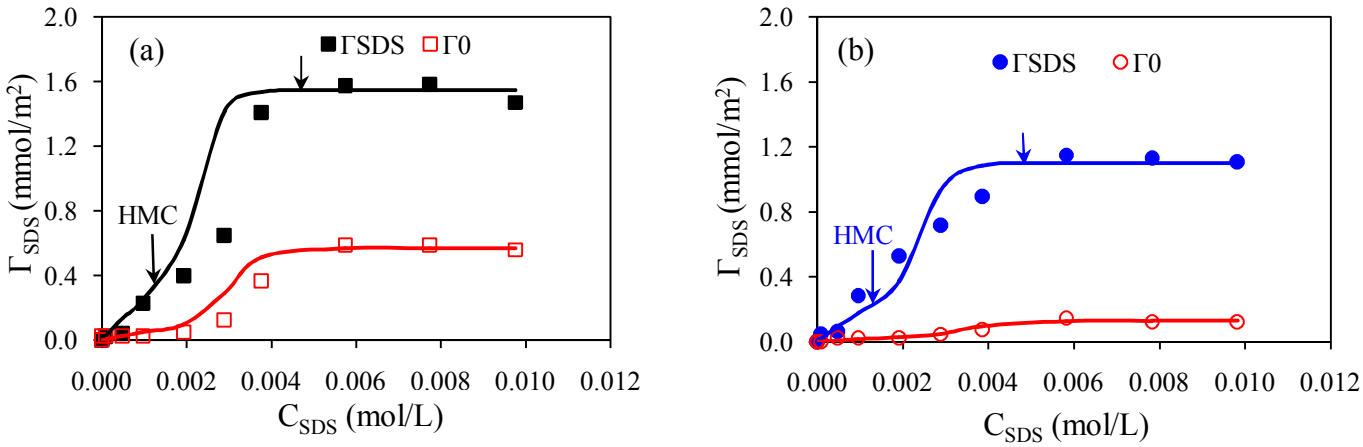

Fig. 4.8. Adsorption isotherms of SDS (Γ_{SDS}) and proton (Γ_0) onto α-Al_2O_3 as a function of the equilibrium SDS concentration at pH 4 (a) and pH 5 (b) in 0.01 M NaCl. The points are experimental data while the solid lines are the results of two-step adsorption model. The above arrows indicate the CMC.

4.4.3.2. Dye adsorption isotherms

Adsorption isotherms of NC onto large α-Al_2O_3 beads with positively charged surface carried out at several pH values and three salt concentrations are shown in Fig. 4.9. The influence of ionic strength is clearly observed at a given pH value. The NC adsorption density decreases with increasing ionic strength that is close to the result of NC adsorption onto positively charged sludge particulates at pH < 3 [52]. The increase in salt concentration increases the number of anions (counter ions) on the positively charged surface of α-Al_2O_3 beads, reducing the electrostatics effect of α-Al_2O_3 surface to dye molecules. In other words, the electrostatic attraction between the negative charge of sulfonic groups of NC dye and positively charged surface is screened by increasing salt concentrations. These trends are similar to the adsorption of SDS below the CIP. However, for dye adsorption, this effect of salt remains from low to high equilibrium concentration of dye so that the CIP is not observed at different pH values. As seen from the isotherms in Fig. 4.9, at different pH and ionic strength, the experimental results were fitted well by general isotherm equation Eq. (4.2) with the fit parameters in Table 4.3.

Tables 4.2 and 4.3 show that the maximum adsorption density of NC ($\Gamma_{\infty,\mathrm{NC}}$) is much lower than one of SDS ($\Gamma_{\infty,\mathrm{SDS}}$) at the same conditions although molecular weight of NC is about 2 times higher than molecular weight of SDS. For SDS adsorption, the micelles are formed with aggregation numbers of hemimicelle ($n_{\mathrm{SDS}} \approx 10$) that are about 5 times higher than n_{NC} ($n_{\mathrm{NC}} \approx 2$) for NC adsorption. It can also be observed that the values of $k_{1,\mathrm{NC}}$ and $k_{1,\mathrm{SDS}}$ are not very different while the values of $k_{2,\mathrm{SDS}}$ are greatly higher than $k_{2,\mathrm{NC}}$ (10^{19} to 10^{20} times). These results reveal that micellization of NC cannot occur on the surface of α-Al_2O_3 as well as on sludge particulates [52]. As shown in Table 4.3, increasing ionic strength induces a decrease in $k_{1,\mathrm{NC}}$ except for 0.1M NaCl while a change in $k_{2,\mathrm{NC}}$ is not significant ($k_{2,\mathrm{NC}} \approx 8.0\times10^{3}$ m^2/mmol). The monolayer adsorption in the case of NC adsorption is influenced by ionic strength but the multilayer adsorption is not affected by ionic strength. Wang et al. [52] indicated that adsorption of NC onto sludge particulates at different pH and ionic strength probably followed multilayer isotherm. In the paper [52], although the values of $k_{1,\mathrm{NC}}$ and $k_{2,\mathrm{NC}}$ are different from our results ($k_{1,\mathrm{NC}}$ is higher than $k_{2,\mathrm{NC}}$), the influence of ionic strength on isotherms seems to be similar to ours. Adsorption of NC onto sludge particles with high surface area reaches equilibrium very fast (about 30 minutes). On the other hand, NC adsorption onto large α-Al_2O_3 beads with small surface area takes long equilibrium time (after

180 minutes: not shown in detail). It implies that the specific surface area could promote equilibrium process of NC adsorption onto solid surface.

Figure 4.9 and Table 4.3 also show that dye adsorption density is strongly dependent on pH and the equilibrium concentration of dye in solutions at a given ionic strength. Adsorption amount of NC onto α-Al_2O_3 beads increases with decreasing pH. The PZC of α-Al_2O_3 is about 6.7 and the decrease of pH induces an increase in the positive charge on surface of α-Al_2O_3. Since the NC dye is negatively charged, the attractive force between anionic dye and positively charged surface α-Al_2O_3 will be enhanced with a decrease in pH. These trends are similar to adsorption of anionic dyes on positively charged metal oxides surface. Adsorption density of azo dyes with sulfonic group on metal oxide surfaces is reported [39, 40] in which adsorption density decreases with increasing solution pH and become negligible for pH values higher than PZC. Furthermore, the change of pH upon NC adsorption is negligible or proton adsorption is not significant, meaning that the surface charge of α-Al_2O_3 is only affected by adsorbed amount of NC. Thus, the IEP of α-Al_2O_3 shifts to the lower pH after NC adsorption (see section 4.4.1).

The results of adsorption isotherms of anionic azo dye onto α-Al_2O_3 indicated above are in good agreement with our electrokinetic and spectroscopic data as well as the results of previous researches [39, 40]. Nevertheless, the influence of ionic strength to adsorption of azo dyes on the metal oxides by experiment and modeling was not shown in published papers [39, 40]. On one hand, the effects of pH and ionic strength to the adsorption of trivalent sulfonic dye, NC onto α-Al_2O_3 in our study are close to the results of Wang et al.[52] who studied adsorption of NC onto sludge particulates. However, in the paper [52], the electrokinetic and spectroscopic data and structure of adsorbed NC have not reported. In current study, we succeeded to relate the electrokinetic and spectroscopic information with adsorption isotherms by two-step model to propose the structure of adsorbed NC onto α-Al_2O_3.

Table 4.3. The fit parameters for NC adsorption, which are maximum adsorbed amount $\Gamma_{\infty,NC}$, the equilibrium constants $k_{1,NC}$ and $k_{2,NC}$ for first layer adsorption and multilayer adsorption, respectively, n_{NC} the aggregation number of NC molecules

C salt (M NaCl)	pH	$\Gamma_{\infty,NC}$ (mmol/m^2)	$k_{1,NC}$ (m^2/mmol)	$k_{2,NC}$ (m^2/mmol)$^{n-1}$	n_{NC}
0.001	4	0.42	2.0×10^3	8.0×10^3	2
0.001	5	0.35	1.9×10^3	8.0×10^3	2
0.001	6	0.30	1.6×10^3	8.0×10^3	2
0.01	4	0.35	1.2×10^3	1.0×10^4	2
0.01	5	0.27	1.0×10^3	8.0×10^3	2
0.01	6	0.20	0.6×10^3	8.0×10^3	1.9
0.1	4	0.27	1.2×10^3	8.0×10^3	2
0.1	5	0.16	1.0×10^3	8.0×10^3	2
0.1	6	0.13	0.6×10^3	8.0×10^3	1.9

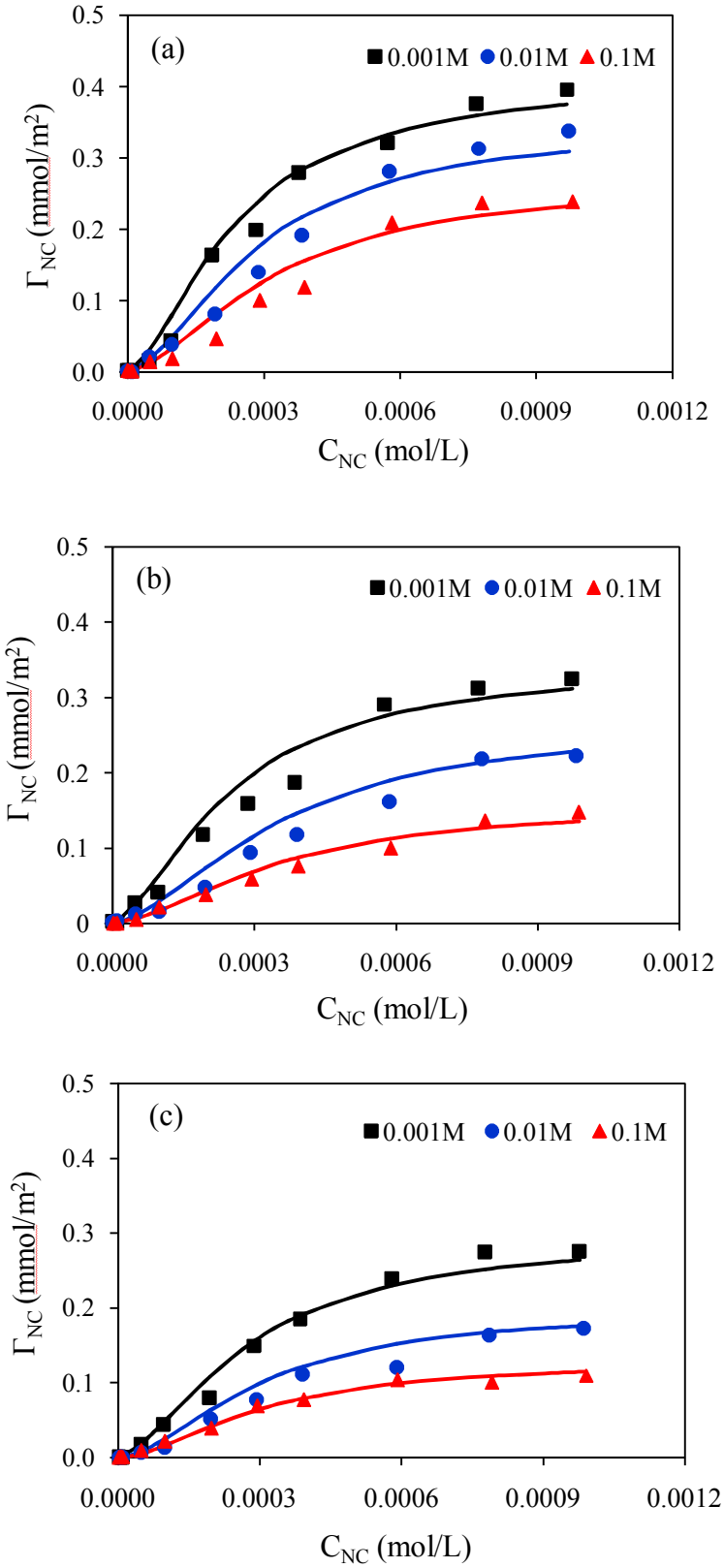

Fig. 4.9. Adsorption isotherms of NC onto α-Al_2O_3 at pH 4 (a), pH 5 (b), pH 6 (c), and three salt concentrations. The points are experimental data while the solid lines are the results of two-step adsorption model.

4.4.4. Structures of adsorbed SDS and NC onto α-Al_2O_3

Anionic surfactant, SDS and anionic dye, NC after adsorption caused the opposite effect in surface charge of α-Al_2O_3 beads that was demonstrated by streaming potential. FTIR-ATR indicated the presence and absence of different functional groups on the surface of α-Al_2O_3 after adsorption of SDS and NC. The streaming potential and FTIR-ATR combined with adsorption isotherms can provide the information about structures of adsorbed surfactant and dye onto α-Al_2O_3. Let us discuss the structures of adsorbed SDS and NC on the surface sites of α-Al_2O_3 beads in more detail.

The structure of adsorbed layer of ionic surfactant onto metal oxides could be dependent on ionic strength. Therefore, it was emphasized by evaluating the change in surface charge upon surfactant adsorption [35, 36, 38]. Surface charge adjustment is one important factor contributing the presence of common intersection point (CIP). Adsorption of anionic surfactant SDS induces an increase in the surface charge of α-Al_2O_3 because at low salt concentration the presence of hemimicelle with head groups toward surface can screen surface charge. This change in surface charge, which was evaluated by streaming potential (section 4.4.1), agreed well with the result of proton uptake upon surfactant adsorption by depletion method. It suggests that beyond the CIP the surfactant molecules keep their head groups toward the surface of α-Al_2O_3 at low salt concentration. The change in proton adsorption still occurs beyond the CIP, demonstrating the head-on is not completed at the CIP. In addition, the adsorption of SDS and proton could be described well by the two-step model with almost the same fit parameters (only small difference in aggregation number), indicating that adsorbing SDS molecules adsorbed protons. In other words, all SDS molecules have their head groups close to the surface than to the solution at low salt concentrations. Figure 4.10a shows a cartoon representation for SDS adsorption onto α-Al_2O_3 [73] in the presence of hemimicelles at low salt concentrations. Although the FTIR-ATR spectra of α-Al_2O_3 after SDS adsorption at 0.01M NaCl (pH 4) indicated that the alkyl bending groups probably appeared, admicelles could only occur after CMC. We support for the hemimicelle concept than admicelle concept at low salt concentrations below CMC.

At high salt concentration (0.1 M NaCl), proton adsorption is too small to be recognized. From the results of the two-step model (Table 4.2), the HMC at high ionic strength is higher than that at low ionic strength but surfactant molecules can form hemimicelles before CIP. The plateau adsorption is not observed near the CMC because the CMC decreases dramatically in 0.1 M NaCl. Above the CMC, admicelles probably appear on the surface when the surface

charge is neutralized by adsorbed surfactant ions and micelles appear in solutions. The value of CMC is also smaller than CIP. Therefore, it suggests that the CIP reveals the formation of local bilayer. After CIP, the electrostatic attraction between charged surface and SDS head groups is negligible and only lateral hydrophobic attraction and the repulsions between head groups remain [36]. In Fig. 4.10b, a cartoon of the adsorbed admicelles of SDS onto α-Al_2O_3 is represented. The surfactant molecules absorbed onto α-Al_2O_3 where SDS molecules are oriented with head groups toward solution and the SDS bilayer [74] on the surface of α-Al_2O_3 is formed. Thus, at high ionic strength, it could argue that admicelles are supported than hemimicelles.

The two-step model was established to describe the NC adsorption onto α-Al_2O_3, suggesting that dye adsorption could occur with cooperative manner. Adsorption of NC decreases with increasing pH due to a decrease of positive surface charge. The change in pH during NC adsorption was not observed so that the net charge of α-Al_2O_3 is strongly dependent on the amount of NC adsorption. A small decrease of surface charge or small reduction of zeta potential was obtained by streaming potential, in accordant with low adsorption amount of NC, compared with SDS adsorption. We confirmed that adsorption of NC onto α-Al_2O_3 surface occurs via only one sulfonic group of azo dye. It was supported by the results of ex situ FTIR-ATR spectra as well as the adsorption isotherms. These results suggest that the adsorption of NC onto α-Al_2O_3 is mainly controlled by the electrostatic attraction between positively charged surface α-Al_2O_3 and negatively charged sulfonic group. In this case, the formation of a bridged bidentate complex can be formed [39] irrespective of salt concentrations. However, the formation of a bidentate inner sphere surface complex is not supported as the cases of adsorption of anionic dye Acid Orange 7 on the TiO_2 [40] or adsorption of azo dye Orange G on α-Fe_2O_3 [39] because NC is easily desorbed in equilibrium and measuring processes of streaming potential (section 4.4.1). In streaming potential measurement, the desorption of NC can be recognized from color change of α-Al_2O_3 beads packed in a glass column. Also, the NC desorption took place quickly at high salt concentration and high pH by batch experiment (not shown in detail).

The adsorption of NC was probably influenced by the positions of sulfonic group. In this research, we suggest that only one sulfonic group on the naphthalene ring without hydroxyl group favors the dye adsorption of NC while two sulfonic groups on another naphthalene ring do not contribute for adsorption. Figure 4.11 shows a cartoon representation of the adsorbed structure of NC onto α-Al_2O_3. In Fig. 4.11, a NC molecule adsorbed onto α-Al_2O_3 via the sulfonic group of the dye, forming a bridge bidentate complex between two aluminum ions

and the surface oxygens. It is close to the results of Bourikas et al. [40], who proposed the similar structure of the adsorbed AO7. The lower adsorption amount of NC onto α-Al_2O_3 can also be explained by a crystalline face and a metal – metal distance rather than specific surface area although the surface area seems to be an important factor to control adsorption. In the paper [39], the same reason was found to demonstrate a higher adsorption of anionic azo dye Orange II on α-Fe_2O_3 than TiO_2 and Al_2O_3 oxides.

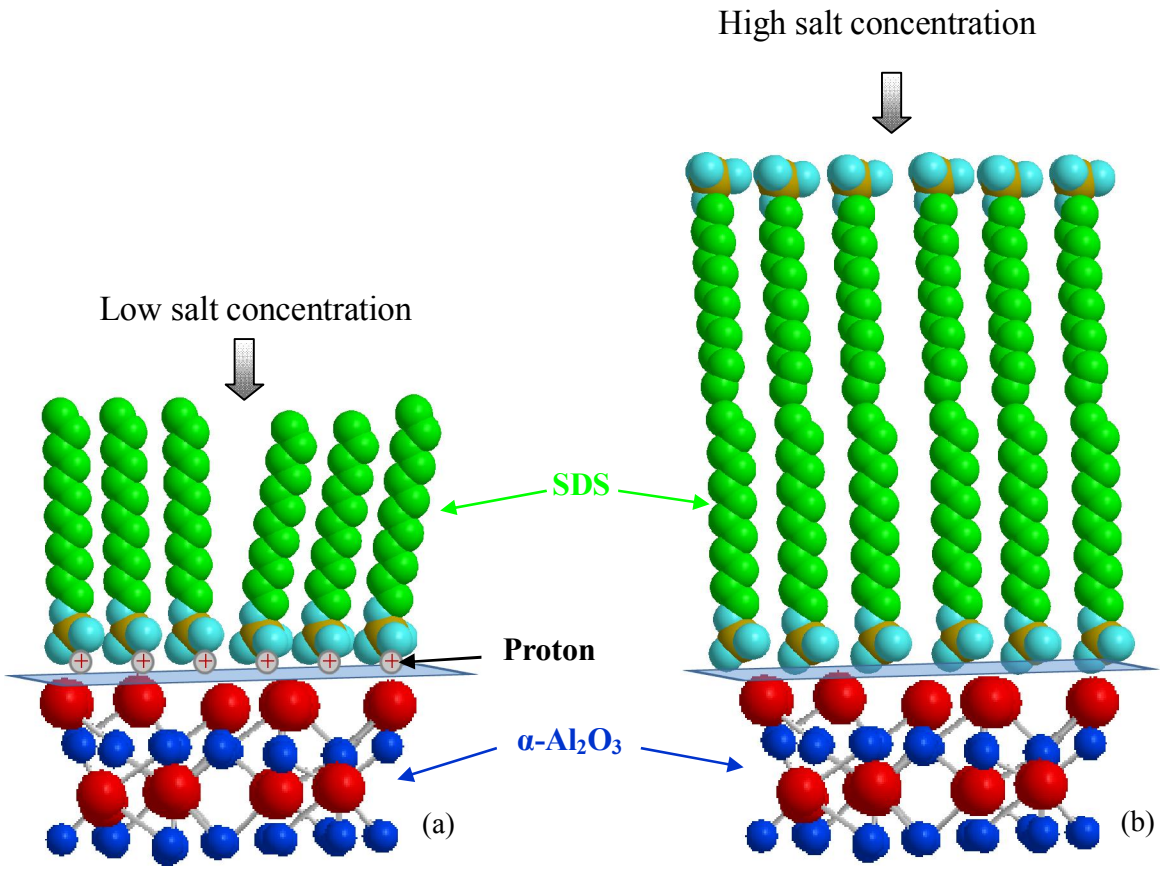

Fig. 4.10. Cartoon showing the adsorbed hemimicelles of SDS (a) and admicelles of SDS (b) onto α-Al_2O_3. Blue spheres represent oxygen atoms, red spheres represent aluminum atoms and grey spheres represent proton.

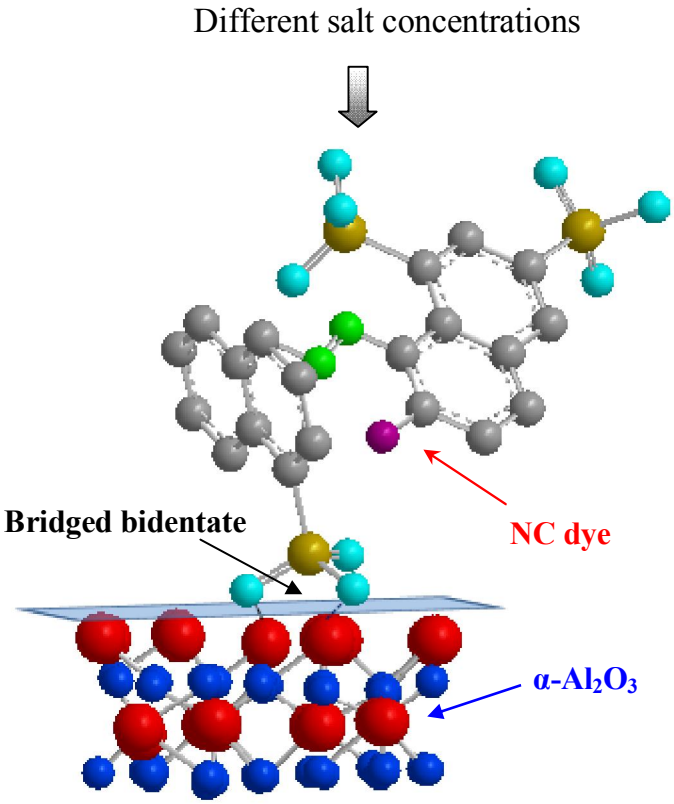

Fig. 4.11. Cartoon representation of structure of the adsorbed NC onto α-Al_2O_3. Two oxygen atoms of the sulfonic group on naphthalene ring favor the adsorption of NC dye by the bridged bidentate complex.

4.5. Conclusions

We have analyzed adsorption properties of anionic surfactant, SDS and anionic dye, NC onto α-alumina with large size in this chapter. Streaming potential indicated that the IEP of α-Al_2O_3 increases after SDS adsorption due to additional proton adsorption while the IEP shifts to the lower pH after adsorption of NC because of the adsorption of negatively charged sulfonic group of the dye. FTIR-ATR confirmed the presence and absence of different active groups of SDS and NC on the surface of α-Al_2O_3. The two-step adsorption model was successfully applied to represent the experimental results of both SDS and NC adsorption isotherms onto α-Al_2O_3. The calculated curves from two-step model for proton adsorption isotherms at low salt concentrations upon surfactant adsorption can also be fitted well, while a change in pH of solutions upon NC adsorption is not observed. Adsorption density of SDS and NC increases with decreasing pH due to an increase in initial positive surface charge of α-Al_2O_3. At a given pH value, the adsorption of SDS below the CIP and NC adsorption decrease with an increase of salt concentration. The salt effect is reversed above the CIP for surfactant adsorption. That is, the adsorption isotherms of SDS and NC are different. Adsorption of SDS is induced by the presence of hemimicelles and admicelles at the α-Al_2O_3/ water interface. Adsorption of NC is affected by the formation of a bridged bidentate complex between two oxygen ions of only one sulfonic group on the naphthalene ring and the surface of α-Al_2O_3, resulting in that adsorption density of surfactant is much higher than that of dye.

References

[1] A. Adak, M. Bandyopadhyay, A. Pal, Removal of crystal violet dye from wastewater by surfactant-modified alumina, Separation and Purification Technology, 44 (2005) 139-144.

[2] Y.C. Wong, Y.S. Szeto, W.H. Cheung, G. McKay, Equilibrium Studies for Acid Dye Adsorption onto Chitosan, Langmuir, 19 (2003) 7888-7894.

[3] E. Forgacs, T. Cserháti, G. Oros, Removal of synthetic dyes from wastewaters: a review, Environment International, 30 (2004) 953-971.

[4] V.K. Gupta, Suhas, Application of low-cost adsorbents for dye removal – A review, Journal of Environmental Management, 90 (2009) 2313-2342.

[5] C.A.P. Almeida, N.A. Debacher, A.J. Downs, L. Cottet, C.A.D. Mello, Removal of methylene blue from colored effluents by adsorption on montmorillonite clay, Journal of Colloid and Interface Science, 332 (2009) 46-53.

[6] M. Doğan, M. Alkan, A. Türkyilmaz, Y. Özdemir, Kinetics and mechanism of removal of methylene blue by adsorption onto perlite, Journal of Hazardous Materials, 109 (2004) 141-148.

[7] B.H. Hameed, M.I. El-Khaiary, Removal of basic dye from aqueous medium using a novel agricultural waste material: Pumpkin seed hull, Journal of Hazardous Materials, 155 (2008) 601-609.

[8] M.A. Schoonen, J.M.T. Schoonen, Removal of crystal violet from aqueous solutions using coal, Journal of Colloid and Interface Science, 422 (2014) 1-8.

[9] F. Al-Momani, E. Touraud, J.R. Degorce-Dumas, J. Roussy, O. Thomas, Biodegradability enhancement of textile dyes and textile wastewater by VUV photolysis, Journal of Photochemistry and Photobiology A: Chemistry, 153 (2002) 191-197.

[10] S.-F. Kang, C.-H. Liao, S.-T. Po, Decolorization of textile wastewater by photo-fenton oxidation technology, Chemosphere, 41 (2000) 1287-1294.

[11] M. Pérez, F. Torrades, X. Domènech, J. Peral, Fenton and photo-Fenton oxidation of textile effluents, Water Research, 36 (2002) 2703-2710.

[12] N. Mohan, N. Balasubramanian, C.A. Basha, Electrochemical oxidation of textile wastewater and its reuse, Journal of Hazardous Materials, 147 (2007) 644-651.

[13] A.G. Vlyssides, M. Loizidou, P.K. Karlis, A.A. Zorpas, D. Papaioannou, Electrochemical oxidation of a textile dye wastewater using a Pt/Ti electrode, Journal of Hazardous Materials, 70 (1999) 41-52.

[14] S. Papić, N. Koprivanac, A. Lončarić Božić, A. Meteš, Removal of some reactive dyes from synthetic wastewater by combined Al(III) coagulation/carbon adsorption process, Dyes and Pigments, 62 (2004) 291-298.

[15] S. Ledakowicz, M. Solecka, R. Zylla, Biodegradation, decolourisation and detoxification of textile wastewater enhanced by advanced oxidation processes, Journal of Biotechnology, 89 (2001) 175-184.

[16] A. Adak, M. Bandyopadhyay, A. Pal, Fixed bed column study for the removal of crystal violet (C. I. Basic Violet 3) dye from aquatic environment by surfactant-modified alumina, Dyes and Pigments, 69 (2006) 245-251.

[17] A. Faki, M. Turan, O. Ozdemir, A.Z. Turan, Analysis of Fixed-Bed Column Adsorption of Reactive Yellow 176 onto Surfactant-Modified Zeolite, Industrial & Engineering Chemistry Research, 47 (2008) 6999-7004.

[18] Y. Su, B. Zhao, W. Xiao, R. Han, Adsorption behavior of light green anionic dye using cationic surfactant-modified wheat straw in batch and column mode, Environ Sci Pollut Res, 20 (2013) 5558-5568.

[19] B. Zhao, Y. Shang, W. Xiao, C. Dou, R. Han, Adsorption of Congo red from solution using cationic surfactant modified wheat straw in column model, Journal of Environmental Chemical Engineering, 2 (2014) 40-45.

[20] S. Chatterjee, D.S. Lee, M.W. Lee, S.H. Woo, Enhanced adsorption of congo red from aqueous solutions by chitosan hydrogel beads impregnated with cetyl trimethyl ammonium bromide, Bioresource Technology, 100 (2009) 2803-2809.

[21] A. Özcan, Ç. Ömeroğlu, Y. Erdoğan, A.S. Özcan, Modification of bentonite with a cationic surfactant: An adsorption study of textile dye Reactive Blue 19, Journal of Hazardous Materials, 140 (2007) 173-179.

[22] M. Kobayashi, H. Nanaumi, Y. Muto, Initial deposition rate of latex particles in the packed bed of zirconia beads, Colloids and Surfaces A: Physicochemical and Engineering Aspects, 347 (2009) 2-7.

[23] Milton J. Rosen, Joy T. Kunjappu, Surfactants and Interfacial Phenomena 4th Edition, John Wiley&Sons, USA, 2012.

[24] A. Ramesh Kumar, M.D. Teli, Electrokinetic studies of modified cellulosic fibres, Colloids and Surfaces A: Physicochemical and Engineering Aspects, 301 (2007) 462-468.

[25] D.W. Fuerstenau, Streaming Potential Studies on Quartz in Solutions of Aminium Acetates in Relation to the Formation of Hemi- micelles at the Quartz-Solution Interface, The Journal of Physical Chemistry, 60 (1956) 981-985.

[26] D.W. Fuerstenau, H.J. Modi, Streaming Potentials of Corundum in Aqueous Organic Electrolyte Solutions, Journal of The Electrochemical Society, 106 (1959) 336-341.

[27] A.M.F. Gaudin, D.W. Fuerstenau, Streaming Potential Studies. Quartz Flotation with Anionic Collectors, Transactions AIME, 202 (1955) 958-962.

[28] P. Somasundaran, T.W. Healy, D.W. Fuerstenau, Surfactant Adsorption at the Solid—Liquid Interface—Dependence of Mechanism on Chain Length, The Journal of Physical Chemistry, 68 (1964) 3562-3566.

[29] T. Wakamatsu, D.W. Fuerstenau, The Effect of Hydrocarbon Chain Length on the Adsorption of Sulfonates at the Solid/Water Interface, Adsorption From Aqueous Solution, American Chemical Society, 1968, pp. 161-172.
[30] D. Bitting, J.H. Harwell, Effects of counterions on surfactant surface aggregates at the alumina/aqueous solution interface, Langmuir, 3 (1987) 500-511.
[31] J.H. Harwell, J.C. Hoskins, R.S. Schechter, W.H. Wade, Pseudophase separation model for surfactant adsorption: isomerically pure surfactants, Langmuir, 1 (1985) 251-262.
[32] M.A. Yeskie, J.H. Harwell, On the structure of aggregates of adsorbed surfactants: the surface charge density at the hemimicelle/admicelle transition, The Journal of Physical Chemistry, 92 (1988) 2346-2352.
[33] A.S. Özcan, B. Erdem, A. Özcan, Adsorption of Acid Blue 193 from aqueous solutions onto Na–bentonite and DTMA–bentonite, Journal of Colloid and Interface Science, 280 (2004) 44-54.
[34] A. Pal, S. Pan, S. Saha, Synergistically improved adsorption of anionic surfactant and crystal violet on chitosan hydrogel beads, Chemical Engineering Journal, 217 (2013) 426-434.
[35] M.R. Bohmer, L.K. Koopal, Adsorption of ionic surfactants on variable-charge surfaces. 1. Charge effects and structure of the adsorbed layer, Langmuir, 8 (1992) 2649-2659.
[36] T.P. Goloub, L.K. Koopal, B.H. Bijsterbosch, M.P. Sidorova, Adsorption of Cationic Surfactants on Silica. Surface Charge Effects, Langmuir, 12 (1996) 3188-3194.
[37] L.K. Koopal, E.M. Lee, M.R. Böhmer, Adsorption of Cationic and Anionic Surfactants on Charged Metal Oxide Surfaces, Journal of Colloid and Interface Science, 170 (1995) 85-97.
[38] T.D. Pham, M. Kobayashi, Y. Adachi, Adsorption of anionic surfactant sodium dodecyl sulfate onto alpha alumina with small surface area, Colloid Polym Sci, (2014), In press, This Thesis: Chapter 3.
[39] J. Bandara, J.A. Mielczarski, J. Kiwi, 1. Molecular Mechanism of Surface Recognition. Azo Dyes Degradation on Fe, Ti, and Al Oxides through Metal Sulfonate Complexes, Langmuir, 15 (1999) 7670-7679.
[40] K. Bourikas, M. Stylidi, D.I. Kondarides, X.E. Verykios, Adsorption of Acid Orange 7 on the Surface of Titanium Dioxide†, Langmuir, 21 (2005) 9222-9230.
[41] T.P. Goloub, L.K. Koopal, Adsorption of Cationic Surfactants on Silica. Comparison of Experiment and Theory, Langmuir, 13 (1997) 673-681.
[42] E. Mączka, J. Luetzenkirchen, M. Kosmulski, The significance of the solid-to-liquid ratio in the electrokinetic studies of the effect of ionic surfactants on mineral oxides, Journal of Colloid and Interface Science, 393 (2013) 228-233.

[43] R.P. Sperline, Y. Song, H. Freiser, Fourier transform infrared attenuated total reflection spectroscopy linear dichroism study of sodium dodecyl sulfate adsorption at the alumina/water interface using alumina-coated optics, Langmuir, 8 (1992) 2183-2191.

[44] R. Zhang, P. Somasundaran, Advances in adsorption of surfactants and their mixtures at solid/solution interfaces, Advances in Colloid and Interface Science, 123–126 (2006) 213-229.

[45] B.-Y. Zhu, T. Gu, Surfactant adsorption at solid-liquid interfaces, Advances in Colloid and Interface Science, 37 (1991) 1-32.

[46] T. Gu, B.-Y. Zhu, The S-type isotherm equation for adsorption of nonionic surfactants at the silica gel—water interface, Colloids and Surfaces, 44 (1990) 81-87.

[47] R. Ndong, W. Russel, Linear viscoelasticity of ZrO 2 nanoparticle dispersions with associative polymers, Rheol Acta, 51 (2012) 771-782.

[48] I. Hoffmann, C. Oppel, U. Gernert, P. Barreleiro, W. von Rybinski, M. Gradzielski, Adsorption Isotherms of Cellulose-Based Polymers onto Cotton Fibers Determined by Means of a Direct Method of Fluorescence Spectroscopy, Langmuir, 28 (2012) 7695-7703.

[49] F. Doulati Ardejani, K. Badii, N.Y. Limaee, S.Z. Shafaei, A.R. Mirhabibi, Adsorption of Direct Red 80 dye from aqueous solution onto almond shells: Effect of pH, initial concentration and shell type, Journal of Hazardous Materials, 151 (2008) 730-737.

[50] A. Kamari, W.S.W. Ngah, M.Y. Chong, M.L. Cheah, Sorption of acid dyes onto GLA and H2SO4 cross-linked chitosan beads, Desalination, 249 (2009) 1180-1189.

[51] J.S. Piccin, C.S. Gomes, L.A. Feris, M. Gutterres, Kinetics and isotherms of leather dye adsorption by tannery solid waste, Chemical Engineering Journal, 183 (2012) 30-38.

[52] J. Wang, C.P. Huang, H.E. Allen, D.K. Cha, D.-W. Kim, Adsorption Characteristics of Dye onto Sludge Particulates, Journal of Colloid and Interface Science, 208 (1998) 518-528.

[53] K. Esumi, Y. Yamanaka, Interaction between Sodium Dodecyl Poly(oxyethylene) Sulfate and Alumina Surface in Aqueous Solution, Journal of Colloid and Interface Science, 172 (1995) 116-120.

[54] J.J. Lopata, K.M. Werts, J.F. Scamehorn, J.H. Harwell, B.P. Grady, Thermodynamics of mixed anionic/nonionic surfactant adsorption on alumina, Journal of Colloid and Interface Science, 342 (2010) 415-426.

[55] P. Somasundaran, D.W. Fuerstenau, Mechanisms of Alkyl Sulfonate Adsorption at the Alumina-Water Interface, The Journal of Physical Chemistry, 70 (1966) 90-96.

[56] R.G. Harris, J.D. Wells, B.B. Johnson, Selective adsorption of dyes and other organic molecules to kaolinite and oxide surfaces, Colloids and Surfaces A: Physicochemical and Engineering Aspects, 180 (2001) 131-140.

[57] V.K. Jain, G.L. Mundhara, J.S. Tiwari, Sorption—desorption studies of anionic dyes on alumina pretreated with acids, Colloids and Surfaces, 29 (1988) 373-389.

[58] B. Yahyaei, S. Azizian, Rapid adsorption of anionic dyes by ordered nanoporous alumina, Chemical Engineering Journal, 209 (2012) 589-596.

[59] K. Hayashi, A rapid determination of sodium dodecyl sulfate with methylene blue, Analytical Biochemistry, 67 (1975) 503-506.

[60] A.V. Delgado, F. González-Caballero, R.J. Hunter, L.K. Koopal, J. Lyklema, Measurement and interpretation of electrokinetic phenomena, Journal of Colloid and Interface Science, 309 (2007) 194-224.

[61] R. J.Hunter, Zeta potential in Colloid Science, Academic Press, London, 1981.

[62] B.-Y. Zhu, T. Gu, General isotherm equation for adsorption of surfactants at solid/liquid interfaces. Part 1. Theoretical, Journal of the Chemical Society, Faraday Transactions 1: Physical Chemistry in Condensed Phases, 85 (1989) 3813-3817.

[63] T.D. Pham, M. Kobayashi, Y. Adachi, Interfacial characterization of α-alumina with small surface area by streaming potential and chromatography, Colloids and Surfaces A: Physicochemical and Engineering Aspects, 436 (2013) 148-157, This Thesis: Chapter 2.

[64] P.M. Karlsson, A.E.C. Palmqvist, K. Holmberg, Adsorption of Sodium Dodecyl Sulfate and Sodium Dodecyl Phosphate on Aluminum, Studied by QCM-D, XPS, and AAS, Langmuir, 24 (2008) 13414-13419.

[65] M.M. Ramos-Tejada, A. Ontiveros-Ortega, E. Giménez-Martín, M. Espinosa-Jiménez, A. Molina Díaz, Effect of polyethyleneimine ion on the sorption of a reactive dye onto Leacril fabric: Electrokinetic properties and surface free energy of the system, Journal of Colloid and Interface Science, 297 (2006) 317-321.

[66] A.R. Hind, S.K. Bhargava, A. McKinnon, At the solid/liquid interface: FTIR/ATR — the tool of choice, Advances in Colloid and Interface Science, 93 (2001) 91-114.

[67] L. Zhao, L. Gao, Coating multi-walled carbon nanotubes with zinc sulfide, Journal of Materials Chemistry, 14 (2004) 1001-1004.

[68] M.K. Singh, A. Agarwal, R. Gopal, R.K. Swarnkar, R.K. Kotnala, Dumbbell shaped nickel nanocrystals synthesized by a laser induced fragmentation method, Journal of Materials Chemistry, 21 (2011) 11074-11079.

[69] M. Del Nero, C. Galindo, R. Barillon, E. Halter, B. Madé, Surface reactivity of α-Al2O3 and mechanisms of phosphate sorption: In situ ATR-FTIR spectroscopy and ζ potential studies, Journal of Colloid and Interface Science, 342 (2010) 437-444.

[70] I.Y. Park, K. Kuroda, C. Kato, Direct synthesis of intercalation compounds between a layered double hydroxide and an anionic dye, Journal of the Chemical Society, Dalton Transactions, (1990) 3071-3074.

[71] P. Somasundaran, J.T. Kunjappu, In-situ investigation of adsorbed surfactants and polymers on solids in solution, Colloids and Surfaces, 37 (1989) 245-268.

[72] F. Aloulou, S. Boufi, D. Beneventi, Adsorption of organic compounds onto polyelectrolyte immobilized-surfactant aggregates on cellulosic fibers, Journal of Colloid and Interface Science, 280 (2004) 350-358.

[73] G.V. Franks, Y. Gan, Charging Behavior at the Alumina–Water Interface and Implications for Ceramic Processing, Journal of the American Ceramic Society, 90 (2007) 3373-3388.

[74] S.-H. Song, P. Koelsch, T. Weidner, M.S. Wagner, D.G. Castner, Sodium Dodecyl Sulfate Adsorption onto Positively Charged Surfaces: Monolayer Formation With Opposing Headgroup Orientations, Langmuir, 29 (2013) 12710-12719.

Chapter 5. Adsorption characteristics of poly(styrenesulfonate) onto large α-alumina beads

5.1. Introduction

Removal organic pollutant is important for water treatment in environmental engineering. Among numerous treatment techniques for organic pollutants from water, adsorption is one of the most commonly used technology that can be applicable for developing countries by using cheap adsorbents [1-3]. Recently, the removal of organic contaminants by adsorption from aqueous solutions using solid surface modified with ionic surfactant or polymers (polyelectrolyte) has attracted intense studies [4-18]. So far, ionic surfactants [4, 14, 19] and polyelectrolyte [20-22] are used to modify large beads or combined clay particles with silica sand to enhance the removal efficiency of organic contaminants. The higher performance for removal organic substances is obtained when ionic surfactants are used combined with polyelectrolyte [11, 23, 24]. In these systems, the binding of micelle and charged surface via polyelectrolyte is achieved in order to get immobilized surfactant with the goal of removing organic pollutants from an aqueous phase [8, 11, 23].

The modifications process of solid surface of adsorbents with ionic surfactant and polyelectrolyte are complicated especially when the adsorption of adsorbates also changes the interfacial properties. Polyelectrolyte is mainly adsorbed on the solid surface by electrostatic attraction between highly charged of polyelectrolyte and oppositely charged solid surface or probably by non-electrostatic interaction [10]. Polyelectrolyte was used as potential sacrificial agents because of their tendency to irreversibly adsorb onto charged metal oxide due to large number of adsorption site on each polymer molecule [25]. For ionic surfactant, solid surface can be changed by not only electrostatic attraction between the oppositely charged hydrophilic components but also hydrophobic interaction between the tails of surfactant molecules. As the results of surfactant adsorption, hemimicelles [26-32] (head groups of surfactants molecules toward solid surface) or admicelles [33-35] (a local bilayer structure with head groups of surfactant toward solution) can be formed at solid-liquid interface while an increase of concentration of surfactant to the critical micelle concentration (CMC) in the bulk solution gives rise to the micellization of surfactants. The existence of different kinds of micelles with large aggregation number of ionic surfactant molecules can modify solid surface and thus improve the removal performance of ionic contaminants.

Many studies focused on adsorption of both surfactants and polyelectrolyte on metal oxides [36-39]. The adsorption of surfactants and polymers were carried out individually or as mixtures (simultaneous or sequential adsorptions). In general, adsorption of surfactants and polymers in aqueous media can be additive, cooperative or competitive [40]. Esumi et al. [41] reported the adsorption of poly(styrenesulfonate) (PSS) with anionic surfactant sodium dodecyl sulfate (SDS) and cationic surfactant hexadecyltrimethylammonium chloride (HTCA) from their binary mixture on positively charged surface of α-Al_2O_3. As the results, adsorbed amounts of PSS decreased with increasing SDS concentration due to stronger adsorption of SDS while in the PSS-HTAC system adsorption of PSS was enhanced due to the formation of a complex of PSS-HTAC. The effect of order of addition of ionic surfactants was intensely studied by this work. In addition, the adsorption of PSS of different molecular weights on α-Al_2O_3 was studied by Blokhus and Djurhuus [42]. The adsorption of PSS was found to increase with increasing ionic strength and the adsorption density of PSS was higher for higher molecular weight than for the lower ones. Blokhus and Djurhuus [42] also investigated the effect of added SDS and found that SDS preferentially adsorbed from both simultaneous and sequential adsorptions so that in all case SDS displaced pre-adsorbed PSS from the solid surface. Very recent study [43] demonstrated that the presence of PSS and PDADMAC (polydiallyldimethylammonium chloride) effectively prevented different surfactants adsorption on alumina and silica with large surface area by blocking charged adsorption sites. Only PSS appears to irreversibly adsorb onto metal oxides surface because of multisite adsorption and kinetic limitations while the adsorption of surfactant is almost completely prevented at the concentration higher than CMC.

As mentioned above, polyanion PSS was chosen in various studies for co-adsorption with surfactant because it has a high charge density statistically distributed along the backbone of polymer and the benzenesulfonate groups that are strong ultraviolet (UV) chromophores [44]. The individual adsorption of PSS and surfactants or mixture adsorption on metal oxide have been addressed through different measurements of adsorption density, zeta potential, fluorescence spectrophotometry, electro spin resonance (ESR) and attenuated total reflection techniques with ultraviolet or infrared spectroscopy [41-44]. Furthermore, Wolterink at el. [45] indicated that the charge regulation of metal oxide upon adsorption of strong electrolyte was obtained theoretically and experimentally. The self consistent field (SCF) calculation showed the large effect of pH and the small effect of the salt concentration on the adsorbed amount while the proton co-adsorption was dependent on both pH and salt concentration. However, the measured adsorption isotherms of PSS on hematite did not show a high affinity

character as inferred by theoretical calculations because of fast flocculation and non-equilibrium polymer conformation. The effect of salt concentrations and the influence of added ionic surfactant have not been investigated experimentally in the paper [45]. It is preferable to make a study using relatively large metal oxide beads which are free from flocculation and can be directly used to analysis of transport phenomena of polymer, surfactant and pollutant.

In this chapter, the results of adsorption isotherms of PSS onto large α-Al_2O_3 beads with variably charged surfaces are reported. The adsorption isotherms of PSS with different molecular weight onto α-Al_2O_3 as functions of pH and salt concentration are fitted by general isotherm equation [46] which was introduced in chapters 3 and 4. The effect in the presence of SDS to the adsorption of PSS will also be investigated. The structures of adsorbed PSS of different molecular weights at low and high salt concentrations onto α-Al_2O_3 are proposed based on the adsorption isotherms and the effect of charge regulation.

5.2. Experimental

5.2.1. Materials

Alpha alumina beads were used as sorbents. The specific properties and initial treated procedure for adsorption studies were described in chapters 3 and 4.

Sodium poly(styrene sulfonate), PSS with a molecular weight (Mw) of 70 and 1000 kg/mol was delivered from Aldrich Chemical Co, Inc, with a degree of polymerization of 340 and 4850, respectively. The structure of PSS is given in Fig. 5.1. Other chemicals used in this study were obtained from Wako Pure Chemical Industries. Ultra pure water, produced from Elix Advantage 5 (Millipore) with electric conductivity around 0.6 μS/cm, was used in preparing solutions and in all measurements.

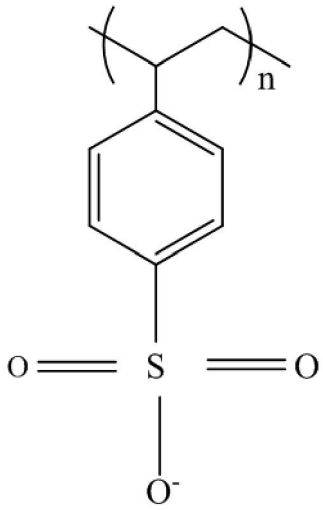

Fig. 5.1. The schematic representation of structure of poly(styrene sulfonate), PSS.

5.2.2. Adsorption isotherms

Adsorption isotherms of PSS onto α-Al_2O_3 were carried out using a depletion method in 100 mL Erlenmeyer flask at room temperature, controlled by air conditioner (22 $\pm$ 2 ^{0}C). For each adsorption experiment, 0.5 g of treated α-Al_2O_3 was mixed with 25 mL of NaCl aqueous solutions at different concentrations by a shaker for 1 h. Then, PSS with concentrations from 0.05 to 0.6 mg/mL was prepared and pH was adjusted to original value. After mixing alumina and PSS and shaking for 3 h, the pH was measured again and if necessary, readjusted by 0.01 or 0.1 M HCl, and 0.1 M NaOH using a Socorex Acura 825 micro pipette with minimum volume of 1 μL. The samples were equilibrated for more than 12 h with vigorous shaking. Then, the pH was checked and, if necessary, readjusted again. This procedure was repeated until no further changes in pH were attained. When equilibrium process was achieved, the α-Al_2O_3 was separated from the solutions. The adsorption density of PSS (Γ_{PSS}) onto α-Al_2O_3 was obtained by the difference in the concentration of PSS solutions before and after adsorption by spectrometric method. By recording the added amount of HCl or NaOH to keep the pH constant after PSS addition, the surface charge adjustment of alpha alumina has been obtained. The surface charge adjustment was combined with initial surface charge of alpha alumina by chromatographic method [47] to calculate the equilibrium surface charge expressed as $\Gamma_{0,PSS} = \sigma_{0,PSS}/F$ with F the Faraday constant.

In order to evaluate the effect of pre-adsorbed SDS on PSS adsorption, SDS was firstly equilibrated with α-Al_2O_3 at the concentration of 1 mM and 8mM of SDS in 0.01M NaCl (pH 4.0) following the SDS adsorption onto α-Al_2O_3 in chapter 4. Thereafter PSS was added in the concentration range 0.05 – 0.6 mg/mL at pH 4. Samples were taken for analysis PSS by spectrometry after shaking solutions for 24 h.

5.2.3. Spectrophotometric method

The concentration of anionic polymer, PSS was measured by spectrophotometry at wavelength 261 nm or 224 nm (according to the results in section 5.4.1) using an UV-vis spectrophotometer (UV-1650PC, Shimadzu) with quartz cuvettes with 1 cm optical path length. All standard calibration curves of PSS in different electrolyte concentrations and pH have a correlation coefficient of at least 0.999. Samples were directly measured or appropriately diluted before measuring the absorbance to quantify PSS concentrations by standard calibration curves.

5.2.4. Potentiometric method

Potentiometry was conducted using a Metrohm 781 pH/Ion meter, Switzerland to determine pH of all solutions and to evaluate CMC of SDS. The detail was presented in previous chapters.

5.3. General isotherm equation

The obtained isotherms were also fitted by general isotherm equation which was firstly derived by assuming that adsorption on solid-liquid interface occurs in two steps [46, 48]. It was originally derived to describe the adsorption of hemimicelle-forming surfactant. The general isotherm equation is

$$\Gamma = \frac{\Gamma_\infty k_1 C \left(\frac{1}{n} + k_2 C^{n-1}\right)}{1 + k_1 C (1 + k_2 C^{n-1})} \quad (5.1)$$

where Γ is amount of PSS adsorbed, Γ_∞ is the maximum adsorption, k_1 and k_2 are equilibrium constants for the adsorption of monomers or first layer adsorption and clusters of n molecules. C is the equilibrium PSS concentration in the bulk solution.

Although the formation of micelle-like structure is unexpected in the case of polyelectrolyte adsorption, polymers can absorb in a cooperative manner to form cluster. The effect of such structure can be described by the parameter *n* [49].

The fitting procedures were described in chapter 3.

5.4. Results and discussion

5.4.1. Spectra of PSS in the absence and presence of SDS

A typical ultra violet (UV) absorbance spectrum of individual PSS with the concentrations ranged from 0.005 to 0.05 mg/mL is shown in Fig. 5.2. At different pH values, the spectra of PSS in the wavelength region 200 – 300 nm have the same shapes with the main absorbance peaks at the wavelength of 224 nm and the secondary peak at 261 nm. The intensity of a maxima at 224 nm is greater than that at 261 nm (about 18 times). These peaks are specific wavelengths for benzene sulfonate group. They are in good agreement with the values of maximum absorbance in published papers [42, 44]. Figure 5.2 also shows that the magnitude of all UV spectra of PSS does not change significantly with pH at a given concentration of PSS. It demonstrates that the dissociation of monomers and structure of PSS are independent of pH [50]. In other word, PSS can be confirmed as strong polyelectrolyte by UV spectroscopic method.

It should be noted that SDS does not absorb ultraviolet light in the region studied. The UV spectra of PSS in the presence of SDS are similar to others in the absence of SDS (not shown in detail). Thus, SDS does not contribute the two peaks mentioned above. Adsorption of PSS in the absence and the presence of SDS can be quantified by measuring absorbance at 224 nm and 261 nm with the standard calibration curves (see Experimental section 5.2.2). Figure 5.3 indicates the standard calibration curves of PSS 1000 in the absence and the presence of SDS (1 mM and 8 mM) at pH 4 and 0.01 M NaCl. The standard calibration curves of PSS 1000 from 0.05 to 0.5 mg/mL with and without SDS have a similar slope with a correlation coefficient of at least 0.999. Again, these curves demonstrate that the effect of SDS to UV method in determining PSS is negligible. These are also helpful to examine the effect of SDS on the processes of adsorption and desorption because the concentration of PSS can be directly determined without any separation.

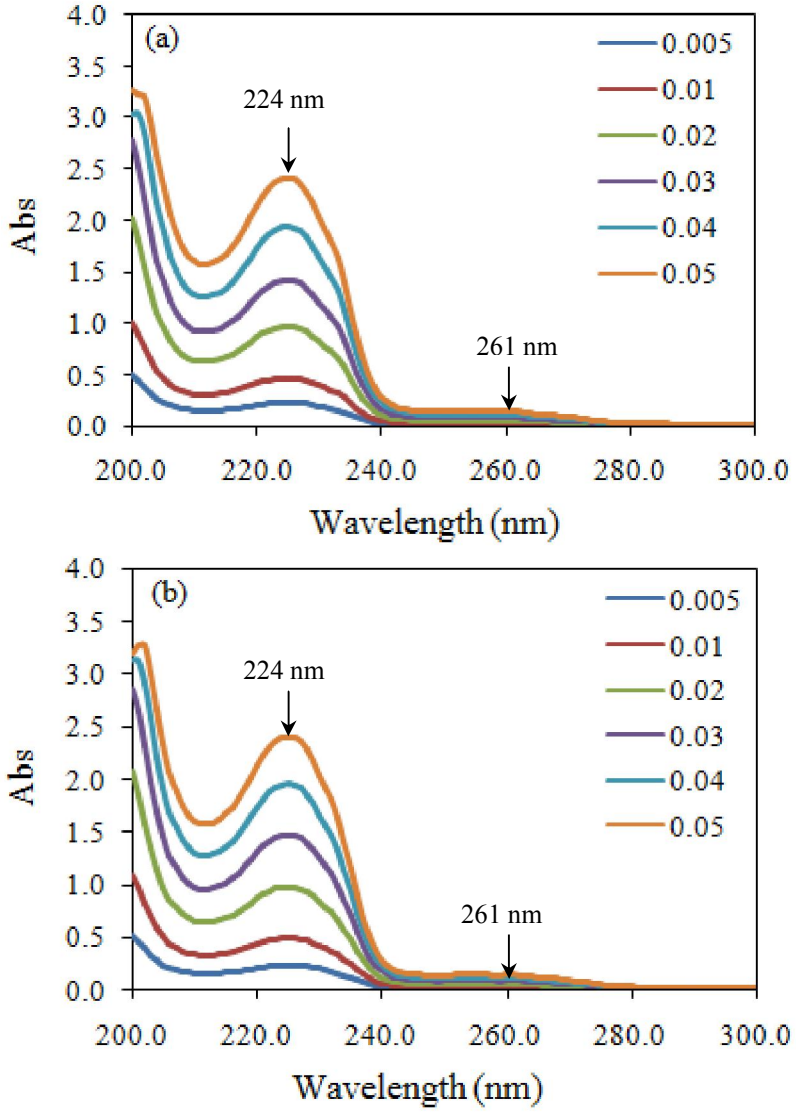

Fig. 5.2. UV spectra of PSS 1000 with different concentrations at pH 4 (a) and pH 5 (b) as a function of wavelength in 0.01M NaCl.

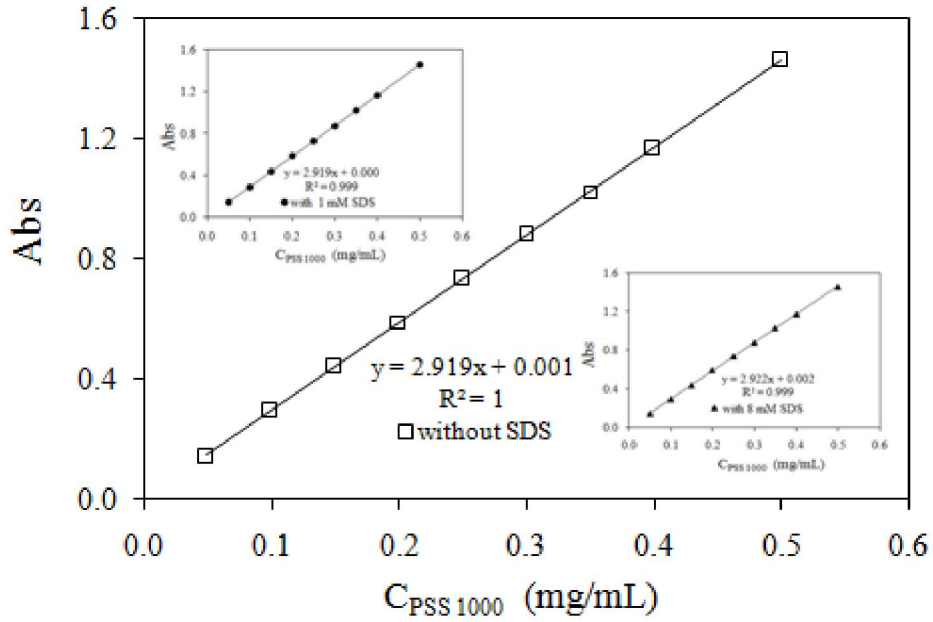

Fig. 5.3. The standard calibration curves of PSS 1000 at pH 4 and at a wavelength of 261 nm in 0.01 M NaCl. The insets show the calibration curves of PSS in the presence of 1 mM SDS (circles) and 8 mM SDS (triangles).

5.4.2. Adsorption isotherms of PSS

The adsorption isotherms of PSS of different molecular weight onto large α-Al_2O_3 beads at two salt concentrations are shown in Fig. 5.4. As can be seen, the adsorption of PSS appears to have the typical high affinity or high adsorption amount that is close to literature data on adsorption of polyanion PSS on positively charged surface α-Al_2O_3 [42] or hematite [51]. Adsorption amounts of PSS of different molecular weights on hematite seem to be remaining from low to high concentrations of polymer [51] while maximum adsorption mounts of PSS onto α-Al_2O_3 appear from 0.025 and 0.1 mg/ml for high and low molecular weights, respectively [42]. Although different molecular weights show the difference in isotherms, the calculated curves fitted by Eq. (5.1) with the fit parameters shown in Table 1 can represent experimental data well. The plateau adsorption increases with increasing the molecular weight of PSS from 70 to 1000 kg/mol at different salt concentrations (Γ_∞ of PSS 1000 > Γ_∞ of PSS 70). At high salt concentration (0.1 M NaCl), the isotherm of PSS 1000 always appears above that of PSS 70. These results are close to the results of published paper [42] in which absorbed amount for higher molecular weight grows up from 70 to 500 kg/mol. However, an increase of molecular weight from 500 to 1000kg/mol does not change the adsorption amounts of PSS on α-Al_2O_3. Due to the different structure of adsorbed layers, the conformation for low molecular weight is more flat than that of high molecular weight. The effect of molecular weight can be evaluated from the difference in the fitting parameters and the isotherms shown in Table 1 and Fig. 5.4, which indicate that the influence of molecular weight is significant at high salt (Fig 5.4b) rather than at low salt (Fig 5.4a). The higher molecular weight is, the higher the value of n is at both two salt concentrations, suggesting that a more flat conformation for adsorbed PSS 70 than that of PSS 1000.

Table 1. The fit parameters for the adsorption of PSS1000 and PSS70 at pH 4, the maximum adsorbed amount $\Gamma_{\infty,PSS}$, the equilibrium constants $k_{1,PSS}$ and $k_{2,PSS}$ for first layer and multilayer, respectively, n is the number of polymer in clusters of polyelectrolyte molecules.

C salt (M NaCl)	Mw (kg/mol)	$\Gamma_{\infty,PSS}$ (mg/m^2)	$k_{1,PSS}$ (m^2/mg)	$k_{2,PSS}$ (m^2/mg)$^{n-1}$	n_{PSS}
0.01	1000	52	1.1	450	4.5
0.01	70	41	1.0	410	4.2
0.1	1000	60	15	500	4.9
0.1	70	44	10	400	4.6

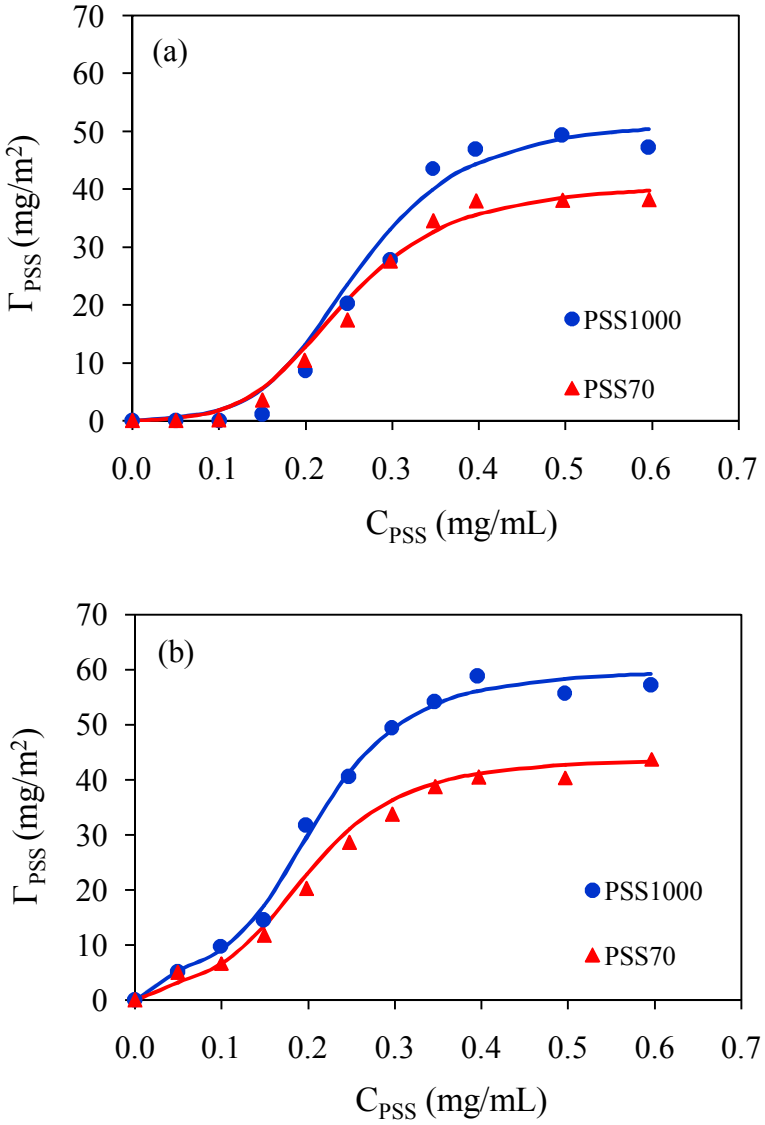

Fig. 5.4. Adsorption isotherms of PSS onto α-Al_2O_3 of different molecular weight at pH 4 in 0.01 M NaCl (a) and 0.1 M NaCl (b) as a function of the equilibrium PSS concentration. While the points are experimental data, the solid lines are the results of 2-step model.

At different salt concentration, the change of pH can be obtained as a function of equilibrium concentration of PSS. The proton adsorption isotherms upon PSS uptake shown in Fig. 5.5 seem to continue even when the equilibrium concentration of PSS is above 0.10 mg/mL. Polyelectrolyte with different molecular weights caused the differences in charge adjustment especially at low salt concentration (Fig. 5.5a) while the change in surface charge is not significant at high salt concentration (Fig. 5.5b). It may be indicated that the charge adjustment could be one factor to evaluate the flat conformation based on molecular weight as mentioned above. However, the adsorption amounts of proton are too small compared with adsorption amounts of PSS (lower than 100 to 200 times). Therefore, it is difficult to explain this effect. Thus, we can suggest that although the proton adsorption isotherms upon PSS adsorption has to be considered, the initial surface charge of α-Al_2O_3 probably seems to be more important for contribution to adsorption.

As mentioned in chapter 2 [47], the surface charge of α-Al_2O_3 is strongly dependent on both pH and ionic strength. Thus, it is necessary to emphasize the effect of electrostatics interaction at different pH and salt concentrations. Figure 5.6 shows the results from the adsorption of PSS 1000 onto α-Al_2O_3 at pH 4 and pH 5 and at two salt concentrations. As can be seen in Fig. 5.6, the adsorption amounts of PSS increase with increasing salt concentration at both pH 4 and pH 5, demonstrating that not only electrostatic attraction but also non-electrostatic interactions induce PSS adsorption. These results agree well with experimental data in published paper [42], where only plateau adsorption of PSS at fixed pH 6 as a function of NaCl concentration is reported. However, in this work, we successfully described salt effect of the experimental adsorption isotherms at different pH and by modeling with general isotherm Eq. (5.1). Table 2 and Fig. 5.6 show that 10 times increase in salt concentrations induces about 13 times in the values of $k_{1,PSS}$ (with both pH 4 and pH 5), while the values of $k_{2,PSS}$ grow up not significantly. It implies that the monolayer adsorption isotherm of PSS expressed by $k_{1,PSS}$ by can be used to evaluate the electrostatic and non-electrostatic interactions. Electrostatic forces and the salt concentration are screened at high salt concentration. If the adsorption is promoted by only attractive electrostatic force, the first layer adsorption or the value of k_1 will decrease with increasing salt concentration. On the contrary, when non-electrostatic interaction occurs, the adsorption of highly charged polyelectrolytes is enhanced by addition of salt [52] that is close to our results. Non-electrostatic interaction can take place due to the presence of the lateral interaction between PSS molecules [45]. The lateral interaction can induce more loops and tails in the structure of adsorbed PSS on α-Al_2O_3 so that adsorption amounts increase with increasing salt concentration.

Table 2. The fit parameters for the adsorption of PSS 1000 at pH 4 and pH 5 in 0.01 M NaCl and 0.1 M NaCl, the maximum adsorbed amount $\Gamma_{\infty,PSS}$, the equilibrium constants $k_{1,PSS}$ and $k_{2,PSS}$ for first layer and multilayer, respectively, n is the number of polymer in clusters of polyelectrolyte molecules.

C salt (M NaCl)	pH	$\Gamma_{\infty,PSS}$ (mg/m^2)	$k_{1,PSS}$ (m^2/mg)	$k_{2,PSS}$ (m^2/mg)$^{n-1}$	n_{PSS}
0.01	4	52	1.1	450	4.5
0.1	4	60	15	500	4.9
0.01	5	43	2	400	4.7
0.1	5	49	25	350	4.9

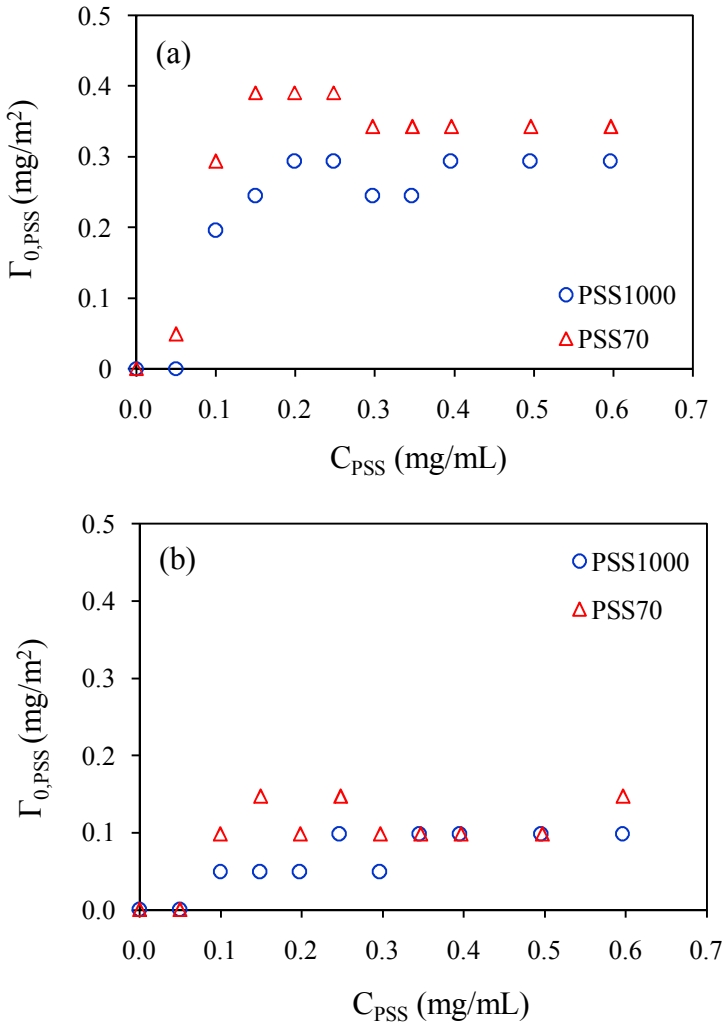

Fig. 5.5. Proton adsorption isotherms upon the adsorption of PSS onto α-Al_2O_3 of different molecular weight at pH 4 in 0.01 M NaCl (a) and 0.1 M NaCl (b) as a function of the equilibrium PSS concentration.

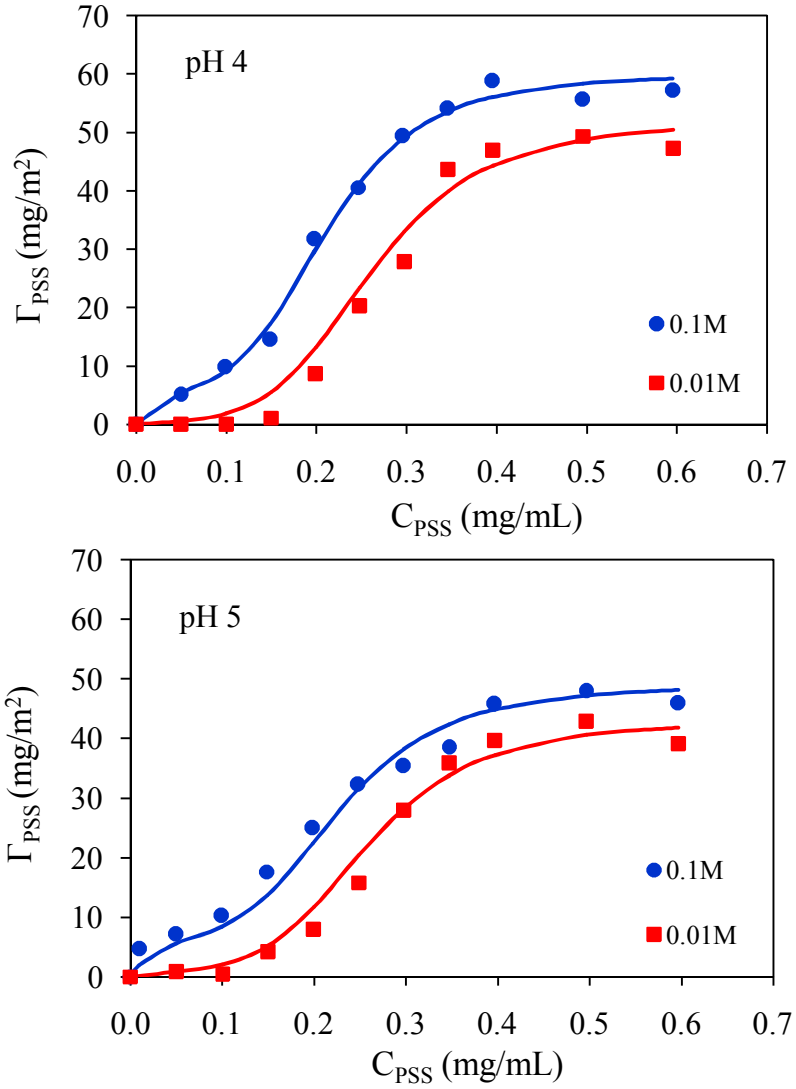

Fig. 5.6. Adsorption isotherms of PSS 1000 onto α-Al_2O_3 at pH 4 and pH 5 in 0.01 M NaCl and 0.1 M NaCl as a function of the equilibrium PSS concentration. While the points are experimental data, the solid lines are the results of 2-step model.

5.4.3. Effect of SDS on the adsorption of PSS

The effect of SDS on the adsorption of PSS onto α-Al_2O_3 beads was studied by a sequential method (section 5.2.2). The adsorption isotherms of PSS in the absence and the presence of SDS are indicated in Figs. 5.7 and 5.8. We can see that the PSS adsorption amounts with pre-adsorbed SDS at concentration of 1 and 8mM seem to be high affinity type due to high loading of polymer on α-Al_2O_3 when the equilibrium concentration of PSS is higher than 0.2 mg/mL. A similar trend was also observed for simultaneous adsorption of difference molecular weight of PSS on α-Al_2O_3 at low concentration of SDS [42]. At low concentration of SDS than hemimicelle concentration (Fig. 5.7), HMC (typically 1 – 2 mM), the adsorption of SDS is low (see results of chapter 3 in this thesis) so that surface sites for adsorption of PSS are available. The pre-adsorbed SDS was conducted with 1 mM that was near HMC can prevent adsorption of PSS. At high concentration of SDS above the CMC (Fig 5.8), the formation of admicelles also prevents adsorption of PSS significantly. However, the prevention in these cases seems to be strong for low concentration of PSS than for higher one. At low concentration of PSS, the adsorption of polyelectrolyte is not significant because the pre-adsorbed surfactant in the presence of hemimicelles or/and admicelles prevents the adsorption of polyelectrolyte. It can be suggested that the adsorption of SDS onto alumina is much stronger than that of PSS [41-43].

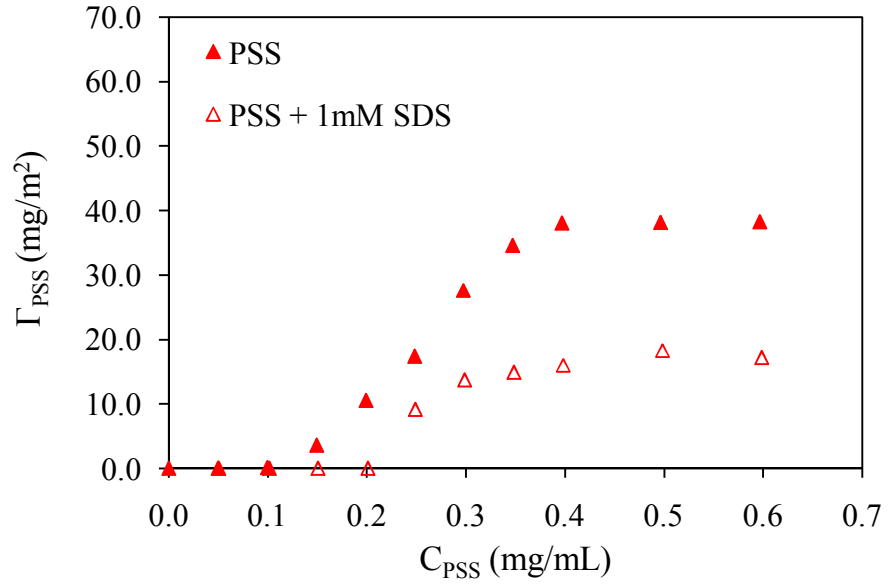

Fig. 5.7. Adsorption isotherms of PSS70 onto α-Al_2O_3 at pH 4 and 0.01 M NaCl without pre-adsorbed SDS and with pre-adsorbed SDS (1 mM) as a function of the equilibrium PSS concentration.

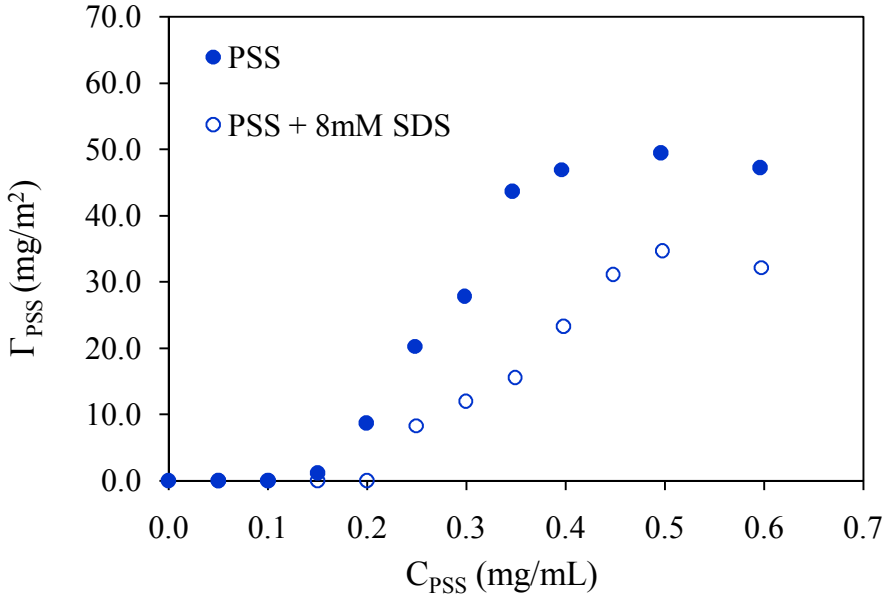

Fig. 5.8. Adsorption isotherms of PSS1000 onto α-Al_2O_3 at pH 4 and 0.01 M NaCl without pre-adsorbed SDS and with pre-adsorbed SDS (8 mM) as a function of the equilibrium PSS concentration.

5.4.4. Structures of adsorbed PSS onto α-Al_2O_3

Polyanion poly(styrenesulfonate), PSS, with different molecular weight adsorbed onto α-Al_2O_3 at different ionic strength induced the difference in the structures of adsorbed PSS. As mentioned in section 5.4.2, the adsorption amounts of PSS 70 are lower than that of PSS 1000 because the conformation for PSS 70 is more flat than PSS 1000. It can be emphasized by the adsorption amount of proton upon the uptake of polyelectrolyte. The more flat conformation for PSS is, the more adsorbed proton is. Even though the adsorption amount of proton is much lower than that of PSS, it is probably useful to explain the structure of adsorbed PSS. In Fig 5.9, a schematic representation shows the different structure of adsorbed PSS 70 and PSS 1000 in the same high salt concentration. As can be seen, based on the less flat conformation, PSS 1000 appears with more loops in adsorbed layer than PSS 70.

An increase in salt concentration also affects the adsorbed structure. By increasing salinity of solution, the adsorption amounts of PSS onto α-Al_2O_3 increase due to both electrostatic and non-electrostatic interactions. The electrostatic repulsion among internal segmental decreased with increasing salt concentrations. Actually, the adsorption of PSS onto α-Al_2O_3 followed a multilayer manner as deduced from the fitting by two-step model. However, to describe the adsorbed structure of polyelectrolyte on the metal oxide surface, we only focused on the first layer adsorption. As the result from adsorption isotherms of both PSS and proton, it can be suggested that the more loops in the adsorbed layer can be formed. Figure 5.10 shows a cartoon of structure of adsorbed PSS 1000 at high and low salt concentration. It is seen that the adsorption of proton in the case of high salt with more loops seems to be smaller than that at low salt concentration. Also, the interaction between polyelectrolyte on the surface of α-Al_2O_3 with polyelectrolyte in bulk solution can be enhanced due to an increase in salt concentration.

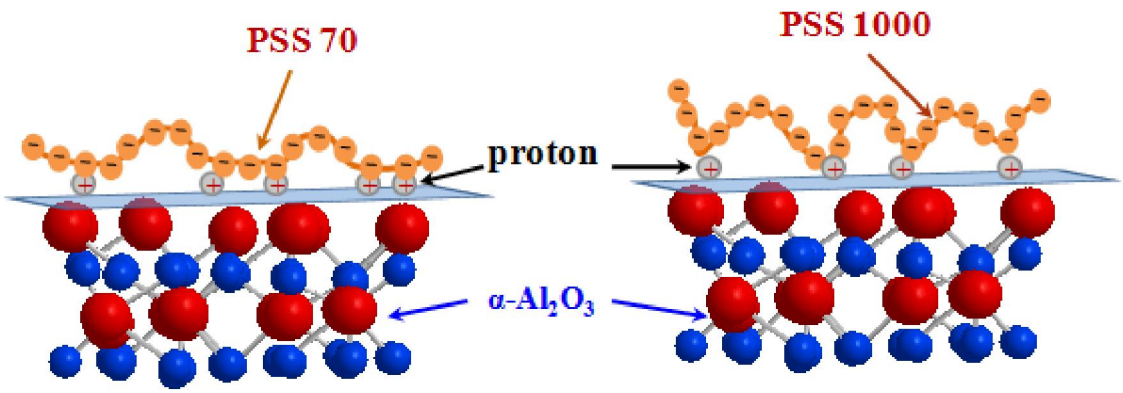

Fig. 5.9. Cartoon representation of structure of the adsorbed PSS 70 and PSS 1000 onto α-Al_2O_3. The conformation for PSS 70 is more flat than PSS 1000.

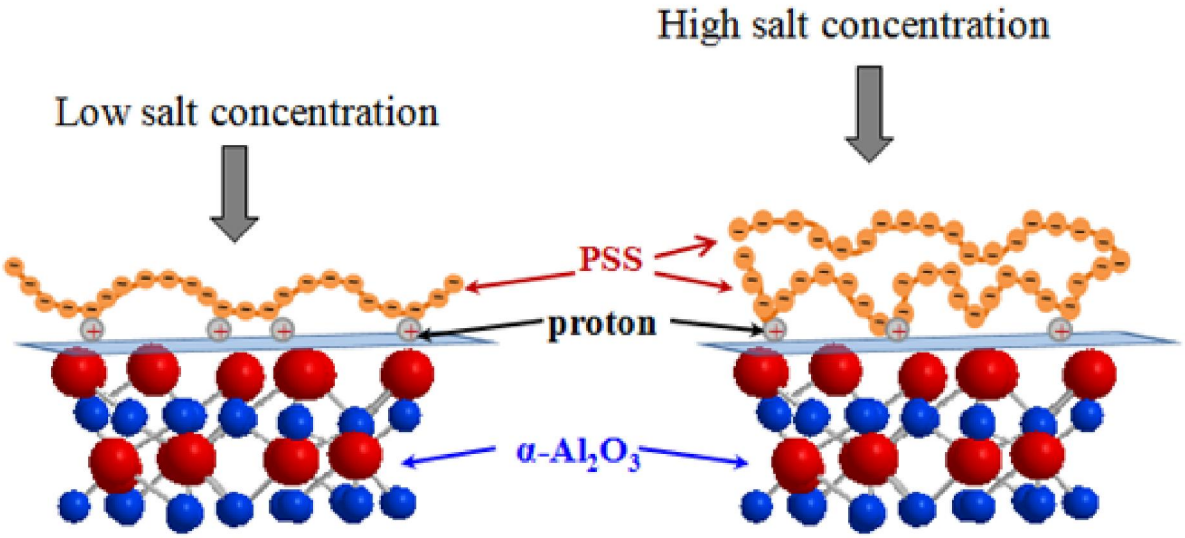

Fig. 5.10. Cartoon showing the structure of the adsorbed PSS 1000 onto α-Al_2O_3 at low and high salt concentrations. While the more proton is adsorbed at low salt, the more loop is obtained in the structure of PSS at high salt concentration.

5.5. Conclusions

In this chapter, we investigated the adsorption of poly(styrene sulfonate), PSS, of different molecular weight onto large α-Al_2O_3 beads. The properties of PSS as a strong polyelectrolyte were confirmed by UV spectrophotometry. An increase in molecular weight of PSS from 70 kg/mol to 1000 kg/mol increases the adsorption amount of PSS and decreases proton uptake on the surface of α-Al_2O_3. It suggested that less flat conformation on the adsorbed structure is expected for high molecular weight rather than lower one. The adsorption is found to increase with increasing salt concentrations, indicating that both electrostatic and non-electrostatic contributions are involved. Electrostatic attraction is screened at high salt concentration while non-electrostatic contribution can be induced by lateral interaction between PSS molecules. The SDS uptake onto α-Al_2O_3 in the presence of hemimicelles or/ and admicelles can prevent the adsorption of PSS at low concentration so that adsorption of PSS decreases with pre-adsorbed SDS.

References

[1] A. Bhatnagar, A.K. Jain, A comparative adsorption study with different industrial wastes as adsorbents for the removal of cationic dyes from water, Journal of Colloid and Interface Science, 281 (2005) 49-55.

[2] G. Crini, Non-conventional low-cost adsorbents for dye removal: A review, Bioresource Technology, 97 (2006) 1061-1085.

[3] V.K. Gupta, Suhas, Application of low-cost adsorbents for dye removal – A review, Journal of Environmental Management, 90 (2009) 2313-2342.

[4] A. Adak, M. Bandyopadhyay, A. Pal, Removal of crystal violet dye from wastewater by surfactant-modified alumina, Separation and Purification Technology, 44 (2005) 139-144.

[5] A. Adak, M. Bandyopadhyay, A. Pal, Fixed bed column study for the removal of crystal violet (C. I. Basic Violet 3) dye from aquatic environment by surfactant-modified alumina, Dyes and Pigments, 69 (2006) 245-251.

[6] F. Al-Momani, E. Touraud, J.R. Degorce-Dumas, J. Roussy, O. Thomas, Biodegradability enhancement of textile dyes and textile wastewater by VUV photolysis, Journal of Photochemistry and Photobiology A: Chemistry, 153 (2002) 191-197.

[7] F. Aloulou, S. Boufi, N. Belgacem, A. Gandini, Adsorption of cationic surfactants and subsequent adsolubilization of organic compounds onto cellulose fibers, Colloid Polym Sci, 283 (2004) 344-350.

[8] F. Aloulou, S. Boufi, D. Beneventi, Adsorption of organic compounds onto polyelectrolyte immobilized-surfactant aggregates on cellulosic fibers, Journal of Colloid and Interface Science, 280 (2004) 350-358.

[9] F. Aloulou, S. Boufi, M. Chakchouk, Adsorption of octadecyltrimethylammonium chloride and adsolubilization on to cellulosic fibers, Colloid Polym Sci, 282 (2004) 699-707.

[10] B. Bolto, J. Gregory, Organic polyelectrolytes in water treatment, Water Research, 41 (2007) 2301-2324.

[11] Y.G. Mishael, P.L. Dubin, Uptake of Organic Pollutants by Silica−Polycation-Immobilized Micelles for Groundwater Remediation, Environmental Science & Technology, 39 (2005) 8475-8480.

[12] Y.G. Mishael, P.L. Dubin, Toluene Solubilization Induces Different Modes of Mixed Micelle Growth†, Langmuir, 21 (2005) 9803-9808.

[13] Y.G. Mishael, T. Undabeytia, G. Rytwo, B. Papahadjopoulos-Sternberg, B. Rubin, S. Nir, Sulfometuron Incorporation in Cationic Micelles Adsorbed on Montmorillonite, Journal of Agricultural and Food Chemistry, 50 (2002) 2856-2863.

[14] A. Özcan, Ç. Ömeroğlu, Y. Erdoğan, A.S. Özcan, Modification of bentonite with a cationic surfactant: An adsorption study of textile dye Reactive Blue 19, Journal of Hazardous Materials, 140 (2007) 173-179.

[15] A.S. Özcan, B. Erdem, A. Özcan, Adsorption of Acid Blue 193 from aqueous solutions onto Na–bentonite and DTMA–bentonite, Journal of Colloid and Interface Science, 280 (2004) 44-54.

[16] Y. Su, B. Zhao, W. Xiao, R. Han, Adsorption behavior of light green anionic dye using cationic surfactant-modified wheat straw in batch and column mode, Environ Sci Pollut Res, 20 (2013) 5558-5568.

[17] D. Zadaka, A. Radian, Y.G. Mishael, Applying zeta potential measurements to characterize the adsorption on montmorillonite of organic cations as monomers, micelles, or polymers, Journal of Colloid and Interface Science, 352 (2010) 171-177.

[18] B. Zhao, Y. Shang, W. Xiao, C. Dou, R. Han, Adsorption of Congo red from solution using cationic surfactant modified wheat straw in column model, Journal of Environmental Chemical Engineering, 2 (2014) 40-45.

[19] S. Chatterjee, D.S. Lee, M.W. Lee, S.H. Woo, Enhanced adsorption of congo red from aqueous solutions by chitosan hydrogel beads impregnated with cetyl trimethyl ammonium bromide, Bioresource Technology, 100 (2009) 2803-2809.

[20] S. Chatterjee, T. Chatterjee, S.H. Woo, Influence of the polyethyleneimine grafting on the adsorption capacity of chitosan beads for Reactive Black 5 from aqueous solutions, Chemical Engineering Journal, 166 (2011) 168-175.

[21] G. Crini, P.-M. Badot, Application of chitosan, a natural aminopolysaccharide, for dye removal from aqueous solutions by adsorption processes using batch studies: A review of recent literature, Progress in Polymer Science, 33 (2008) 399-447.

[22] E.S. Dragan, Design and applications of interpenetrating polymer network hydrogels. A review, Chemical Engineering Journal, 243 (2014) 572-590.

[23] Y. Wang, J. Banziger, P.L. Dubin, G. Filippelli, N. Nuraje, Adsorptive Partitioning of an Organic Compound onto Polyelectrolyte-Immobilized Micelles on Porous Glass and Sand, Environmental Science & Technology, 35 (2001) 2608-2611.

[24] D. Zadaka, Y.G. Mishael, T. Polubesova, C. Serban, S. Nir, Modified silicates and porous glass as adsorbents for removal of organic pollutants from water and comparison with activated carbons, Applied Clay Science, 36 (2007) 174-181.

[25] E.S. Pagac, D.C. Prieve, R.D. Tilton, Kinetics and Mechanism of Cationic Surfactant Adsorption and Coadsorption with Cationic Polyelectrolytes at the Silica−Water Interface, Langmuir, 14 (1998) 2333-2342.

[26] D.W. Fuerstenau, Streaming Potential Studies on Quartz in Solutions of Aminium Acetates in Relation to the Formation of Hemi- micelles at the Quartz-Solution Interface, The Journal of Physical Chemistry, 60 (1956) 981-985.

[27] D.W. Fuerstenau, H.J. Modi, Streaming Potentials of Corundum in Aqueous Organic Electrolyte Solutions, Journal of The Electrochemical Society, 106 (1959) 336-341.

[28] D.W. Fuerstenau, T. Wakamatsu, Effect of pH on the adsorption of sodium dodecane-sulphonate at the alumina/water interface, Faraday Discussions of the Chemical Society, 59 (1975) 157-168.

[29] A.M.F. Gaudin, D.W. Fuerstenau , Streaming Potential Studies. Quartz Flotation with Anionic Collectors, Transactions AIME, 202 (1955) 958-962.

[30] P. Somasundaran, D.W. Fuerstenau, Mechanisms of Alkyl Sulfonate Adsorption at the Alumina-Water Interface, The Journal of Physical Chemistry, 70 (1966) 90-96.

[31] P. Somasundaran, T.W. Healy, D.W. Fuerstenau, Surfactant Adsorption at the Solid—Liquid Interface—Dependence of Mechanism on Chain Length, The Journal of Physical Chemistry, 68 (1964) 3562-3566.

[32] T. Wakamatsu, D.W. Fuerstenau, The Effect of Hydrocarbon Chain Length on the Adsorption of Sulfonates at the Solid/Water Interface, Adsorption From Aqueous Solution, American Chemical Society, 1968, pp. 161-172.

[33] D. Bitting, J.H. Harwell, Effects of counterions on surfactant surface aggregates at the alumina/aqueous solution interface, Langmuir, 3 (1987) 500-511.

[34] J.H. Harwell, J.C. Hoskins, R.S. Schechter, W.H. Wade, Pseudophase separation model for surfactant adsorption: isomerically pure surfactants, Langmuir, 1 (1985) 251-262.

[35] M.A. Yeskie, J.H. Harwell, On the structure of aggregates of adsorbed surfactants: the surface charge density at the hemimicelle/admicelle transition, The Journal of Physical Chemistry, 92 (1988) 2346-2352.

[36] E. Grządka, Competitive adsorption in the system: carboxymethylcellulose/surfactant/electrolyte/Al2O3, Cellulose, 18 (2011) 291-308.

[37] L. Meagher, G. Maurdev, M.L. Gee, Interaction Forces between a Bare Silica Surface and an α-Alumina Surface Bearing Adsorbed Polyelectrolyte and Surfactant, Langmuir, 18 (2002) 2649-2657.

[38] K. Sakai, T. Yoshimura, K. Esumi, Direct Force Measurements between α-Alumina Surfaces with Adsorption of Anionic Surfactant/Polymer Mixtures, Langmuir, 19 (2003) 1203-1208.

[39] P. Somasundaran, J. Cleverdon, A study of polymer/surfactant interaction at the mineral/solution interface, Colloids and Surfaces, 13 (1985) 73-85.

[40] L.H. Torn, A. de Keizer, L.K. Koopal, J. Lyklema, Mixed adsorption of poly(vinylpyrrolidone) and sodium dodecylbenzenesulfonate on kaolinite, Journal of Colloid and Interface Science, 260 (2003) 1-8.

[41] K. Esumi, A. Masuda, H. Otsuka, Adsorption of poly(styrenesulfonate) and ionic surfactant from their binary mixtures of alumina, Langmuir, 9 (1993) 284-287.

[42] A.M. Blokhus, K. Djurhuus, Adsorption of poly(styrene sulfonate) of different molecular weights on α-alumina: Effect of added sodium dodecyl sulfate, Journal of Colloid and Interface Science, 296 (2006) 64-70.

[43] J.S. Weston, J.H. Harwell, B.J. Shiau, M. Kabir, Disrupting Admicelle Formation and Preventing Surfactant Adsorption on Metal Oxide Surfaces Using Sacrificial Polyelectrolytes, Langmuir, 30 (2014) 6384-6388.

[44] D.J. Neivandt, M.L. Gee, C.P. Tripp, M.L. Hair, Coadsorption of Poly(styrenesulfonate) and Cetyltrimethylammonium Bromide on Silica Investigated by Attenuated Total Reflection Techniques, Langmuir, 13 (1997) 2519-2526.

[45] J.K. Wolterink, L.K. Koopal, M.A.C. Stuart, W.H. Van Riemsdijk, Surface charge regulation upon polyelectrolyte adsorption, hematite, polystyrene sulfonate, surface charge regulation: Theoretical calculations and hematite-poly(styrene sulfonate) system, Colloids and Surfaces A: Physicochemical and Engineering Aspects, 291 (2006) 13-23.

[46] B.-Y. Zhu, T. Gu, Surfactant adsorption at solid-liquid interfaces, Advances in Colloid and Interface Science, 37 (1991) 1-32.

[47] T.D. Pham, M. Kobayashi, Y. Adachi, Interfacial characterization of α-alumina with small surface area by streaming potential and chromatography, Colloids and Surfaces A: Physicochemical and Engineering Aspects, 436 (2013) 148-157, This thesis: Chapter 2.

[48] B.-Y. Zhu, T. Gu, General isotherm equation for adsorption of surfactants at solid/liquid interfaces. Part 1. Theoretical, Journal of the Chemical Society, Faraday Transactions 1: Physical Chemistry in Condensed Phases, 85 (1989) 3813-3817.

[49] I. Hoffmann, C. Oppel, U. Gernert, P. Barreleiro, W. von Rybinski, M. Gradzielski, Adsorption Isotherms of Cellulose-Based Polymers onto Cotton Fibers Determined by Means of a Direct Method of Fluorescence Spectroscopy, Langmuir, 28 (2012) 7695-7703.

[50] A.W.M. de Laat, PhD Thesis: Adsorption of water-soluble polymers onto barium titanate and its effec on colloidal stability, Wageningen Agricultural University, 1995.

[51] R. Ramachandran, P. Somasundaran, Polyelectrolyte interactions at the hematite/water interface. Part 1, Colloids and Surfaces, 32 (1988) 307-317.

[52] N.G. Hoogeveen, M.A.C. Stuart, G.J. Fleer, Polyelectrolyte Adsorption on Oxides: I. Kinetics and Adsorbed Amounts, Journal of Colloid and Interface Science, 182 (1996) 133-145.

Chapter 6. Conclusions and perspectives

6.1. Conclusions

The treatment of wastewater by adsorption is widely used to remove organic pollutants from aqueous solutions. The understanding of adsorption properties of organic ions onto charged surface is very important in environmental science and technology. Adsorption of organic waste such as ionic dyes is effectively enhanced by surfactant and/or polyelectrolyte modified solid surface. However, the adsorption characteristics of ionic surfactant, ionic dye and polyelectrolyte on to solid surfaces are still inadequate when adsorbents have large size. Furthermore, so many scientific papers studied adsorption of various ions onto silica sand with negatively charged surface. Nevertheless, a few studies focused on adsorption using large beads with positive surface charge. Therefore, the purpose of this thesis is to extend knowledge of adsorption of organic anions onto large α-Al_2O_3 beads with positively charged surface. For this purpose adsorption of anionic surfactant, sodium dodecyl sulfate (SDS), anionic azo dye, new coccine (NC), and strong polyanion, polystyrene sulfonate (PSS), onto α-Al_2O_3 have been systematically studied and successfully analyzed with two-step adsorption model. Furthermore, the structures of adsorbed SDS, NC and PSS onto α-Al_2O_3 were also discussed on the basis of charge effect, surface modification and adsorption isotherms. The results were described in chapter 2 to chapter 5.

In chapter 2 the interfacial properties of α-Al_2O_3 beads with small surface area were investigated by streaming potential and chromatography. The zeta potential from streaming potential and the surface charge density of α-Al_2O_3 were obtained as a function of pH. Streaming potential was used to obtain the zeta potential at several pH values to evaluate electrokinetic property and to identify isoelectric point (IEP) of α-Al_2O_3 materials. The surface charge density of α-Al_2O_3 was evaluated by chromatographic method from measured pH breakthrough curves. A good agreement between the charge density obtained from column pH breakthrough curves and 1-pK Stern model was confirmed in the pH range without dissolution effect. Although streaming potential and chromatography are not new techniques, our results indicated that their combinations compared with 1-pK Stern model are convincing to characterize the electrokinetic potential and surface charge density of large beads.

Chapter 3 deals the measurement and analysis of adsorption of SDS onto large Al_2O_3 beads with variably charged surface as functions of pH and NaCl concentration. The obtained comprehensive data clarified the applicability of two-step adsorption and four-region models to describe the adsorption isotherms of SDS onto Al_2O_3 beads. Proton adsorption upon surfactant uptake could be fitted by two-step adsorption model with almost the same parameters for surfactant adsorption for 0.001 and 0.01 M NaCl concentration, indicating that proton adsorption took place onto the adsorbed SDS. Adsorption isotherms of SDS at different salt concentrations had a common intersection point (CIP) corresponding to charge neutralization. After passing through CIP, proton adsorption onto α-Al_2O_3 increased at low ionic strength while the amount of proton adsorption did not change for 0.1 M NaCl. Proton adsorption amounts as a function of SDS adsorption suggested that only hemimicelles are plausible for case of low ionic strength. The increase in the proton adsorption was not significant at high ionic strength, suggesting the presence of admicelles on the surface of α-Al_2O_3 beads.

In chapter 4, a comparison of SDS with NC in terms of adsorption onto α-Al_2O_3 beads was intensively studied. Streaming potential demonstrated that the IEP of α-Al_2O_3 increases after SDS adsorption due to additional proton adsorption while the IEP shifts to the lower pH after adsorption of NC because of the adsorption of the negatively charged sulfonic group of NC. The surface modifications of α-Al_2O_3 after adsorption of SDS and NC were confirmed by Fourier transform infrared attenuated total reflection spectroscopy (FTIR-ATR). The calculated curves from two-step model can reasonably represent experimental results of both SDS and NC adsorption isotherms onto α-Al_2O_3. The proton adsorption isotherms at low salt concentrations upon surfactant adsorption were able to be described well by two-step model, while proton adsorption upon dye adsorption was negligible. The decrease of adsorption of SDS onto α-Al_2O_3 with increasing electrolyte concentration below CIP was similar to NC adsorption. Nevertheless, above CIP, the salt effect was reversed and the adsorption density of SDS reduces at lower ionic strength. This trend is different from dye adsorption. Adsorption of SDS is induced by the presence of hemimicelles and admicelles at the α-Al_2O_3/ water interface. Adsorption of NC was affected by formation of a bridged bidentate complex between only one sulfonic group on the naphthalene ring and surface of α-Al_2O_3, resulting in that adsorption density of surfactant was much higher than that of dye.

Chapter 5 focused on the adsorption of strong polyelectrolyte PSS of different molecular weights onto α-Al_2O_3 beads. The ultraviolet (UV) absorption spectra of PSS at different pH and salt concentrations confirmed that PSS was independent of pH. With increasing in the

molecular weight from 70 to 1000 kg/mol, adsorption amount of PSS increased and proton co-adsorption on the surface of α-Al_2O_3 decreased at given pH and salt concentration. It suggested that higher molecular weight of PSS was less flat conformation than lower one. The adsorption density decreased with decreasing salt concentrations, indicating that both electrostatic and non-electrostatic interactions occurred. Electrostatic attraction was screened at high salt concentration while non-electrostatic contribution could be induced by lateral interaction between PSS molecules. The effects of molecular weight and salt concentration were explained by structure of adsorbed PSS onto α-Al_2O_3. The effect of added SDS on the isotherms was evaluated from sequential adsorption. The SDS uptake onto α-Al_2O_3 in the presence of hemimicelles or/and admicelles prevented the adsorption of PSS at low concentration so that adsorption of PSS decreased with pre-adsorbed SDS.

6.2. Perspectives and further studies

In this thesis, adsorption characteristics of strong anionic ions, anionic surfactant, anionic azo dye, and strong polyanion onto large α-Al_2O_3 beads with positively charged surface were experimentally investigated. The experimental data were compared with theoretical calculation by two-step adsorption model. The experimental data and calculation by modeling indicated that adsorption of these strong organic anions onto α-Al_2O_3 beads was similarly dependent on pH. The adsorption amounts increased with decreasing pH due to strong electrostatic attraction induced by highly positively charged surface of α-Al_2O_3 at lower pH. However, the adsorption of SDS onto α-Al_2O_3 was much stronger than that of PSS and NC due to the presence of hemimicelles and admicelles. The CIP appears only in the adsorption isotherms of SDS at different salt concentrations because of charge adjustment upon surfactant adsorption and the strong effect of hydrophobic interaction between chains. While the adsorption of NC was only controlled by electrostatic attraction, both electrostatic and non-electrostatic interactions induced PSS adsorption. Therefore, these differences in adsorption properties of surfactant, dye and polyelectrolyte can be a convincing argument to explain the enhancement of removal efficiency of dyes after modification of large beads by surfactants and/or polyelectrolytes.

The general isotherm equation derived by the concept of two-step adsorption was successfully applied to various types of surfactant adsorption isotherms and used for some kinds of polymers. The adsorption of complex multilayer adsorption of ionic dyes fitted by the general equation has been reported in this thesis. In addition, an improvement of two-step

model to describe the proton/SDS adsorption inferences is important to understand the interaction of surfactant and proton with surface. Thus, two-step model may be applied to not only surfactant systems but also proton, complexes, polyelectrolytes, dyes, and so on.

As mentioned in this thesis, the use of large size particles with positively charged surface such as our beads are useful to make an analysis of transport phenomena directly. It can be also compared with negatively charged sand to better understand the adsorption and the transport in natural porous materials. Furthermore, large particles are of great importance in the chemical engineering process and chemical industry as packed bed adsorbents in columns for wastewater treatment in environmental remediation. In its current studies, this thesis need to be further developed.

For the application in analytical science, surfactant and/or polyelectrolyte can be used to enhance the separation efficiency of organic substances due to the presence of micelles or complexes in aqueous solutions. Thus, the high performance liquid chromatography with reserved phase and/or capillary electrophoresis chromatography are applicable. The used surfactant and/or polyelectrolyte for this purpose seem to be effective in bulk solutions because of the interactions of these with organic compounds. However, surfactant and/or polyelectrolyte modified stationary phase need to be considered.

The α-Al_2O_3 beads used in this research has IEP around pH 7. We only investigated adsorption of organic anions onto α-Al_2O_3 with positively charged surface at pH < IEP. It can also be applicable to use this adsorbent at higher pH than IEP for absorbing organic cations. Another feature is that surfactants or/and polyelectrolytes can modify solid surface of large beads to enhance removal efficiency of dyes with opposite charge than the same one. The combination of surfactants and polyelectrolytes are also highly performed with opposite charge. This thesis has a need to be extended for further investigation on the complex systems with both organic cations and anions. Moreover, the removal efficiency of inorganic ions such as heavy metals which are not easily biodegradable can be improved by adsorption with surfactants or/and polyelectrolytes modified solid surface. Therefore, surfactants or/and polyelectrolytes modified alumina system will be subjected to more intense studies.

List of publications

Related to Doctoral thesis:

1. **Tien Duc Pham**, Motoyoshi Kobayashi, Yasuhisa Adachi, Interfacial characterization of α-alumina with small surface area by streaming potential and chromatography, *Colloids and Surfaces A: Physicochem. Eng. Aspects*, 436 (2013) 148 – 157.

2. **Tien Duc Pham**, Motoyoshi Kobayashi, Yasuhisa Adachi, Adsorption of anionic surfactant sodium dodecyl sulfate onto alpha alumina with small surface area, *Colloid and Polymer Science* (2014), Accepted.

3. **Tien Duc Pham**, Motoyoshi Kobayashi, Yasuhisa Adachi, Adsorption characteristics of anionic surfactant and anionic dye onto large α-alumina beads, In preparation.

References:

1. Motoyoshi Kobayashi, Takuya Sugimoto, Kenta Yamada, **Tien Duc Pham** and Yuta Honjo, Soil and related interfacial electric phenomena. 3. Electrokinetic phenomena and their applications, *Journal of Soil Science and Plant Nutrition* 85, No. 3(2014) 250 – 257 (in Japanese).

2. **Pham Tien Duc**, Pham Thi Ngoc Mai, Nguyen Thi Anh Huong, Hoang Trong Khiem (2012), Simultaneous determination of impurities metals in pure Tungsten powder by ICP-MS, *Journal of Analytical Sciences* 17, No. 3 (2012) 22 – 27 (in Vietnamese with English Abstract).

3. Dang Hoai Nhon, Tran Duc Thanh, Dinh Van Huy, Nguyen Thi Kim Anh, Nguyen Mai Luu, Nguyen Dinh Khang, Phan Son Hai, Nguyen Manh Ha, **Pham Tien Duc**, Lai Thi Bich Thuy, The sedimentary processes on tidal flats in the North of Vietnam: initial results and implication future, *Proceedings of VAST – IRD Symposium on Marine Science*, (2013) 164 – 178.

Acknowledgements

Without the help of many people who contributed to this thesis in various ways, I could not finish it. I would like to express my deep gratitude to all those who gave me the possibility to complete this thesis.

First of all, I would like to express my indebtedness to my supervisor, Prof. Yasuhisa Adachi for his whole – hearted guidance that help me throughout my work. I could not have an opportunity to study in Colloid laboratory at University of Tsukuba without his help.

I would like to convey my deep appreciation to Assoc. Prof. Motoyoshi Kobayashi for his valuable advice and suggestions during the time I worked my PhD project. His enthusiasm in Colloid and Interface Science has inspired my love for Colloid Chemistry.

I would like to thank Prof. Munehide Ishiguro at Hokkaido University and Dr. Mikio Kajiyama, Dr. Kasayoshi Ogawa at University of Tsukuba for their suggestions to further improve this thesis.

I thank all of professors and staff of Graduate School of Life and Environmental Sciences, University of Tsukuba to support my work and student life.

I would like to express my gratitude for all members in Colloid laboratory for their help and encouragements, especially Mr. Kenta Yamada and Dr. Yoko Tsujimoto.

I wish to thank Ms. Nakayama, Ms. Ishii and also Ms. Hasegawa for their kind help in all administrative and non-administrative problems.

I also thank my colleagues at Faculty of Chemistry, Vietnam National University, Hanoi for their assistance in some measurements.

I am grateful for the financial support from University of Tsukuba. I also thank to support from Vietnamese government scholarship (approved by VIED-MOET) for study Doctoral course abroad.

Finally, I owe my deepest gratitude to my family, my wife and my daughter for their endless support and help.

September, 2014

Tien Duc PHAM